Spring 2018

Differentiation of Pseudomonas sp. strain ADP biofilms and planktonic cells using methods in gene expression analysis

Michael Asher Delcau
University of Iowa

DIFFERENTIATION OF *PSEUDOMONAS* SP. STRAIN ADP BIOFILMS AND PLANKTONIC CELLS USING METHODS IN GENE EXPRESSION ANALYSIS

by

Michael Asher Delcau

A thesis submitted in partial fulfillment
of the requirements for the Doctor of Philosophy
degree in Chemical and Biochemical Engineering in the
Graduate College of
The University of Iowa

May 2018

Thesis Supervisor: Professor Tonya L. Peeples

Graduate College
The University of Iowa
Iowa City, Iowa

CERTIFICATE OF APPROVAL

PH.D. THESIS

This is to certify that the Ph.D. thesis of

Michael Asher Delcau

has been approved by the Examining Committee for
the thesis requirement for the Doctor of Philosophy degree
in Chemical and Biochemical Engineering at the May 2018 graduation.

Thesis Committee: _____
Tonya L. Peeples, Thesis Supervisor

_____
Alexander R. Horswill

_____
Craig L. Just

_____
David W. Murhammer

_____
Aliasger K. Salem

To My Loving Father, Carey M. Delcau

The most dangerous thing about an academic education is that it enables my tendency to over-intellectualize stuff, to get lost in abstract thinking instead of simply paying attention to what's going on in front of me.

David Foster Wallace
This is Water

ACKNOWLEDGEMENTS

It has been a spirited, intense, and fascinating journey as I come close to finishing my time as doctoral student at the University of Iowa in Chemical and Biochemical Engineering. First and foremost, I would like to thank my advisor, Dr. Tonya Peeples, for providing me with wisdom and guidance, advice, and unwavering support from the beginning of my time as an incoming graduate student to the very end of my voyage as a PhD graduate in Chemical and Biochemical Engineering. Without her, I would not be where I am today in terms of my personal, professional, and academic development.

I would like to thank my family, including my mother Roxanne Delcau, my father Carey Delcau, my brother David Delcau, and my uncle James Roedel for their love, patience, and understanding while I pursue higher education to fulfill my greatest goals. The phone calls, text messages, and road trips to visit me in Iowa City from my loving friends, Ryan Lund and Kevin Robb, have helped me retain my sanity in graduate school.

The Chemical and Biochemical Engineering Department and administrative staff, including Sara Hartman and Megan Delaney, for their promptness and aid regarding both personal and professional matters. My current and former graduate lab mates, Richard Gonzales, Felipe Nicolau-Manterola, and Victoria Henry, for their patience in familiarizing me to the graduate work environment and their willingness to help in any aspect of my project and training. A great thanks to the undergraduate research assistants who have helped progress my research, Emily R. Pattee, Sarah Keith, Megan Martin, and Andrea Diaz. The SSTP student, Yiheng Xie, I would like to recognize for performing an incredible amount of research work in a fleeting period.

I am grateful for my committee members Dr. Alexander Horswill, Dr. Craig Just, Dr. David Murhammer, and Dr. Aliasger Salem for providing sustained guidance and feedback during my greatest doctoral milestones. A big thanks to Dr. Chantal Allamargot for consulting and assistance at the Central Microscopy Research Facility. The wonderful staff at the DNA facility I owe my gratitude, Mary Boes and Gary Hauser, for an infinite amount of help in troubleshooting and experimental validation.

I would like to acknowledge The Center for Biocatalyis and Bioprocessing along with the National Institutes of Health for providing me with funding for two years and encouraging me to pursue experience in industrial biotechnology via an internship. I would like to thank my advisor from Matis Ohf, Bjorn Adalbjornsson, for his leadership and direction in helping me succeed as a biotechnology intern abroad in Iceland and encouraging me to continue my academic career.

Lastly, and not least, I would like to recognize my graduate and undergraduate support system at the University of Iowa. My fellow graduate students in my class have given me an overwhelming amount of support throughout my five years. My friends at Alpha Chi Sigma, for being present and offering companionship throughout my time at the University of Iowa. Without them, I would not have a social outlet to balance my life as a graduate research student. My work achieved as a graduate student, including the research, the oral and poster presentations, the grants, the fellowships, the scholarships, and even networks built would not be possible without the help of the aforementioned people and departments. As my life as a PhD student ends, and new chapter in my life begins, I want to ensure that even if I am away from Iowa, these people are documented for their role in my life.

ABSTRACT

Bacterial strain *Pseudomonas* sp. ADP is capable of degrading atrazine via an enzymatic pathway in six sequential steps to yield carbon dioxide and ammonia. Atrazine is a persistent herbicide that frequently contaminates soil, drinking water, and ground water throughout areas of heavy use in the United States. A biological remediation approach using *Pseudomonas* sp. APD is considered as an effective and environmentally conscious method of decreasing atrazine concentration in areas of high contamination. Each enzyme in the degradation pathway is encoded by a corresponding gene, *AtzA-AtzF*, and is located on a self-transmissible 108-kb plasmid.

Due to their prevalence in nature, and their unique genetic and physical characteristics, biofilms are of great interest in the field of bioremediation. Biofilms exhibit high tolerance for harsh environmental stressors/conditions, prodigious potential for recalcitrant compound entrapment via an extracellular polymeric matrix, quorum sensing, and increased horizontal gene transfer compared to their planktonic counterparts. Despite frequent genetic and chemical analyses performed on atrazine-degrading genes on planktonic cells of strain *Pseudomonas* sp. APD, the genetics and degradation potential of *Pseudomonas* sp. ADP biofilms is relatively unexplored.

Real-time quantitative PCR was used to differentiate the expression of six genes involved in the process of atrazine degradation. Relative expression experiments revealed no statistically significant difference in the expression of atrazine-degrading genes in *Pseudomonas* sp. ADP cells grown as biofilms relative to *Pseudomonas* sp. ADP cells grown as planktonic cells. In biofilms alone, the

expression of genes *AtzDEF* was differentiated via temperature of biofilm growth in cells grown at 25 ^{o}C, 30 ^{o}C, and 37^{o}C.

Analytical techniques, including GC-MS and HPLC, were used to elucidate atrazine remediation potential of *Pseudomonas* sp. ADP biofilms and our previously collected genetic data. Stable decreases in atrazine degradation following a first-order kinetic model have been demonstrated for planktonic cells compared to a complex degradation pattern, including transient increases, observed for corresponding biofilm-mediated cells. This is attributed to the unique structure of the biofilm and the potential of atrazine to be entrapped in the substances of the extracellular polymeric matrix and subsequently released into the effluent. Overall, the biodegradation efficiency was statistically significantly higher for *Pseudomonas* sp. ADP biofilm-mediated cells compared to their planktonic counterparts.

A novel methodology of using confocal microscopy and *in situ* reverse transcription was proposed to visualize the expression of atrazine-degrading genes in fixed *Pseudomonas* sp. ADP biofilms. The sugar composition of *Pseudomonas* sp. ADP was evaluated using fluorescent lectin binding analysis and was determined to exhibit a prominent level of diversity and was dependent upon the growth medium. The results from these experiments will play a role in application of biofilms grown in bioreactors for atrazine remediation throughout areas of persistent and high contamination throughout the US. The new step in methodology development of an *in situ* visual gene expression technique can be extended to bioremediation of alternate recalcitrant compounds. The results may also be aid progress in alternate biofilm-related studies in medicine & human health, metallurgy, and engineering.

PUBLIC ABSTRACT

Atrazine is the second most common herbicide in the United States, used to prevent the pre-and post-emergence of broad-leaved and grassy weeds. While effective, atrazine is classified as an endocrine disruptor compound (EDC) that frequently pollutes groundwater sources and drinking water in levels exceeding the EPA's maximum contaminant level of 3 parts per billion. A conscious approach to removing atrazine from the environment is bioremediation; this method relies on exploiting a microbe's natural ability to degrade a chemical compound. Bacterial strain *Pseudomonas* sp. ADP degrades atrazine in six sequential steps. In the natural environment, the strain can form a 'biofilm', in which the microbes attach to a surface, proliferates, and produces an enclosed matrix of bio macromolecules. This structure is of heightened interest in the field of bioremediation due to its unique abilities to entrap chemicals within the matrix and increased bacterial genetic activity.

Genetic techniques were used to survey the metabolic activity, and the strain's biodegradation potential, in a biofilm compared to free-floating 'planktonic' cells. Degradation of atrazine and its metabolites were monitored chemically to evaluate the differences between *Pseudomonas* sp. ADP's atrazine degradation capacity by mode of growth. Genetic methods revealed no difference while chemical methods demonstrated complex degradation kinetics in the biofilm mode of growth and sustained degradation of atrazine in planktonic cells. Additionally, methods to visualize the *in situ* metabolic activity of the strain in biofilms were explored using confocal microscopy, which may be applied in a general manner to biofilms.

TABLE OF CONTENTS

Contents

LIST OF TABLES xiii

LIST OF FIGURES xv

PREFACE xxi

CHAPTER 1: INTRODUCTION 1

Project Description 1

Specific Aims 2

Background 3

Atrazine 3

Bioremediation 5

Pseudomonas sp. strain ADP 7

Catabolic pathway for degradation 10

Biofilms 12

Gene expression 15

Addressed research gaps 19

CHAPTER 2: GROWTH OF *PSEUDOMONAS* SP. STRAIN ADP AND OPTIMIZATION OF RNA EXTRACTION FROM BIOFILMS 22

Introduction 22

Materials and Methods 24

Bacterial strain and reagents 24

Culture media 24

Planktonic cell preparation 26

Bacterial calibration for growth 26

Construction of P.ADP growth curves 27

RNA extraction from P.ADP planktonic cells 28

Preparation for P.ADP biofilm growth in DFR 30

Construction of DFR for biofilm growth 30

Sterilization of DFR 31

P.ADP biofilm growth in DFR 32

Optimized RNA extraction of P.ADP biofilms 33

Environmental synthesis of atrazine 35

Results and Discussion 36

Growth curves for P.ADP by media 36

Quality control of RNA following various extraction methods 41
Characterization: MS and NMR analysis for atrazine synthesis 51
Conclusion 56
CHAPTER 3: EXPRESSION OF ATRAZINE-DEGRADING GENES IN *PSEUDOMONAS* SP. ADP BIOFILMS 59
Introduction 59
Materials and Methods 65
Bacterial strain, cultivation medium, and culture conditions 65
Growth of P.ADP planktonic cells 65
Drip-flow reactor for P.ADP biofilm growth 66
Temperature dependence and mode of growth 66
RNA extraction and quantification 67
Reverse transcription (cDNA synthesis) 67
Validation of primers 68
Quantitative PCR 69
Growth of cyanuric acid as a sole-nitrogen source 70
Expression of AtzDEF in response to cyanuric acid 71
Growth of P.ADP under nitrogen sources 71
UV-Vis degradation assay under various nitrogen sources 71
Expression of atzABC by nitrogen source 72
Statistical analysis 72
Results and Discussion 73
No difference in expression by mode of growth 73
Regulation dependence on biofilm growth temperature 74
Growth and expression of P.ADP on CYA as sole nitrogen source 78
Conclusion 89
CHAPTER 4: MICROSCOPY TO CHARACTERIZE *PSEUDOMONAS* SP. ADP BIOFILMS 91
Introduction 91
Materials and Methods 95
Optimization of ISRT 95
Prior work for RNA preparation for ISRT 95
Atrazine-degrading system and growth of planktonic cells 96
Fixation 97
Paraformaldehyde solution (4% in PBS) 97
Permeabilization 98

Dehydration 98
Hybridization 99
Construction of humidity chamber for hybridization 100
Reverse transcription 100
Confocal laser scanning microscopy 100
SEM to differentiate biofilms and planktonic cells 101
Antibiotic testing on P.ADP for GFP Constructs 101
FLBA for monosaccharide analysis 102
Results and Discussion 103
Differentiation of surface properties by mode of growth 103
Qualitative measure of cell density by media using SEM 105
Optimization of ISRT in planktonic P.ADP for AtzD 106
ISRT optimization of planktonic P.ADP with GADPH 109
Effect of select antibiotics on P.ADP 111
Optimization of ISRT in planktonic P.ADP with EUB338 113
Mean intensity ratio of glycoconjugates in P.ADP biofilms 116
IMARIS generated images of FLBA for P.ADP biofilms 119
Lectin dependence upon media in P.ADP biofilms 126
Conclusion 128
CHAPTER 5: KINETICS OF ATRAZINE DEGRADATION BY ANALYTICAL METHODS 132
Introduction 132
Materials and Methods 134
Sample collection for P.ADP planktonic cells 134
Sample collection for P.ADP biofilms 134
Mode of growth dependence using GC-MS 135
Temperature-dependence using GC-MS 136
Atrazine concentration in biofilms using GC-MS 136
HPLC 137
ELISA 138
Results and Discussion 138
Dependence of biodegradation on mode of growth by P.ADP 138
Dependence of biodegradation on temperature by P.ADP biofilm 143
Atrazine detection in DFR-grown P.ADP biofilms 144
Conclusion 146
CHAPTER 6: CONCLUSION AND FUTURE PERSPECTIVES 148

Thesis Conclusion 148
Scientific Impact 151
Future Work 151
Component optimization of ISRT by a DOE approach 152
Whole-transcriptome analysis of P.ADP biofilms and planktonic cells 154
Detection of atrazine by Raman spectroscopy 156
Optimization of atrazine-degradation for P.ADP biofilms 158
APPENDIX A: RNA GEL ELECTROPHORESIS 160
APPENDIX B: CALIBRATION CURVES 162
APPENDIX C: NANODROP RNA QUALITY ANALYSIS 163
APPENDIX D: MASS SPECTROMETRY SPECTRA 165
APPENDIX E: FLUORESCENT LECTIN BINDING ANALYSIS 169
APPENDIX F: NOMENCLATURE TABLE 171
REFERENCES 173

LIST OF TABLES

Table 2.1. Growth parameters of *Pseudomonas* sp. strain ADP, including: doubling time (t_d), specific growth rate (μ), and range of the logarithmic phase, are reported for each type of growth medium.....39

Table 2.2. Micro-spectrophotometric parameters for quality control of RNA following extraction of total RNA using RNeasy Mini Kit. Concentration, absorbance ratios, and multiplication factor are reported above and organized by column.....42

Table 2.3. Capillary gel electrophoresis parameters for quality control of RNA following extraction of total RNA using RNeasy Mini Kit. Concentration, peak areas, ribosomal ratios, and RNA integrity numbers are reported above and organize by column.....44

Table 2.4. Sample concentrations reported from *Pseudomonas* sp. strain ADP biofilms as measured by micro-spectrophotometry. Absorbance ratios (260/280) and (260/230) are reported, in addition to approximate RNA concentrations from sample.....47

Table 2.5. Sample concentrations reported from *Pseudomonas* sp. strain ADP biofilms as measured by gel capillary electrophoresis. Area, ribosomal ratio, and RNA integrity number are reported in addition to approximate RNA concentrations from sample.....48

Table 3.1. Sample 96-well plate for qPCR containing log-range span of endogenous control primer pair and experiment primer pair to evaluate amplification efficiencies. No template controls (NTC) and no reverse-transcriptase controls (NRT) are negative controls used for the qPCR validation experiment. Each (X) represents a well without cDNA or other qPCR components. Each numeric value represents the amount of cDNA in nanograms.....69

Table 4.1. Model bacterial strains permeabilized with optimized concentrations and incubations.....98

Table 4.2. Ethanol dehydration series with an increasing amount of ethanol in each of the following steps.....99

Table 4.3. Monosaccharide specificities for rhodamine-bound lectins.....103

Table 4.4. Probes tested in In Situ Reverse Transcription (ISRT) protocol for optimization in *Pseudomonas* sp. strain ADP planktonic cells. Primer, direction, and sequence are listed for each specific probe.....107

Table 4.5. Mean Intensity Ratio (MIR), associated error, and indicated presence or absence of specified sugar as demonstrated by fluorescent lectin binding analysis (FLBA) and confocal microscopy (CLSM) for *Pseudomonas* sp. strain ADP biofilms grown in DSMZ medium containing 30 mg L^{-1} atrazine.....119

Table 4.6. Mean Intensity Ratio (MIR), associated error, and indicated presence or absence of specified sugar as demonstrated by fluorescent lectin binding analysis (FLBA) and confocal microscopy (CLSM) for *Pseudomonas* sp. strain ADP biofilms grown in LB medium.....119

Table 6.1. Fixation time factor in design-of-experiments approach to ISRT.....153

Table 6.2. Permeabilization time and concentration in design-of-experiments approach to ISRT, each concentration and time are independent of each other and factored separately.....153

Table 6.3. Hybridization time and temperature of probe in design-of-experiments approach to ISRT, each temperature and time are independent and factored separately.....153

Table E.1. Sample calculations of Mean Intensity Ratio (MIR) for fluorescent lectin binding analysis (FLBA) of Concanavalin A (ConA). S designates sample, and T in table above designates trial. LB is the medium used for this set of samples.....170

LIST OF FIGURES

Figure 1.1. Indicator plates containing atrazine demonstrate moderate Clearing zones 48 h after inoculation (A) surrounding areas of bacterial Streaking, and substantial clearing zones 72 h following initial inoculation of *Pseudomonas* sp. strain ADP (B).[30] 8

Figure 1.2. Atrazine (100 mg L^{-1}) was completely degraded by *Pseudomonas* sp. strain ADP cells after 25 h as measured by radioactivity of c-14 ring labeled atrazine and scintillation counting. Boiled cells were used as a negative control.[1] 9

Figure 1.3. The 108-kb self-transmissible plasmid, pADP-1, containing all six genes encoding for atrazine-degradation isolated from Pseudomonas sp. strain ADP.[2] 10

Figure 1.4. The complete catabolic pathway of atrazine taken by *Pseudomonas* sp. strain ADP, involving enzymes AtzA-AtzF.[3] 11

Figure 1.5. Biofilms are characterized by four to five sequential stages of development from planktonic cells. These include reversible attachment, irreversible attachment, maturation I / microcolony formation, maturation II, and dispersal/dispersion.[4] 14

Figure 1.6. Expression of the complete set of atrazine-degrading genes in *Pseudomonas* sp. strain ADP planktonic cells in response to (A) no atrazine (circles) and (B) atrazine at 55 mg L^{-1} (squares) over a timescale of 400 min. Values identified with a different letter at each sampling point differ significantly at $p<0.05$ as a result of Fisher's test between *atz* transcripts of control and atrazine-treated conditions [3] 18

Figure 1.7. Expression of todC1 gene in *Pseudomonas putida* F1 cells by In Situ Reverse Transcription (ISRT), (A) Red fluorescent cells are expressing todC1 (arrows are positive cells), (B) DAPI counterstaining (arrows are negative cells) to view whole community.[59] 19

Figure 2.1. Methodology of constructing bacterial growth curve of *Pseudomonas* sp. strain ADP on various growth media using spectrophotometry. Initial cells are retrieved from a streak plate; however, cells may be retrieved from frozen P.ADP stock if there is no known contamination 28

Figure 2.2. Four-chamber polycarbonate drip-flow reactor with septa and filter units used for growth of P.ADP biofilms.[5,9] 31

Figure 2.3. Set up of the drip-flow reactor for biofilm growth. The influent consisting of DSMZ medium (30 mg L^{-1} atrazine), connected to peristaltic pumps running to the DFR chamber, and subsequently to the effluent (waste) container 32

Figure 2.4. (A) Growth of P.ADP at 30°C, shaking at 250 rpm, in planktonic mode of growth for 32 h under the following media conditions: LB (●), ammonium nitrate (■), DSMZ with atrazine (100 mg L^{-1}) (▲), and DSMZ with atrazine (50 mg L^{-1}) (▼) (B) Semi-logarithmic plot of growth curves in (A).....37

Figure 2.5. (A) Growth of P.ADP at 30°C, shaking at 250 rpm, in planktonic mode of growth for 32 h under the following media conditions: ammonium nitrate (■), DSMZ with atrazine (100 mg L^{-1}) (▲), and DSMZ with atrazine (50 mg L^{-1}) (▼). LB media removed to demonstrate the growth of P.ADP under minimal Media conditions more clearly (B) Semi-logarithmic plot of growth curves in (A).....38

Figure 2.6. Electropherogram of capillary gel electrophoresis, displaying 16s and 23s ribosomal peaks, along with RNA area, concentration, integrity number, and spectra for extraction of RNA from planktonic *Pseudomonas* sp. strain ADP cells. Two samples, AS (top) and BS (bottom), are illustrated, respectively. 45

Figure 2.7. Digital renderings of *Pseudomonas* sp. strain ADP biofilms grown at 30°C for 5-days under a drip-flow reactor with DSMZ media containing atrazine (30 mg L^{-1}). Each image illustrates a mature biofilm, performed in triplicate in drip-flow reactor. Each biofilm is attached to a Silane-coated microscope slide in images above.....46

Figure 2.8. Electropherogram of capillary gel electrophoresis, displaying 16s and 23s ribosomal peaks, along with RNA area, concentration, integrity number, and spectra for extraction of RNA from biofilm *Pseudomonas* sp. strain ADP cells. Two samples, SR (top), and TR (bottom), are illustrated, respectively.....49

Figure 2.9. Electropherogram of capillary gel electrophoresis, displaying 16s and 23s ribosomal peaks, along with RNA area, concentration, integrity number, and spectra for extraction of RNA from biofilm *Pseudomonas* sp. strain ADP cells. Three samples (TRB), (TRC), and (TRD), are illustrated above at top, middle, and bottom, respectively.....50

Figure 2.10. Spectrum from TOF MS EI+ designating three peaks, representing the mixture of three compounds synthesized from cyanuric chloride. The compounds appeared at 10.39 s, 10.67 s, and 10.93 s.....52

Figure 2.11. Mass spectra from TOF MS EI+ displaying the fingerprint for each of the three compounds detected in varying abundances: 1,3,5-Triazine-2,4-diamine, 6-chloro-N-N'-bis(1-methylethyl), s-Triazine, 1-chloro-3-ethylamino-5-isopropylamino -2,4,6-triazine (atrazine), and 2-chloro-4,6-bis(ethylamino). The abscissa displays the mass to charge ratio and the ordinate displays the relative abundance of each molecular fragment from time of flight mass spectrometry electron ionization (TOF MS EI+).....54

Figure 2.12. Crude ^{1}H-NMR spectrum of synthesized atrazine from cyanuric chloride.....56

Figure 3.1. RT-qPCR workflow consisted of initial cellular growth, followed by extraction of total ribonucleic acid, DNase treatment, purification, cDNA synthesis, qPCR, and analysis. Each experiment involving gene expression involved the use of the above RT-qPCR schematic.....64

Figure 3.2. Expression of atrazine-degrading genes in *Pseudomonas* sp. strain ADP cells grown in biofilm mode of growth (experimental) relative to suspended planktonic mode of growth reported as n-fold changes. Error bars represent 95% confidence intervals. Baseline is represented by (+1/-1) dependent upon upregulation and downregulation of expression, respectively.....74

Figure 3.3. Expression of atrazine-degrading genes in *Pseudomonas* sp. strain ADP biofilms measured by growth temperature. Temperature of 30°C (control) was used a baseline for relative expression experiments to temperatures 25°C and 37°C (experimental). Error bars represent 95% confidence intervals for non-control conditions. Baseline temperature is set at a fold change of 1, downregulation is designated as bars below 0, and upregulation is designated as bars above 0-fold-change.....75

Figure 3.4. Figure a (top) represents the growth curve of *Pseudomonas* sp. strain ADP on cyanuric acid as a sole nitrogen source over a period of approximately 250 h. Error associated is represented as positive and negative bars representing 95% confidence intervals, with n = 3. Figure b (bottom) displays the n-fold changes in expression of atrazine-degrading genes *AtzDEF* in *Pseudomonas* sp. strain ADP planktonic cells grown on cyanuric acid relative to cells grown on atrazine at 30 mg L^{-1} as a sole nitrogen source. Error bars represent 95% confidence intervals. Baseline is at zero (atrazine) with each bar representing the change for cyanuric acid-grown cells.....79

Figure 3.5. Growth curves of *Pseudomonas* sp. strain ADP under the following sole or dual nitrogen sources: urea (●), urea + atrazine (■), cyanuric acid (▲), cyanuric acid + atrazine (▼), and atrazine (♦). Measurements up to 66 h, ranging from an optical density (OD_{600}) 0.05 to 0.4.....82

Figure 3.6. Spectrophotometric determination of atrazine remaining after *Pseudomonas* sp. strain ADP planktonic cells (A_{225}) growing on one of the following sole or dual nitrogen sources: urea + atrazine, cyanuric + atrazine, and atrazine. After 66 h, the final concentration was reported as above in each bar (grey) compared to the initial concentrations represented in each bar (black).....83

Figure 3.7. Expression of atrazine-degrading genes in *Pseudomonas* sp. strain ADP planktonic cells on various sole or dual nitrogen sources (urea, urea + atrazine, cyanuric acid, cyanuric acid + atrazine) relative to atrazine as a sole nitrogen source. Error bars represent 95% confidence intervals. Atrazine is illustrated with a baseline of 1-fold change as the control condition, other nitrogen sources reported as upregulation (values greater than 1) and downregulation (values less than 1).....86

Figure 4.1. A schematic of In Situ Reverse Transcription (ISRT), from initial cell culture of *Pseudomonas* sp. strain ADP cells and *Escherichia coli* DH5α in LB medium.....95

Figure 4.2. The panel above displays SEM micrographs of *Pseudomonas* sp. strain ADP cells grown as a mature five-day biofilm under DSMZ medium containing atrazine (A-B), and SEM micrographs of *Pseudomonas* sp. strain ADP free-cells under DSMZ medium containing atrazine (C-D).....104

Figure 4.3. The panel above displays SEM micrographs of planktonic *Pseudomonas* sp. strain ADP cells grown in A) DSMZ medium containing 100 mg L^{-1} of atrazine, B) LB medium, C) LB medium (magnified), and D) ammonium nitrate medium.....106

Figure 4.4. Initial ISRT confocal (A, C) and transmission (B, D) micrographs illustrating planktonic *Pseudomonas* sp. strain ADP cells with positive *AtzD* expression with DAPI counterstain and Alexa Fluor 488 conjugated dye (A) and negative *AtzD* expression with DAPI counterstain (blue) and Alexa Fluor 488 conjugated dye (C).....108

Figure 4.5. ISRT confocal (A, B) and transmission (C) micrographs illustrating planktonic *Pseudomonas* sp. strain ADP cells with positive GAPDH expression with DAPI (blue) counterstain (A) and Alexa Fluor 488 (green) conjugated dye (B).....110

Figure 4.6. Minimum inhibitory concentration (MIC) data for antibiotic carbenicillin on *Pseudomonas* sp. strain ADP cells growing on LB.....112

Figure 4.7. Minimum inhibitory concentration (MIC) data for antibiotics gentamicin (●) and tetracycline (■) on *Pseudomonas* sp. strain ADP cells growing on LB.....112

Figure 4.8. Micrographs of ISRT *Pseudomonas* sp. strain ADP cells under confocal laser scanning microscope (C, D) and transmission (A, B) in single-layer (A, C, D) and z-stack (B) conformations. Image in panel (C) is the negative control of DAPI counterstain with no probe containing Alexa Fluor 488 in dual channel mode, and image in panel (D) is DAPI counterstain (blue) with eubacterial probe EUB338 conjugated to Alexa Fluor 488 (green) in dual channel mode.....114

Figure 4.9. Confocal laser scanning micrograph of *Pseudomonas* sp. strain ADP in planktonic mode of growth viewed as a z-stack with DAPI counterstain (blue) and Alexa Flour 488 conjugated to EUB338 probe (green).....115

Figure 4.10. Mean Intensity Ratios, the ratio of the mean intensities for rhodamine (red) conjugated to lectins relative to the mean intensities for DAPI (blue), for each lectin was calculated for *Pseudomonas* sp. strain ADP biofilms grown under DSMZ medium (30 mg L^{-1} atrazine). Error bars represent 95% confidence intervals.....117

Figure 4.11. IMARIS generated images of *Pseudomonas* sp. strain ADP biofilms with DAPI counterstain (blue) of whole cell population and rhodamine-bound lectins (red) of Dolichos Biflorus Agglutinin (DBA) from a top-view (A) and sectional view (B) with aid of confocal laser scanning microscopy (CLSM).....120

Figure 4.12. IMARIS generated images of *Pseudomonas* sp. strain ADP biofilms with DAPI counterstain (blue) of whole cell population (B), rhodamine-bound lectin (red) of Concanavalin A (ConA) (A), and dual-channels (C) from a top-view with aid of confocal laser scanning microscopy (CLSM).....121

Figure 4.13. IMARIS generated image of *Pseudomonas* sp. strain ADP biofilms with DAPI counterstain (blue) of whole cell population in dual-channel with rhodamine-bound lectin (red) of Concanavalin A (ConA) from a three-dimensional view (A), and Z-stack confocal lasers scanning microscopy (CLSM) superimposed with transmission image (B) displaying DAPI (blue), ConA (pink), and the combination (purple).....122

Figure 4.14. Rhodamine-bound Peanut Agglutinin (PNA) (A, B), rhodamine-bound Wheat Germ Agglutinin (WGA) (C, D), rhodamine-bound Ricin Communis Agglutinin (RCA) (E, F) from top-view (A, C, E) and sectional-view (B, D, F). DAPI counterstain (blue) is displayed in all confocal laser scanning (CLSM) micrographs for *Pseudomonas* sp. strain ADP biofilms.....123

Figure 4.15. IMARIS generated images of *Pseudomonas* sp. strain ADP biofilms viewed under a confocal laser scanning microscope in single-channel mode displaying rhodamine-bound lectins Peanut Agglutinin (PNA) (A), Wheat Germ Agglutinin (WGA) (B), Ricinus Communis Agglutinin (RCA) (C) from a top-view.....125

Figure 4.16. Relative distributions of rhodamine-bound lectins normalized to cell material in *Pseudomonas* sp. strain ADP biofilms grown in DSMZ medium (A) and grown in LB medium (B). Total represents fluorescence intensity ratio (arbitrary units).....127

Figure 5.1. Atrazine concentration measured by GC-MS over five days in shake flasks containing a planktonic cell medium (■) and a DFR-grown biofilm containing reactor effluent (●) as a result of microbial degradation.[5] 139

Figure 5.2. 96-well microtiter plate for atrazine-based ELISA assay demonstrating colorimetric change of enzyme-substrate binding.....140

Figure 5.3. ELISA results for tracking atrazine concentration in samples from biofilm effluent and planktonic cell culture. Samples were diluted 1000-fold and inhibition curve was constructed for calibration.....141

Figure 5.4. Atrazine concentration measured by GC-MS over five days in a DFR-grown biofilm (reactor effluent) at incubation temperatures of 30°C (●) and 37°C (■) as a result of microbial degradation.....144

Figure 5.5 Constructed calibration curve of atrazine concentrations ranging from 1.0-50.0 mg L^{-1} and peak area using GC-MS.....145

Figure 6.1. RNA-Seq workflow for *de novo* transcriptome assembly of *Pseudomonas* sp. strain ADP biofilms and planktonic cells.....157

Figure A.1. RNA denaturing gel electrophoresis. RNA ladder (L) is the left-most band. Bands 2,4, and 6 are not DNase treated while bands 1,2, and 3 are DNase treated.....161

Figure B.1. Calibration curve for P.ADP bacterial growth for LB medium using Colony Forming Units per mL and optical density at 600 nm.....162

Figure B.2. Calibration curve for P.ADP bacterial growth for LB medium using Colony Forming Units per mL and optical density at 600 nm.....162

Figure C.1. Nanodrop spectrophotometry graph displaying the spectrum from 220-340 nm at 10 mm absorbance.....164

Figure D.1. The first peak reported from MS: atrazine. The experimental mass spectrum (top) along with the mass spectrum of the library hit for atrazine (bottom) is displayed.....166

Figure D.2. The second peak reported from MS: atrazine. The experimental mass spectrum (top) along with the mass spectrum of the library hit for atrazine (bottom) is displayed.....167

Figure D.3. The second peak reported from MS: atrazine. The experimental mass spectrum (top) along with the mass spectrum of the library hit for s-Triazine, 2-chloro-4,6-bis(ethylamino)- (bottom) is displayed.....168

PREFACE

The following work was carried out in accordance with guidelines set forth by the University of Iowa's Department of Chemical and Biochemical Engineering with more specific goals determined by my advisor, Dr. Tonya Peeples. The broader context of the work aims to further the development of gene expression techniques used for biofilms to systems beyond atrazine remediation. This includes biofilms pervasive in the medical and dental fields, biofilms present in the natural environment, and biofilms manifested as corrosion in industrial settings.

Furthermore, the work presents the everchanging journey of a graduate project. The proposed experiments were often modified and/or appended depending on the goal and specific objectives we set out to achieve and based on early results and findings. The work is split into three core objectives, each representing a different, but vital component of the bioremediation research project. Differentiation of gene expression in *Pseudomonas* sp. ADP cells is a core objective, however, confirmation of these results from a chemical standpoint, and visualization/microscopy aids in yielding a more complete view of the complex degradation occurring in bacterial biofilms.

The ensuing dissertation serves only as a blueprint of the work to come in genetic analysis of degradation genes in *Pseudomonas* sp. ADP biofilms. From a practical standpoint, the purpose of the work is to evaluate the efficiency of bacterial biofilms in environmentally-conscious remediation efforts based on genetics and chemical profiling of an atrazine-degrading strain. It is my pleasure to present my thesis on a special topic in chemical and biochemical engineering.

CHAPTER 1: INTRODUCTION

Project Description

Environmental biotechnology is a vital sector of research in the principal field of chemical and biochemical engineering. The process of degrading chemical pollutants via microbial metabolism, termed bioremediation, is an environmentally conscious alternative to traditional contaminant removal methods.[6] A large body of most research and applications of this technique are centered around the use and dispersal of free-floating or 'planktonic' cells. However, in the natural environment, microbes frequently attach to a surface, proliferate, and secrete a self-produced extracellular matrix of biomolecules, to produce structures called 'biofilms'.[7]

Due to their unique structural and genetic properties, microbes in the biofilm mode of growth are able to survive in periods of stress, attain sustained protection from the surrounding environment, harbor amplified nutrient availability, possess frequent cell-to-cell communication, and exhibit an increased exchange of genetic material.[8] Previous studies on *Pseudomonas* sp. strain ADP biofilms have focused on reactor kinetics and the use of Raman spectroscopy as a tool for differentiation of mode of growth and metabolite identification.[9,10]

In this work, experiments in expression of atrazine-degrading genes and chemical confirmation have been performed to further elucidate the bioremediation capabilities of bacterial biofilms. Furthermore, the development of genetic visualization strategies using confocal microscopy have been explored for application to *Pseudomonas* sp. strain ADP planktonic cells/biofilms, and for extension to alternate model microbes. By completing this work, a better understanding of the

role of biofilms in bioremediation will be greatly illuminated by uncovering genetic and chemical aspects of microbial catabolic processes.

Specific Aims

The purpose of the following work is two-fold: a) to objectively evaluate the efficiency of a biofilm-based bioremediation approach for the model atrazine-degrading bacterium *Pseudomonas* sp. strain ADP, and b) to develop a method for visualizing gene expression that may be applied to the catabolic strain of interest and extended to biofilms across the medical and environmental industries. Additionally, further characterization of the *Pseudomonas* sp. strain ADP biofilm system shall be elucidated using laser scanning confocal microscopy.

Our hypothesis is: Atrazine-degrading genes present in biofilm-mediated cells of bacterium *Pseudomonas* sp. strain ADP will exhibit greater catabolic activity, in the form of increased gene expression, relative to planktonic cells due to the unique properties of bacterial biofilms. The ensuing specific aims were implemented to test our principal hypothesis:

1. Determine the expression of the complete set of atrazine-degrading genes in *Pseudomonas* sp. strain ADP in biofilm-mediated cells relative to planktonic cells.
2. Evaluate kinetics of atrazine-degradation and the strains' metabolites in planktonic cells and biofilm-mediated cells to chemically assess the potential efficiency in bioremediation.
3. Demonstrate further characterization and visualization of *Pseudomonas* sp. strain ADP biofilms using confocal laser scanning microscopy.

Background

Atrazine

By the year 2050, the global population is expected to increase to 9.1 billion people. In order to meet the demand of sustainable food production in the worldwide economy, it is essential to consider the use of herbicides to decrease weed proliferation and subsequently increase crop production.[11] Since 2000, the second-most applied herbicide in the United States is atrazine, only behind glyphosate, with approximately 70 million pounds of the chemical applied annually.[12,13] Atrazine is widely used for the control of broad leaved and grassy weeds to increase yields on crops such as sorghum, maize, and sugarcane.[14] Atrazine (1-Chloro-3-ethylamino-5-isopropylamino-2,4,6-triazine) falls within the triazine class of herbicides based on its structure and mechanism of action. Physically, atrazine appears as a white or colorless crystalline solid. The chemical is slightly soluble in aqueous solutions (34.7 mg L^{-1} at 26^{o}C) and possesses variable solubility in organic solvents (183 g kg^{-1} DMSO, 52 g kg^{-1} chloroform, 28 g kg^{-1} ethyl acetate, and 18 g kg^{-1} methanol at 26^{o}C).[15]

Despite the effectiveness of atrazine as a selective herbicide, the chemical draws national and international concern regarding the risks associated with human and aquatic organismal exposure. The herbicide is classified as an endocrine disruptor compound (EDC), but does not demonstrate compelling evidence as a carcinogenic molecule.[16] Both human and animal studies have established mixed results concerning the carcinogenicity of the chemical compound.[17] However, in certain species of rats, no incidence of breast cancer occurred throughout moderate levels of atrazine exposure.[18] In humans, atrazine revealed to disrupt endocrine function though hypothalamic control of pituitary-ovarian function.[19] The effects of atrazine

exposure on African clawed frogs and marine crabs revealed de-masculinization of male larvae and respiratory distress, respectively. In other aquatic organisms, exposure to the herbicide resulted in genome-wide changes and the generation of reactive oxygen species (ROS).[20–22] Often times, the concentration of the herbicide to present a risk to organismal health is extremely low. In American leopard frogs, atrazine levels as low as 0.1 parts per billion demonstrated induced hermaphroditism and gonadal dysngenesis.[23]

In October 2003, the European Union (EU) banned the use of atrazine due to the pervasive and unpreventable water contamination.[24] In the United States, the Environmental Protection Agency (EPA) limits the concentration of atrazine in drinking water to 0.003 mg L^{-1} (3 parts per billion), which is designated as the maximum contaminant level (MCL).[25] Regardless of regulations set forth by the EPA and other governmental regulatory agencies, the concentration of atrazine is frequently higher in drinking water and groundwater sources. The Natural Resource Defense Council (NRDC) reports, in more than 35,000 samples of drinking water, 80 percent of them were contaminated with atrazine in 2010. In all water systems,100 systems contained atrazine concentrations above the MCL for their high maximum peaks, and six systems contained levels sustained above the maximum contaminant level based on a running annual average. Watersheds monitored by the EPA demonstrated high atrazine spikes (18 of 20 watersheds with levels exceeding 20 ppb), and the Big Blue River watershed in Nebraska exhibited a high maximum peak concentration of 147.65 ppb in May 2008, which lasted for twelve days.[26]

Due to the ubiquitous contamination of atrazine in soil, groundwater, and drinking water, and the potential associated hazards, including damage to the central

nervous system, endocrine system, and immune system, efforts are being made to reduce the concentration of the pollutant in natural water and soil sources.[27] Atrazine is still prevalently used in the United States and Australia as a prolific herbicide to target the growth of grassy and broad-leaved weeds at pre- and post-emergence. Despite its current ban in the EU, atrazine continues to be the 2nd most used herbicide in the world with 90 million pounds applied annually in the U.S. alone. It is therefore vital to reduce the amount of contamination of the chemical in the environment, especially with concerns to the health risks to humans and aquatic wildlife One such method to reduce the concentration of a recalcitrant compound by microbial action is bioremediation.

Bioremediation

An attractive technological process that relies on the use of microbial systems to degrade target pollutants in the environmental industry is termed bioremediation.[28] Traditionally, remediation is done by removal of the contaminated soil to another site or a landfill. The issue concerning this method is the creation of contamination elsewhere, the risks in transport and handling of hazardous material, and the prohibitive costs associated with finding disposal sites. Another alternative approach to remediation is pollutant destruction and/or transformation to non-hazardous substances. Elevated temperature incineration, and chemical decomposition are included in this category of remediation technologies. The major drawbacks of these techniques include expenses, public acceptance, and technical complexity. Bioremediation is an innovative technique that eludes some of the disadvantages associated with traditional remediation technologies, and is significant for its low-technology, low-cost, and environmentally conscious properties.[6]

Strategies in bioremediation range in effectiveness depending on the contaminant, environmental constraints, microbial ecology, and procedure of culture introduction. In addition, bioremediation may be classified as *ex situ* or *in situ,* and further classified by approach within *in situ* technologies: natural attenuation, biostimulation, and bioaugmentation.[29] The treatment of contaminated water and/or soil at its origin is an *in situ* process, whereas the removal of the soil and/or water via excavation or pumping for decontamination is an *ex situ* bioremediation process.[30]

The processes of biostimulation and bioaugmentation demonstrate higher effectiveness than natural attenuation based on the 4-Chloroaniline contaminated soil system. Natural attenuation, the least invasive and controversial method, involves reliance on natural processes to degrade pollutants via biotransformation activity. Biostimulation is the method of adding agents, such as optimal nutrient conditions, to the site of contamination to stimulate the metabolic activity of indigenous microbes. Conversely, bioaugmentation is a process in which microbes are added to the environment at which contamination has occurred for degrading the parent compound. The various *in situ* and *ex situ* strategies vary in effectiveness depending on the method, the pollutant, and microbial system used for decontamination.[31] Common *ex situ* applications of bioremediation include the development of biofilm-based reactors for waste-water treatment. Contaminated water would enter the bioreactor, be treated at a remote location, and the treated water would be re-introduced for human consumption. As for in situ applications of bioremediation, commonly biostimulation and bioaugmentation are employed 'on site' (*in situ*) to remediate the site of contamination. At a chemical spill site, the introduction of microbes capable of metabolizing the pollutant of interest is of great interest to environmental scientists.

A large number of successful strategies for degradation of atrazine have been demonstrated using bacterial-based remediation, mycoremediation, phytoremediation, and plant-microbe association.[27]

Since the 1990s, an assortment or bacterial strains capable of degrading atrazine were isolated independently. Each of the strains catalyze the initial hydrolytic dechlorination of atrazine to yield hydroxyatrazine, which does not possess herbicidal properties nor any known risks to human health.[32] Furthermore, the strain *Agrobacterium radiobacter* J14a degraded atrazine (94%, 50 micrograms) in 72 h in nitrogen-free medium with sucrose and citrate as carbon sources. The metabolites resulting from the strain degradation yielded hydroxyatrazine, deethylatrazine, and deethylhydroxyatrazine.[33]

Similarly, numerous *Rhodococcus* strains screened for their ability to degrade atrazine demonstrated catabolic activity and the appearance of metabolites from s-triazines including simazine, propazine, cyanazine, and atrazine under aerobic conditions.[34] The model bacterium for atrazine degradation, *Pseudomonas* sp. strain ADP, was isolated from an atrazine spill site in rural Minnesota and revealed high catabolic activity in the presence of the herbicide.[1]

Pseudomonas sp. strain ADP

The bacterium *Pseudomonas* sp. strain ADP (P.ADP, obtained from Deutsche Sammlung von Mikroorganismen und Zellkulturen) was first identified and isolated in 1995 by Mandlebaum, Allan, and Wackett from a herbicide spill site in rural Minnesota. The strain was isolated upon advanced sub-culturing and was revealed to be a novel bacterial strain most closely related to *Pseudomonas citronellosis* as evidenced by 96.1% identity match of 16s rRNA sequences and high similarity in Biolog biochemical

tests.[35] The strain demonstrated an amplified amount of clearing zones on indicator plates containing 1000 parts per million of atrazine from 48 h (Figure 1.1A) to 72 h (Figure 1.1B) following inoculation.[35]

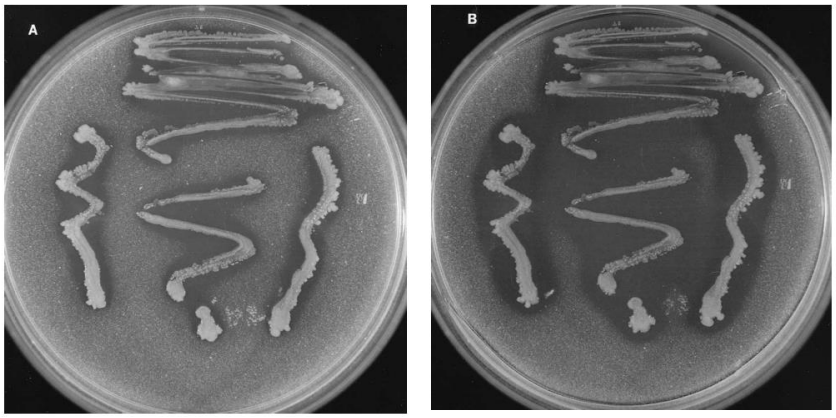

Figure 1.1. Indicator plates containing atrazine demonstrate moderate clearing zones 48 h after inoculation (A) surrounding areas of bacterial streaking, and substantial clearing zones 72 h following initial inoculation of *Pseudomonas* sp. ADP (B).[30]

In liquid medium, C-14 ring-labeled atrazine (100 parts per million) was used to measure the timescale of metabolic atrazine degradation by *Pseudomonas* sp. strain ADP. Boiled cells were used as a negative control to eliminate the possibility of confounding variables in atrazine degradation. Atrazine was completely metabolized 25 h from the point of inoculation as measured by scintillation counting (Figure 1.2).[35] All genes encoding for the metabolic degradation of atrazine were determined to be located on a single 108 kilo base pair catabolic plasmid, pADP-1. Additionally, the complete nucleotide sequence of pADP-1 in *Pseudomonas* sp. strain ADP was determined (Figure 1.3).[2] One potential problem in the use of the catabolic strain in bioremediation applications is *Pseudomonas* sp. strain ADP's affinity for alternate nitrogen sources that support rapid growth in the presence of atrazine. The rate of atrazine degradation decreases in the cells in nitrogen-limited conditions, and the presence of atrazine in addition to alternate nitrogen sources does not stimulate

degradation. For the bacterial strain to overcome this limitation of nitrogen repression in the catabolic pathway, select mutant variants may be used to maintain or increase the rate of atrazine degradation.[36] It was established that the enzyme atrazine chlorohydrolase, encoded by the gene *AtzA*, has a homologous sequence and broad substrate specificity across multiple atrazine-degrading strains.[37] This enzyme catalyzes the initial biotransformation of atrazine to yield hydroxyatrazine, an innocuous and non-herbicidal chemical compound. The six-step catabolic pathway to complete the biotransformation from atrazine to carbon dioxide and ammonia was discovered and illuminated the role of the enzymes and aspects of gene expression in *Pseudomonas* sp. ADP.[3]

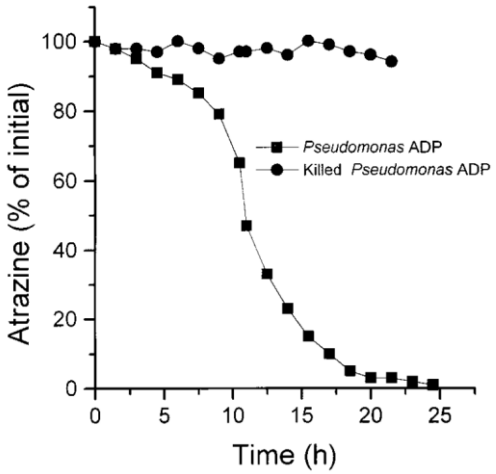

Figure 1.2. Atrazine (100 mg L^{-1}) was completely degraded by *Pseudomonas* sp. strain ADP cells after 25 h as measured by radioactivity of c-14 ring labeled atrazine and scintillation counting. Boiled cells were used as a negative control.[1]

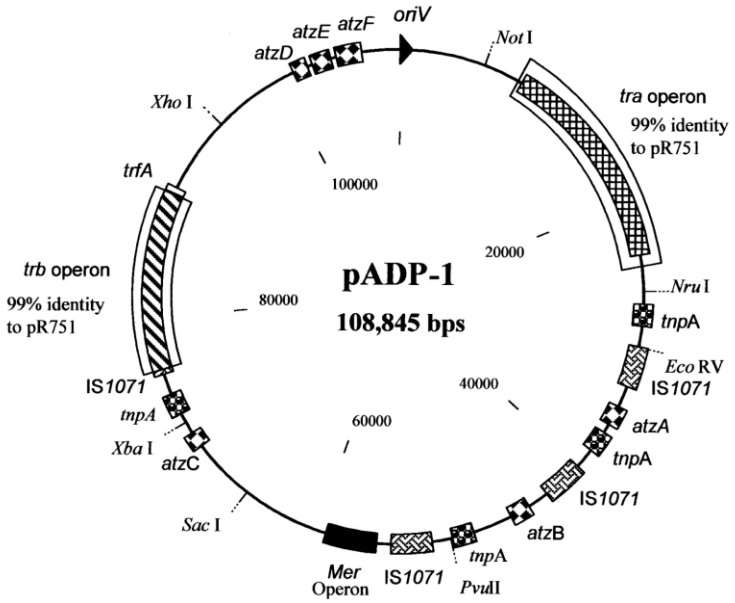

Figure 1.3. The 108-kb self-transmissible plasmid, pADP-1, containing all six genes encoding for atrazine-degradation isolated from *Pseudomonas* sp. strain ADP.[2]

Catabolic pathway for degradation

All six genes encoding for the degradation of atrazine are located on the large catabolic plasmid, pADP-1. The catabolic plasmid pADP-1 is self-transmissible as evidenced by mating experiments with *Escherichia coli*. The genes *AtzABC* encode for the enzymes which catalyze the biotransformation from atrazine to cyanuric acid.[37–40] The remainder of the genes catalyze the remainder of the biotransformation from cyanuric acid to ammonia and carbon dioxide.

Initially, atrazine undergoes a hydrolytic dechlorination by enzyme AtzA to yield hydroxyatrazine. Following, enzymes AtzB and AtzC perform two subsequent deamidations to form N-isopropylammelide and cyanuric acid, respectively. The ring opening of cyanuric acid is catalyzed by AtzD to form biuret. The last two steps of the degradation pathway involve enzymes AtzE and AtzF, which yield allophanate, and mineralization products, respectively. Each of the six enzymes are encoded by

corresponding genes, *AtzA-AtzF*. As formerly specified, all atrazine-degradation genes are located on the catabolic plasmid, pADP-1.[1,3,27,37,40,41] (Figure 1.4)

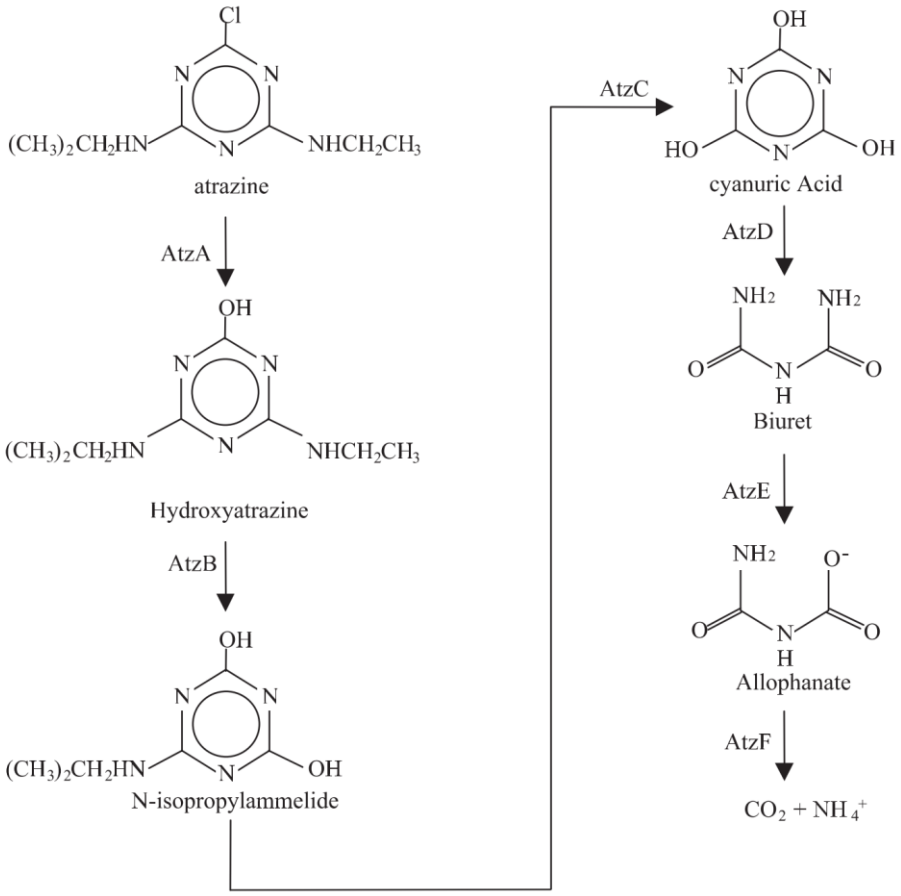

Figure 1.4. The complete catabolic pathway of atrazine taken by *Pseudomonas* sp. strain ADP, involving enzymes AtzA-AtzF.[3]

Genes *AtzABC* are constitutively expressed and dispersed throughout the catabolic plasmid, while genes *AtzDEF* are clustered on a strongly regulated operon. The first three genes are relatively spread out by a 47-kb region, with 8-kb from *AtzA* to *AtzB*, and a distance of 25-kb from *AtzB* to *AtzC*. Additionally, the plasmid pADP-1 contains a mercury resistance operon, *Mer*, which is used a selective marker and is able to detoxify any presence of mercury. [36,41,42] These dispersed genes are comparatively unstable on pADP-1 and may be lost in the absence of selection pressure with atrazine as a sole nitrogen source. This would produce strains incapable

of the initial biotransformation step (Atr-). The latter set of genes, conversely, are stable on the pADP-1 plasmid and are not spontaneously lost. However, the absence of selection pressure the strain may trigger a the plasmid pADP-1 to be lost, in which the strain would no longer be able to degrade atrazine or its metabolites (Cya-).[38]

The remaining catabolic genes *AtzDEF*, encoding for the enzymatic biotransformation from cyanuric acid to ammonia and carbon dioxide, are subjected to dual regulation in response to nitrogen limitation and cyanuric acid. The cyanuric acid degradation operon could be subject to general nitrogen control based on the LysR regulator.[43] Until recently, in *Pseudomonas* sp. strain ADP and other atrazine-degrading bacteria, urease was assumed to function as the enzyme in the catabolic pathway from cyanuric acid. However, the presence of enzyme allophanate hydrolase and the appearance and subsequent isolation of allophanate as the metabolite following cyanuric acid degradation validated the absence of urease and urea.[44]

Recent advances have further developed methods for detecting of metabolites in the catabolic pathway of *Pseudomonas* sp. strain ADP. Henry et al. evaluated the use of Raman spectroscopy as a tool to measure the concentration of pure metabolites and metabolites from active degradation processes of atrazine. Furthermore, Henry successfully developed a method to differentiate planktonic (free-floating) *Pseudomonas* sp. strain ADP cells from biofilm-mediated cells based on signals from the extracellular polymeric substances (EPS) matrix.[9]

Biofilms

Biofilms are assemblages of microbes attached to an abiotic or biotic surface that secrete a self-produced extracellular (EPS) matrix consisting of water, polysaccharides, proteins, and other biological macromolecules.[45] The presence of a

complex matrix in which the microbes reside along with intracellular interactions distinguish the mode of growth from planktonic, or free-floating cells. Despite the ubiquity of surface-associated biofilms, cells in this mode of growth are able to mobilize in 'flocs' in which the substratum is absent.[7] The focus of most research in the fields of biochemistry, molecular biology, and biochemical engineering have been focused on pure, planktonic cultures. However, it is now known that most microbes in industrial, clinical, and natural settings are in the biofilm mode of growth.[46]

Biofilms are the predominant form of growth in the natural environment, and the preferred mode of growth for prokaryotes due to optimum positioning regarding available nutrients and an advantageous strategy for microbial survival. Natural aquatic environments, medical biomaterials (e.g., intravenous catheters, sutures, wound drainage tubes, & hemodialysis buttons), teeth manifested as dental plaque, and in the food processing industry are a few of the common environments in which biofilms are prevalent.[47,48] In most industries, biofilms harbor a negative impact due to their invasive and resistant nature. However, in the field of environmental biotechnology, biofilms are of great interest for use in bioremediation. This is due to their unique physical and genetic characteristics which may substantially enhance the efficiency of contaminant remediation compared to their planktonic counterparts in both *in situ* and *ex situ* pollution circumstances. Despite their complexity and differentiation at maturity, the development of biofilms begins with growth of planktonic, free-floating cells.

The stages of biofilm development include five distinct stages: (1) initial attachment, (2) irreversible attachment, (3) maturation I, (4) maturation II, and (5) dispersion (Figure 1.5).[4] Cell-to-cell communication has demonstrated to play a major

role in biofilm development and maturation.[49] Initially, the microbes attach to a substratum (e.g., glass, blood, polymers) in a manner which is reversible, i.e., the cells are able to easily detach. The second stage involves irreversible attachment, in which the planktonic microbes adhere strongly to the surface, or substratum. Stages (3) and (4) consist largely of biofilm maturation. In these stages, the bacterial colonies, with aid of quorum sensing, secrete extracellular polymeric substances (EPS) to form an enclosed matrix. The matrix, largely consisting of biological macromolecules and water, encapsulates the microbes which aids in survival and protection from outside stressors. Once the biofilm has completely matured, microbes in the biofilm begin to disperse in the final stage. The dispersed biomass is then able to colonize a surface at a proximate location.[46] Biofilms, particularly when mature, are able to provide environmental benefits as they are explored as communities for use in bioremediation of pollutants.[8,46]

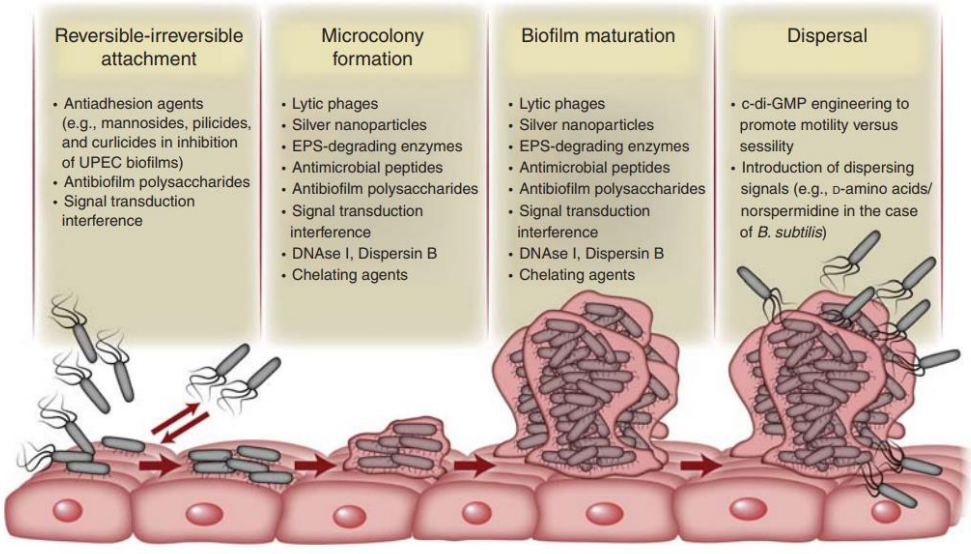

Figure 1.5. Biofilms are characterized by four to five sequential stages of development from planktonic cells. These include reversible attachment, irreversible attachment, maturation I / microcolony formation, maturation II, and dispersal/dispersion.[4]

Due to the ubiquity of persistent pollutants continually being created and disposed, it has become vital to search for more efficient strategies in bioremediation. Low activity and abundance, along with nutrient limitations, has stalled planktonic-based bioremediation efforts and novel research with respect to atrazine contamination. Some clear advantages of employing biofilms in bioremediation research include increased genetic and nutrient exchange, protection from the outside environment due to the presence of an EPS matrix (e.g., chemical stresses, predation, shear stress), and ability to entrap pollutants due to the biofilm's beneficial structure.[8,28,50,51] Additionally, cells in a biofilm have increased odds of adaptation. The accelerated use of xenobiotics and consequently immobilization and degradation of target pollutants, due to the close physiological interactions among organisms within a biofilm, is another distinct advantage of biofilms compared to planktonic, free-floating cells.[50]

Prior research focused on *Pseudomonas* sp. strain ADP biofilms concerned degradation kinetics and the ability to use Raman as an analytical tool for monitoring atrazine degradation.[9,10] The characterization of *Pseudomonas* sp. strain biofilms is essential for moving forward in application of biofilms in bioremediation of atrazine. One method of analyzing the active degradation of atrazine and pathway enzymes past the surface level of physio-chemical interactions is by utilizing techniques in molecular biology to explore gene expression.

Gene expression

Devers, De Souza, and Solomon have studied the expression of atrazine-degrading genes in planktonic *Pseudomonas* sp. strain ADP as a means of evaluating bacterial catabolic processes and to understand their role in bioremediation .[3,52,53]

Despite extensive work regarding cloning, characterization, and gene expression analyses on the model strain under various conditions, gene expression analyses on *Pseudomonas* sp. strain ADP biofilms is relatively unexplored.

The objective of studying gene expression is to gather insight into the genetic level of bacterial catabolic processes. Understanding the metabolism of bacteria, with persistent xenobiotics as a substrate, allows researchers to evaluate the effectiveness of remediation strategies from an intimate position. Once the genetic and chemical based information is evaluated with respect to biodegradation efficiency, engineers and research scientists are able to apply the results to technology development in the field of environmental biotech. The primary method of evaluating gene expression with a limited number of genes is real-time quantitative reverse transcription polymerase chain reaction (RT-qPCR).[54]

Analysis of gene expression can be divided into two categories: visual and non-visual. Non-visual methodology largely consists of destructive, quantitative techniques such as RT-qPCR, RNA-seq, DNA microarrays, and northern blotting. Conversely, visual methods in gene expression analysis are based primarily on the aid of microscopy and non-destructive: fluorescent in situ hybridization (FISH), in situ reverse transcription (ISRT), green fluorescent protein (GFP), red fluorescent protein (RFP) fusions, and antibody labeling. Laser scanning confocal microscopy (CLSM) and scanning electron microscopy (SEM) are the aids with respect to visual gene expression analysis. Essential studies by Devers et al. explored the use of RT-qPCR on atrazine-degrading genes in *Pseudomonas* sp. ADP planktonic cells.[3]

An RT-qPCR protocol was developed to analyze the expression of all atrazine-degrading genes in *Pseudomonas* sp. strain ADP free-cells. The complete set of genes

were basally expressed without any atrazine treatment. However, genes *AtzA*, *AtzB*, and *AtzC* were all upregulated in response to 55 mg L^{-1} of atrazine within growth medium at approximately 200 min. The expression of *AtzD* and *AtzE* demonstrated slight upregulation downstream at 300 min, while expression of *AtzF* was relatively unchanged in the presence or absence of atrazine (Figure 1.6).[3] These results corroborate Martinez's findings on the relative disparate location of the first three and remaining three genes on the catabolic plasmid.[2] Studies on genetic regulatory elements and the expression of planktonic cells in response to cyanuric acid treatment in certain conditions has been performed on the strain of interest.[53,55]

The comparison of biofilm and free-cell communities has yielded interesting results about alternate bacterial strains. For illustration, expression patterns were largely differentiated in *Staphylococcus aureus* and *Salmonella tymphimurium* by mode of growth in various growth media and pH conditions.[56] In strains with environmental significance, the model strain for toluene degradation *Pseudomonas putida* demonstrated growth phase dependent expression of catabolic genes.[57] RNA-seq, an emerging technology, is frequently used to differentiate expression of the entire transcriptome in two states, such as biofilm-mediated cells relative to free cells.[58]

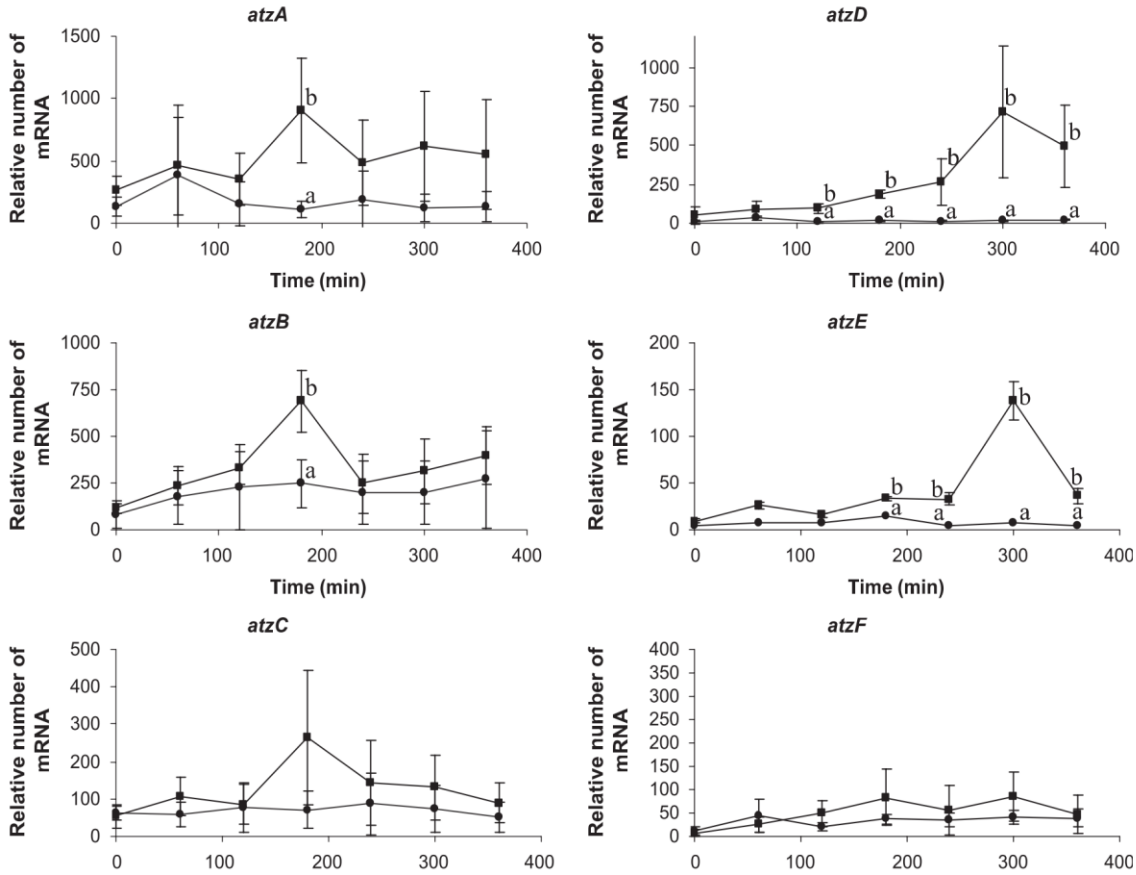

Figure 1.6. Expression of the complete set of atrazine-degrading genes in *Pseudomonas* sp. strain ADP planktonic cells in response to (A) no atrazine (circles) and (B) atrazine at 55 mg L^{-1} (squares) over a timescale of 400 min. Values identified with a different letter at each sampling point differ significantly at $p<0.05$ as a result of Fisher's test between *atz* transcripts of control and atrazine-treated conditions.[3]

In Situ Reverse Transcription (ISRT) is a visual gene expression method that has been successfully developed, optimized, and applied to toluene-degrading *Pseudomonas putida*.[59,60] The method was used to detect mRNA of the *todCI* gene in *P. putida* F1 cells using this highly specific and sensitive technique (Figure 1.7). One potential drawback regarding ISRT is the optimization required in sample preparation for each bacterial strain.

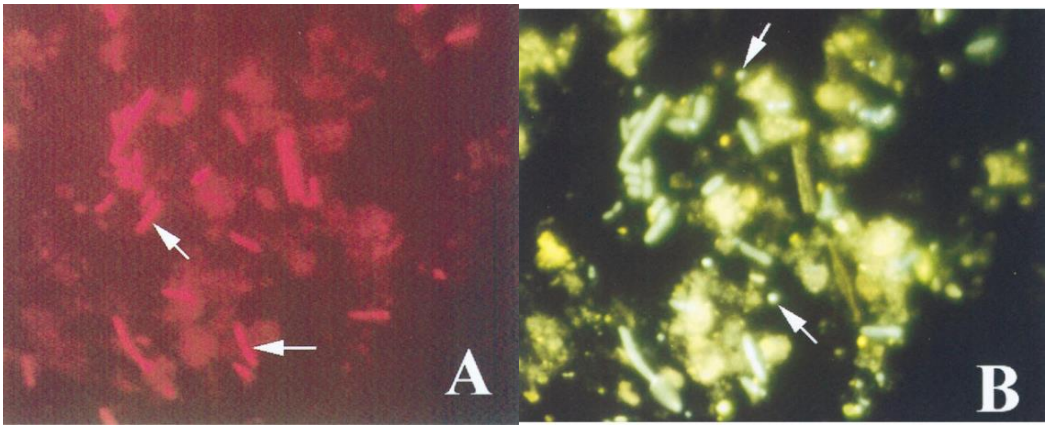

Figure 1.7. Expression of todC1 gene in *Pseudomonas putida* F1 cells by In Situ Reverse Transcription (ISRT), (A) Red fluorescent cells are expressing todC1 (arrows are positive cells), (B) DAPI counterstaining (arrows are negative cells) to view whole community.[59]

Due to such difficulties regarding optimization of ISRT for bacterial biofilms, other methods including antibody labeling, fluorescent protein fusions, and fluorescent in situ hybridization (FISH) are often considered to achieve comparable goals. Regardless, both visual and non-visual gene expression methods are frequently complimentary in nature and provide a more complete understanding of the genetics of environmentally-relevant bacterial biofilms.

Addressed research gaps

There is an overabundance of research performed on the model atrazine-degrading bacterium *Pseudomonas* sp. strain ADP in the planktonic mode of growth. Wackett, Sadowsky, Martinez, Mandelbaum, Devers, De Souza, and Garcia-Gonzalez have contributed greatly to furthering our understanding and knowledge of planktonic *Pseudomonas* sp. strain ADP with respect to discovery, gene expression, gene regulation, cloning, and metabolomics.[1,3,36,40,43,52] Despite extensive research on the planktonic form, there is much to be studied on biofilm-mediated *Pseudomonas* sp. strain ADP cells.

Biglione evaluated degradation rates, yields, and Monod kinetics of the strain grown in different bioreactors and shake flasks with varied shaking speed and temperature.[10] Following, Henry applied Raman spectroscopy as an analytical tool to quantify atrazine and its metabolites in *Pseudomonas* sp. strain ADP free-cells and biofilms. The extracellular polymeric substances were successfully differentiated by Raman fingerprints to demonstrate the significance of the EPS in biofilm-mediated cells compared to free-cells.[9] Though a noteworthy amount of work has been performed on characterization on *Pseudomonas* sp. strain ADP biofilms, no studies have illuminated the strains' catabolic activity on atrazine degradation at the genetic level. Additionally, no comprehensive study has been performed analyzing the biodegradation of atrazine and its metabolites in free-cells compared the biodegradation of atrazine and its metabolites in biofilms. This is vital, as it would provide a direct comparison of a flow vs. batch system and their respective efficiencies on a bioremediation system.

Lastly, the development of novel tools in gene expression and microscopy would be crucial for: a) expanding the use of the method to biofilms across other disciplines, including medical technology, dentistry, and the food industry, and b) application of visual gene expression methods for application of monitoring pollutants real-time in biofilm-based systems for *in situ* bioremediation. To address this gap, the following dissertation explores methods and optimization in In Situ Reverse Transcription (ISRT), red/green fluorescent protein fusions (RFP), and fluorescent lectin binding analysis (FLBA). The last method would allow further characterization of sugar moieties involved in *Pseudomonas* sp. strain ADP biofilm formation, rather than aid in development of a novel visual gene expression technique.[61]

In the following work, the above gaps are thoroughly addressed. In Chapter 2, the growth rates of *Pseudomonas* sp. strain ADP under various nutrient conditions is performed to set the baseline for the remainder of experiments. Furthermore, total ribonucleic acid extraction from *Pseudomonas* sp. strain ADP biofilms is optimized via a design of experiments (DOE) approach for both quality and quantity considerations. Chapter 3 dives into work involving differentiation of expression in atrazine-degrading genes based on RT-qPCR experiments. Free-cells and biofilm mediated cells, along with differentiation based on biofilm growth temperature have been analyzed. In Chapter 4, an ISRT procedure was attempted for optimization in biofilms and visualization of atrazine-degrading genes with the aid of confocal microscopy. Antibiotics were tested for use in GFP/RFP fusion experiments, and FLBA was successfully used to evaluate the diversity of monomers in *Pseudomonas* sp. ADP biofilms based on growth media. Finally, atrazine degradation and its metabolites were quantified in biofilms and free-cells based on analytical chemistry methods (GC and HPLC) to gauge biodegradation efficiency by mode of growth in Chapter 5. Future prospective work in environmental biotechnology, specifically with regards to: bioremediation, biofilms, and characterization of the atrazine-degrading strain *Pseudomonas* sp. ADP, is explored in the last chapter.

CHAPTER 2: GROWTH OF *PSEUDOMONAS* SP. STRAIN ADP AND OPTIMIZATION OF RNA EXTRACTION FROM BIOFILMS

Introduction

The model atrazine-degrading bacterium *Pseudomonas* sp. strain ADP (P.ADP) possesses great variability in growth dependent upon nutrient concentration, temperature, shaking speed, pH, ion/salt concentration, and water content. It was demonstrated the variability in P.ADP growth in a fed-batch culture in a cyanuric acid limited medium in concentrations of the nitrogen source ranging from 0-100 μM.[55] In experiments focused on fluctuating the presence and concentration of a glutamine synthase inhibitor (MSX), the growth medium identity (ammonium compared to nitrate) had a significant effect on the growth rate of P.ADP in a relatively short timeframe from 0-25 h and 0-15 h. It was then confirmed erraticism in growth curves by utilizing a Monod kinetic model, and varied several factors including the initial atrazine concentration, reactor type, temperature, and agitation speed.[10,114]

The purpose of establishing a growth curve with a specified set of conditions prior to further experimentation sets the stage for consistency and prevention of erroneous conclusions. Furthermore, the relative growth rate based on optical density at 600 nm (OD_{600}) and consequently CFUs can be determined by a standard curve. Establishing growth curves based upon the medium to be used at experimental conditions allows for extraction of parameters such as time at mid-exponential phase and doubling time. The former parameter, time at mid-exponential phase, is vital because cells are generally healthiest and most uniform in the exponential growth phase as indicated by the growth curve. Experiments downstream rely on halting growth or extraction of nucleic acids once the exponential phase is determined.

Downstream experiments, including gene expression experiments relying on nucleic acid extractions are of upmost importance to harvest at mid-exponential phase.

Gene expression experiments based on the method of RT-qPCR follow a general workflow: cellular growth and proliferation, RNA extraction, RNA quality control, cDNA synthesis, real-time PCR, and data analysis.[54,62] Due to the presence of the extracellular polymeric substances in a bacterial biofilm's matrix, microbes within the biofilm are often difficult to lyse and may contain inhibitory substances. Interference from the EPS may greatly reduce the quantity and quality of RNA extracted from biofilms by use of traditional methods (e.g. organic solvent based and spin column kits) for qPCR.[64,65,75] Sonication, additional washes with phosphate buffered saline, liquid nitrogen, phase separation gels, and combinatory extraction methods are some of the factors that may affect both the quantity and quality of total RNA extracted from *Pseudomonas* sp. strain ADP biofilms. Once the RNA is extracted, the nucleic acid may be analyzed with gel capillary electrophoresis and micro-spectrophotometry for quality and use for subsequent steps in the RT-qPCR workflow.[75,122]

The overarching objective of optimizing the RNA extraction process is to ensure consistency in gene expression results from qPCR analysis. A robust extraction method would allow for high quality cDNA synthesis and subsequent qPCR. The gene expression experiments provide an understanding of the catabolic pathway in *Pseudomonas* sp. strain ADP biofilms and give insight into the mechanism of remediation action (e.g. entrapment of compound in EPS matrix of biofilm, active degradation, or an amalgamation) and the overall biodegradation efficiency of bacterial biofilms.

Materials and Methods

Bacterial strain and reagents

Pseudomonas sp. strain ADP was generously provided by Dr. Lawrence Wackett (Minneapolis, Minnesota) and stored at -80°C in Lysogeny Broth (LB) with 50% (v/v) glycerol to protect cells in cryogenic conditions. *Escherichia coli* DH5α cells were purchased from Life Technologies (Carlsbad, California) and stored in the same conditions as *Pseudomonas* sp. strain ADP cells. LB capsules, ammonium nitrate, and glycerol were purchased from Sigma Aldrich (St. Louis, Missouri). Atrazine was generously provided by Monsanto (St. Louis, Missouri) and D-glucose was purchased from Research Products International (Mount Prospect, Illinois). TRIZOL reagent and RNeasy Kit were purchase from Thermo Fisher Scientific (Waltham, Massachusetts) and Qiagen (Hilden, Germany), respectively. Phase Lock Gels for aid in nucleic acid extraction were purchased from VWR (Radnor, Pennsylvania).

Culture media

Leibniz Institut Deutsche Sammlung von Mikroorganisnmen und Zulkulturen GmbhH (DSMZ) adapted medium was used as a minimal medium for growth of *Pseudomonas* sp. strain ADP with the addition atrazine as a sole nitrogen source and glucose as a sole carbon source. Trace element solution SL-6 consisted of $ZnSO_4 \cdot 7H_2O$ (0.10 g L^{-1}), $MnCl_2 \cdot 4H_2O$ (0.03 g L^{-1}), H_3BO_3 (0.30 g L^{-1}), $CoCl_2 \cdot 6H_2O$ (0.2 g L^{-1}), $CuCl_2 \cdot 2H_2O$ (0.01 g L^{-1}), $NiCl_2 \cdot 6H_2O$ (0.02 g L^{-1}), and $Na_2MoO_4 \cdot 2H_2O$ (0.03 g L-1) in distilled water. Trace element solution SL-4 consisted of EDTA (0.50 g L^{-1}), $FeSO_4 \cdot 7H_2O$ (0.20 g L^{-1}), SL-6 (100 mL), and distilled water (900 mL). The mineral medium, adjusted to a pH of 7.25 contained $Na_2HPO_4 \cdot 2H_2O$ (3.50 g L^{-1}), KH_2PO_4 (1.00 g L^{-1}), $MgCl_2 \cdot 6H_2O$ (0.10 g), $CaCl_2$ (0.05 g), SL-4 (1.00 mL L^{-1}), and distilled

water. Atrazine (2-chloro-4(ethylamino)-6-(isopropylamino)-1,3,5-triazine) was suspended in methanol (10 mg mL^{-1}) and briefly sonicated to reduce particle size. Once mineral medium was autoclaved at 121°C, 15 Bar, for 20 min and cooled, stock suspension of atrazine was added to a final concentration of 30 mg L^{-1} atrazine in 2L of mineral medium. The carbon source, d-glucose, was added at a concentration of 1 g L^{-1} from a concentration stock of 100 g L^{-1} in distilled, deionized water. The final concentration of atrazine in all experiments ranged from 30 mg L^{-1} to 100 mg L^{-1}, based on the addition of stock suspension in final source of minimal medium. The above medium will be referred to as DSMZ in the following work.

Lysogeny Broth (LB), a complex medium, was used as a nutritionally-rich source of growth medium for P.ADP cells. LB was prepared from tryptone (10 g L^{-1}), sodium chloride (10 g L^{-1}), yeast extract (5 g L^{-1}), and distilled water. The medium was autoclaved at 121°C, 15 Bar, for 20 min prior to refrigeration and storage.

DSZM with ammonium nitrate, a relatively rich source of nitrogen for bacteria, was substituted for atrazine at the same concentration. The biologics, including phosphate salts, SL-4, SL-6, and glucose as a carbon source, remained unchanged. This medium was used as an intermediate for P.ADP between LB and DSMZ. Additionally, TY medium was formulated for constructing a calibration curve. TY medium consisted of Bacto-tryptone (10 g L^{-1}), sodium chloride (10 g L^{-1}), and yeast extract (5 g L^{-1}) in distilled water.

The above medium will be referred to as ammonium nitrate medium in the following work. All the above media contains a source of carbon and nitrogen for sufficient bacterial growth of *Pseudomonas* sp. strain ADP planktonic cells.

Planktonic cell preparation

A frozen stock of P.ADP (-80°C) was retrieved and subsequently thawed aseptically. Frozen stock was thawed at room temperature in biosafety cabinet for approximately five minutes, and vortexed prior to streaking. The cells were streaked onto agar plates containing i) LB, ii) DSMZ, and iii) ammonium nitrate in triplicate. Plates were incubated at 30°C overnight. Once growth was readily observed on each streak plate, a few small colonies were inoculated in liquid culture (10 mL) of the same medium in a 50 mL Erlenmeyer flask in an aseptic manner. Liquid cultures were incubated and shaken overnight at 30°C and 250 rpm, respectively.

Bacterial calibration for growth

Spread plates were prepared in triplicate for *Pseudomonas* sp. strain ADP on i) LB and ii) TY nutrient-rich medium. For each plate, 1 mL of log phase liquid culture from each respective medium was retrieved and dispensed on a plate. The culture was spread evenly across the plate containing solid medium of the same nature. Due to the high concentration of bacteria in culture, serial dilutions were made (1:10 x 8) for more attainable and accurate counts of colony forming units (CFU). Plates were incubated overnight at 30°C and observed for CFUs the following day. The spread plate containing between 10-50 CFUs was used for measurement, and the total CFUs from the parent cell culture was calculated. This was repeated at numerous phases in the cellular growth curve for the parent liquid culture to form a calibration curve between optical density and CFUs. At each sectioned interval, the optical density at 600 nm (OD_{600}) was measured via spectrophotometry (Thermo Fisher BioMate 3s Spectrophotometer, Waltham, Massachusetts) and correlated to the CFUs of a specific spread plate. Blank samples used for OD_{600} quantification were measured in

triplicate and consisted of growth medium (DSMZ medium containing 30 mg L^{-1} atrazine) without cells. The OD_{600} values were determined relative to blank medium, and each liquid cell culture was diluted to an OD_{600} of 0.05 with each medium in a 250 mL Erlenmeyer flask

Construction of P.ADP growth curves

Once a calibration curve has been constructed, the relative number of CFUs and OD_{600} is related by a linear equation as demonstrated in the results. P.ADP cells in each growth medium (LB, DSMZ, and ammonium nitrate) were measured for cell growth indirectly by spectrophotometry. The following experiments were all performed in triplicate and the methodology is outlined in Figure 2.1. A sample of 1 mL was retrieved immediately upon dilution and measured in a cuvette spectrophotometrically. All cell cultures were incubated at 30°C and shaken at 250 rpm.

Samples were retrieved for measurement every hour for approximately 30-40 h. If additional samples were taken past 40 h, intervals were increased to capture extended stationary and death phase of cells. Samples measuring greater than 0.5 OD_{600} were diluted 1:10 in growth medium and re-measured. The re-measured values were then calculated to reflect the original culture to ensure accuracy. This step was essential to prevent erroneous spectrophotometric values exceeding the instrument's upper limit of detection. Essential parameters, including specific growth rate, doubling time, and time at mid-exponential phase, were extracted from each curve. Growth curves were constructed for *Pseudomonas* sp. strain ADP cells with a) DSZM containing 50 mg L^{-1} atrazine b) DSMZ containing 100 mg L^{-1} atrazine, c) LB, and d) ammonium nitrate.

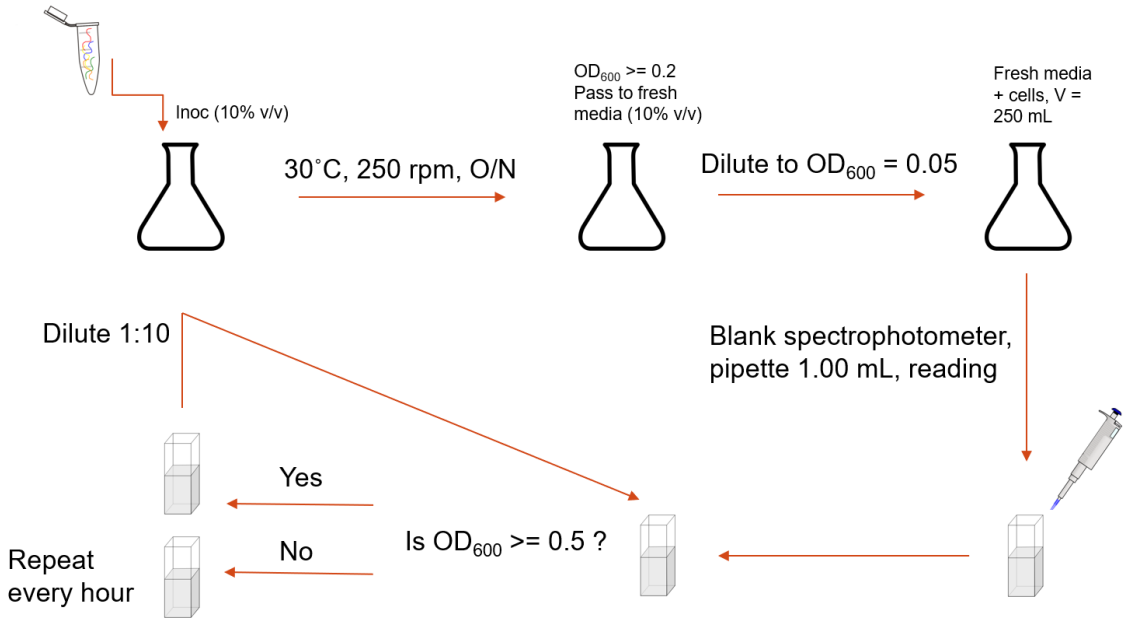

Figure 2.1. Methodology of constructing bacterial growth curve of *Pseudomonas* sp. strain ADP on various growth media using spectrophotometry. Initial cells are retrieved from a streak plate; however, cells may be retrieved from frozen P.ADP stock if there is no known contamination.

RNA extraction from P.ADP planktonic cells

Total Ribonucleic acids (RNAA) from *Pseudomonas* sp. strain ADP free-cells were extracted using the RNeasy Mini Kit following the manufacturer's instructions with additional modifications. Briefly, P.ADP cells in DSMZ containing atrazine reached mid-exponential phase, based on previous growth curve data, and were suspended in a lysozyme/TE mixture (100 µL). Cells were thoroughly mixed, vortexed for 10 s, and shaken in an incubator at 175 rpm at 30°C for 10 min. Buffer RLT mix (350 µL), containing β-mercaptoethanol, was added to cell mixture and vortexed vigorously. Ethanol (100%, 250 µL) was added to lysate, and mixed by pipetting. The mixture (750 µL) was transferred to a spin0column, centrifuged for 15 s at 8000 x g, and the flow-through was discarded. Buffer RW1 (350 µL) was added to the RNeasy column, centrifuged for 15 s at 8000 x g, and the flow through was discarded. Sample was then treated with DNAse following the manufacturer's instructions

(RNase free DNAse set, Qiagen, Hilden, Germany). Buffer RW1 (350 µL) was added to the spin-column, centrifuged for 15 s at 8000 x g, and the flow through was discarded. RPE (500 µL), containing ethanol, was added to the spin-column, centrifuged at 8000 x g, with the flow through discarded. This was performed twice, at 15 s and 120 s. The sample was transferred to a 1.5 mL collection tube, and RNAse-free water (50 µL) was dispensed to elute the RNA. The sample was centrifuged for 60 s at 8000 x g. The sample was transferred to a sterile, 0.5 mL tube for analysis of quantity and quality.

All extracted RNA samples were subjected to micro-spectrophotometry (NanoDrop 8000 Spectrophotometer, Thermo Fischer, Waltham, Massachusetts) for initial quantification of total RNA prior to capillary gel electrophoresis for integrity. Sample of RNA was briefly vortexed, and 3 µL of sample was dispensed onto the surface of the instrument. The spectrophotometric curve, 260/280 Ratio, and 260/230 Ratio were measured to assess purity and approximate quantity. Nucleic acids, both RNA and DNA, have absorbance maxima at 260 nm. The ratio of this absorbance maxima to two other wavelengths, 280 nm and 230 nm, are used as a quantitative measure of purity. Ideal 260/280 and 260/230 ratios for RNA hover around 1.8 and 2.0, respectively. Abnormal values may signify contamination or lower quality RNA. It is vital to use pure RNA for reverse transcription and subsequent qPCR applications. Contaminating DNA is exhibited from spectrophotometry, and is difficult to distinguish without additional methods, such as capillary gel electrophoresis. If quantity measured is higher than 50 ng μL^{-1}, sample is subjected to capillary gel electrophoresis (Agilent Genomics, 2100 Bioanalyzer, Santa Clara, California) to assess quality through an RNA integrity number (RIN). The RNA integrity

number is a value assigned to RNA samples calculated from an algorithm to assess the quality of a sample. The value is based on a computational model using Bayesian learning to generate an algorithm that would accurate assess nucleic acid integrity.[56] Samples with a RIN greater than 8.0 were used for downstream processes in the RT-qPCR workflow. Samples with a RIN less than 8.0 were discarded from further modification and analysis.

Preparation for P.ADP biofilm growth in DFR

Suspended *Pseudomonas* sp. strain ADP cells were harvested from shake flasks in mid-exponential phase when optical density reached 0.3 AU. If culture did not reach OD_{600} = 0.3 AU, the suspension was concentrated to achieve the desired cellular density. The bacterial culture (50 mL) was transferred to centrifuge tubes and centrifuged at 10,000 x g for 10 min at -4°C to pellet cells in quadruplicate. Supernatant from suspension was collectively discarded in biological waste, leaving only the cell pellet. Pellets were re-suspended in fresh DSMZ containing 30 mg L^{-1} atrazine (10 mL) and vortexed thoroughly for 10 s. Prior to dispensing concentrated cell culture on microscope slides within the drip-flow reactor (DFR), the biofilm growth apparatus was sterilized to prevent contamination.

Construction of DFR for biofilm growth

The bioreactor used for biofilm growth consisted of a drip-flow reactor (Figure 2.2) connected to an influent and effluent port, with aid of two peristaltic pumps and tubing. The drip flow reactor is comprised of a polycarbonate base with four chambers capable of containing four Silane-coated microscope slides. The lid covered all chambers with metal twists to secure the bottoms, septa to allow for influent, and air vents to prevent pressurization of the bioreactor.

Figure 2.2. Four-chamber polycarbonate drip-flow reactor with septa and filter units used for growth of P.ADP biofilms.[5,9]

The dimensions of the DFR are 10 cm x 2.5 cm x 2 cm and the dimensions of each Silane-coated microscope slide inserted are 75 mm x 25 mm x 1 mm. The posterior of the bioreactor contains four tubes emanating from the bottom of each chamber to allow for effluent to escape to waste container. Septa located on the posterior allow for needles to be pierced to drip fresh medium (influent) to stimulate biofilm growth.

Two (2L) Pyrex bottles containing sterile DSMZ medium (30 mg L^{-1} atrazine) were connected to two peristaltic pumps, propelled at 0.8 mL min^{-1} to the needles at the anterior of the DFR. The DFR was placed at a 10^{o} angle to ensure the medium flowed down the surface of the microscope slide at a steady rate. The effluent was collected in a 4L waste container. The complete setup of the drip-flow reactor is illustrated in Figure 2.3. The flow rate of medium was controlled by each peristaltic pump, which each of controls two of the four ports in the reactor chamber.

Sterilization of DFR

DFR was sterilized according to Tolker-Nielson with modifications. Briefly, all tubing from the bioreactor setup was rinsed with 0.5% sodium hypochlorite at a rate of 4.5 mL min^{-1} for five min. The sodium hypochlorite remained in the line for two h, followed by a flush of sterile distilled deionized water at a rate of 4.5 mL min^{-1}. This

was performed three times, with air between each pass, for a total of 30 min. Following the flush, sterile distilled deionized water was driven overnight at a rate of 0.2 mL min^{-1}. Lastly, hydrogen peroxide (1% v/v solution) was pumped at a rate of 0.8 mL min^{-1} for ten min for additional sterilization. The bioreactor, tubing, along with all fittings and necessary components, were autoclaved for 20 min at 121°C and 15 psi.

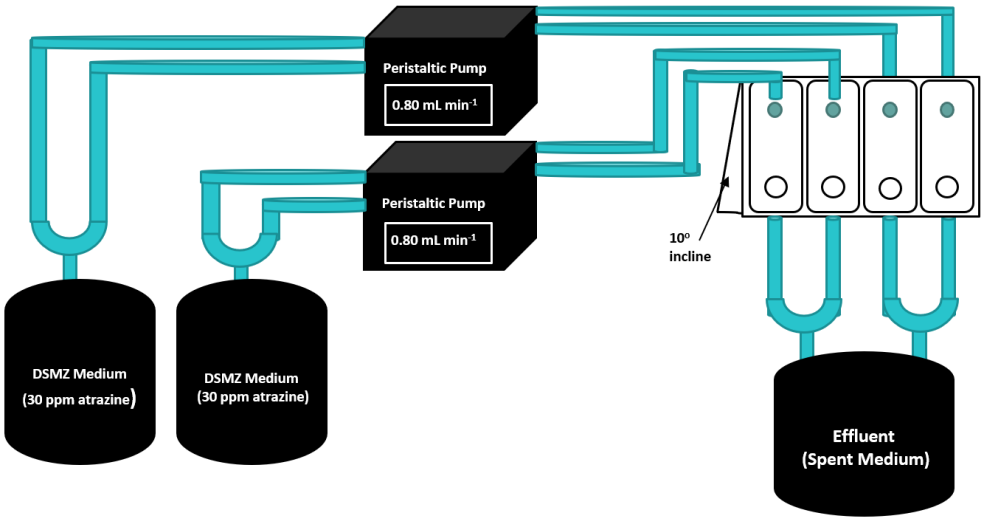

Figure 2.3. Set up of the drip-flow reactor for biofilm growth. The influent consisting of DSMZ medium (30 mg L^{-1} atrazine), connected to peristaltic pumps running to the DFR chamber, and subsequently to the effluent (waste) container.

P.ADP biofilm growth in DFR

The concentrated cell culture (10 mL) was dispensed into each of the four chambers and allowed for bacterial attachment in batch for a period of 6-8 h in batch phase. Once P.ADP cells attached to Silane-coated slides, the drip-flow reactor set up with influent and effluent was constructed. The drip-flow reactor was adjusted to a 10° incline to allow for medium to coat the maximum surface of the slide prior to entering the effluent. DSMZ medium containing 30 mg L^{-1} of atrazine was propelled

via peristaltic pumps and allowed to drip on the Silane-coated slides continuously for five days continuously.

Medium was replaced approximately every 30 h, aseptically to minimize bacterial and fungal contamination. The effluent container was replaced with an empty container every 30 h. Once the biofilm was mature (typically after 5 days), the drip-flow reactor was dismantled from the influent and effluent containers. Each biofilm was scraped into individual centrifuge tubes (50 mL) and immersed with 2 mL of trizol reagent to prevent enzymatic degradation of ribonucleic acids in samples. Despite a robust method for planktonic RNA extraction, a method of biofilm-based RNA extraction was to be developed in an efficient manner, utilizing an design-of-experiments (DOE) approach.

Optimized RNA extraction of P.ADP biofilms

Total ribonucleic acids from P.ADP biofilms were extracted without the aid of lysing matrix beads, phase lock gel tubes, storage of cells in a mixture of ammonium acetate/ethanol, and lysed cells from liquid nitrogen. Rather, P.ADP biofilms followed a combination approach of phenol extraction using Trizol and spin columns emanating from RNeasy Mini Kits based on a DOE approach.

The sample, previously scraped into centrifuge tube (50 mL) with trizol reagent (2 mL) was vortexed for 60 s. Cell material was sonicated with a sterile probe sonication needle for 10 s at medium-high output. If copious amounts of insoluble materials were still present, centrifugation was used at 6,000 x g for 10 min at 4^{o}C. RNA was initially isolated by a method with Trizol, and subsequently purified by RNeasy spin columns combined with DNAse digestion.

Once P.ADP cells were centrifuged, supernatant was discarded, leaving only the cell pellet. Trizol (1-2 mL) was added to re-suspend the pellet, and the sample was briefly vortexed. Chloroform (200 µL) was added to the mixture, and each sample was transferred to microcentrifuge tubes (1.5 mL). Tubes were shaken vigorously for 15 s and incubated for 2-3 min at approximately room temperature (15°C to 30°C). Each sample was centrifuged at 12,000 x g for 15 min at 4°C for phase separation. The upper layer, consisting of RNA, was removed from the microcentrifuge tube without disrupting the interphase or bottom layer by carefully angling at 45°. The interphase and lower phase were discarded, and the upper phase was transferred to a new micro tube. The total RNA was precipitated by the addition of ethanol (0.5 mL per 1 mL Trizol, 100%) at room temperature. The solution was mixed gently by inverting ten times.

Following isolation of RNA, the total nucleic acid was purified using the RNeasy Kit with modifications. Samples were transferred to RNeasy spin columns, with a maximum volume of 700 µL. The sample was then centrifuged at 9,600 x g for 30 s at room temperature (15°C to 30°C) and the supernatant was discarded. If the volume exceeded 700 µL, then aliquots were loaded successively onto the spin column and centrifugation steps were repeated. The flow through was discarded after each step.

To remove DNA contamination, DNase was used to remove remaining DNA. Buffer RW1 (350 µL) was added to the column. The sample was centrifuged at 9,600 x g for 30 s at room temperature (15°C to 30°C). Buffer RDD (35 µL) was added to DNase I stock solution (5 µL) and mixed gently by pipetting. The resulting incubation mix (40 µL) was placed directly onto silica gel membrane of the spin column. The

samples were incubated at room temperature for 15 min, and then Buffer RW1 (350 µL) was subsequently added to the column. The samples were centrifuged at 9,600 x g for 30 s at room temperature, and the flow through was discarded.

Purification of RNA was finalized by the addition of Buffer RPE containing ethanol (500 µL) to the column, centrifuged at 9,600 x g for 30 s at room temperature. Once the flow through was discarded, the previous step was repeated prior to placing the column in a new collection tube (2 mL). The sample was then centrifuged at 16,000 x g for 120 s at room temperature. The RNA was eluted by the addition of RNase-free water onto the silica gel membrane of the column and centrifugation at 9,600 x g for 60 s at room temperature. The RNA was stored at -80^{o}C prior to submission for quality control analysis.

Environmental synthesis of atrazine

Synthesis of atrazine was conducted according to previously published literature with slight modifications. A three-neck flask was charged with chlorobenzene (40 L), cyanuric chloride (4.07 g, 0.020 mole), and isopropylamine (1.32 g, 0.020 mole). The solution was cooled below 0^{o}C and controlled under 10^{o}C while being stirred for two h. Sodium hydroxide (10% v/v solution) was added to the mixture to neutralize the formation of the acid. Approximately two h later, ethylamine (0.99 g, 0.020 mole) was added, and the temperature was controlled at 15-20^{o}C. One hour later, sodium hydroxide (0.88 g, 0.020 mole) was supplemented to neutralize the acid, and the reaction was subsequently mixed for two h. The crude product was obtained by evaporating the chlorobenzene. After triturating the residue with petroleum ether, the crude product (powder) was obtained. The synthesized product was characterized by NMR and GC-MS for identity and purity.

Results and Discussion

Here, we present the results of the bioanalyzer and nanodrop quality analysis of RNA from optimization of nucleic acid in *Pseudomonas* sp. strain ADP biofilms, the Plackett-Burman DOE table aiding in our extraction decision, and the NMR/GC-MS spectra from our attempts to synthesize atrazine from cyanuric chloride as a starting material. The growth curves, along with parameters extracted, are illustrated to demonstrate the role of media in P. ADP growth. These results set a baseline for the experiments discussed in Chapters 3, 4, and 5. The growth curve parameters allow us to predict the time at mid-exponential phase for RNA extraction for use in the RT-qPCR experiments for gene expression.

Growth curves for P.ADP by media

Bacterial cells are normally characterized for growth by four distinct phases: lag, logarithmic (exponential), stationary, and death. The lag phase can be diminished by pre-inoculating bacterial cells in the same medium prior to OD_{600} measurements.[62] The growth curve, from t = 0 to t = 32 h, clearly illustrates three of the four phases for P.ADP cells grown in rich medium (lysogeny broth) in Figure 2.4(A). To demonstrate the growth phases more clearly, a semi-logarithmic plot has been generated from data displayed in the original experimental data (Figure 2.4(B)). In Figure 2.5(A), where LB has been removed to demonstrate the growth of cells in minimal medium in an evident manner, the data has been semi-log transformed akin to Figure 2.4 to demonstrate the growth phases (Figure 2.5(B)). On a semi-logarithmic plot, the lag phase is demonstrated by a horizontal line, logarithmic or exponential phase is demonstrated by a linearly increasing trendline, stationary phase is established as a flat, horizontal line, and death phase is manifested as a linearly, decreasing line.

P.ADP grown in LB, a rich medium, illustrates each of these phases to a greater extent in the planktonic mode of growth compared to P.ADP grown in alternate medium conditions (ammonium nitrate and minimal medium DSMZ containing atrazine).

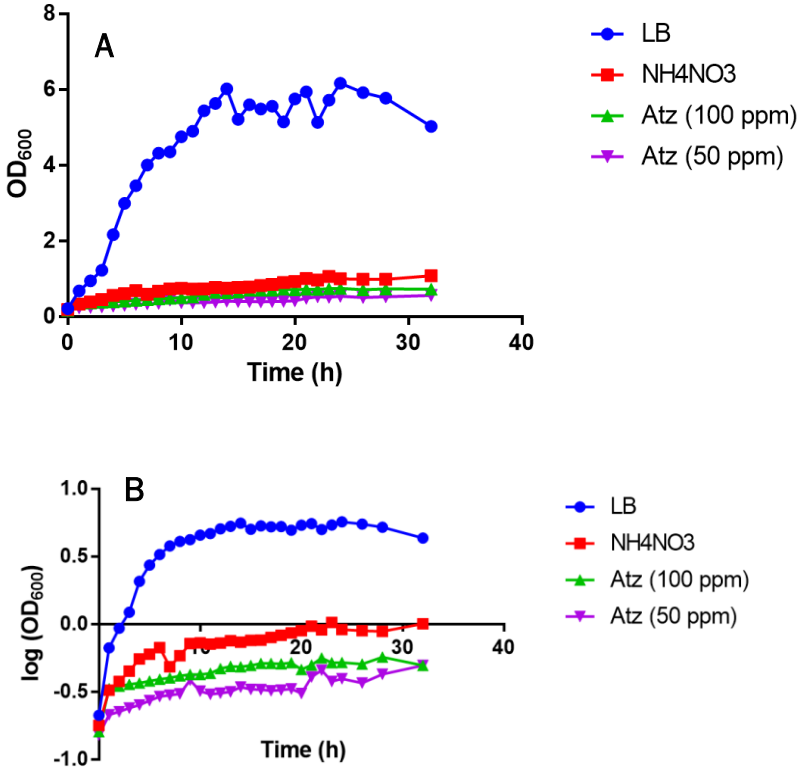

Figure 2.4. (A) Growth of P.ADP at 30°C, shaking at 250 rpm, in planktonic mode of growth for 32 h under the following media conditions: LB (●), ammonium nitrate (■), DSMZ with atrazine (100 mg L^{-1}) (▲), and DSMZ with atrazine (50 mg L^{-1}) (▼). (B) Semi-logarithmic plot of growth curves in (A).

Lag phase has effectively been diminished by pre-inoculation of P.ADP in LB prior to measurements, and cells demonstrate log growth from approximately 0-15 h. A brief stationary phase follows from 15-25 h prior to a decline in OD_{600} from 25-33 h. The former characterizes stationary phase, while the latter is a distinct death

phase for P.ADP bacteria. During this stage, cells have exhausted nutrients, accumulate toxic byproducts, and lyse at an increasing rate compared to the cells growing. The doubling time at 1.54 h is comparatively low to cells grown in minimal growth medium. This is primarily due to the availability of rich carbon and nitrogen sources from LB medium, compared to the relatively sparse availability of nutrients in ammonium nitrate, DSMZ (100 mg L^{-1} atrazine), and DSMZ (50 mg L^{-1} atrazine) To further illustrate the growth curves of P.ADP on minimal medium, LB was removed in Figure 2.5(A). A corresponding semi-logarithmic plot, as previously described, has been generated (Figure 2.5(B)).

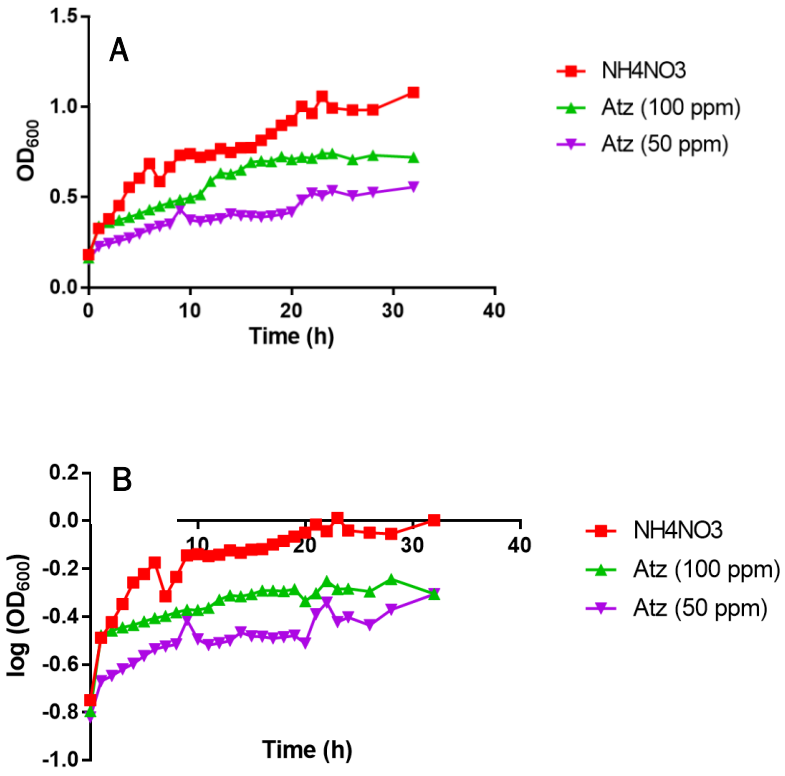

Figure 2.5. (A) Growth of P.ADP at 30°C, shaking at 250 rpm, in planktonic mode of growth for 32 h under the following media conditions: ammonium nitrate (■), DSMZ with atrazine (100 mg L^{-1}) (▲), and DSMZ with atrazine (50 mg L^{-1}) (▼). LB media removed to demonstrate the growth of P.ADP under minimal media conditions more clearly. (B) Semi-logarithmic plot of growth curves in (A).

Methods have been unchanged, and therefore the lag phase is not present in the cells grown in each of these sources of growth media. However, from the timespan of the P.ADP cells for OD_{600} measurements, 0-33 h, a noticeable lack of distinct stationary and death phases are present. Rather, most of each growth curve just appears to have a longer phase of exponential growth. It is clear the rate of growth is highest for ammonium nitrate, followed by DSMZ with 100 mg L^{-1} atrazine, and DSMZ with 50 mg L^{-1} atrazine. This is expected: the source of carbon has been unchanged, and ammonium nitrate contains a greater level of bioavailable nitrogen compared to atrazine. The higher concentration of atrazine allows for greater rate of growth (100 mg L^{-1}), due to more nitrogen available to P.ADP cells. Lastly, P.ADP cells grown with 50 mg L^{-1} of atrazine establishes the lowest specific growth rate. Table 2.1 summarizes the growth rate parameters that are necessary for experiments carried out in Chapters 3, 4, and 5.

Table 2.1. Growth parameters of *Pseudomonas* sp. strain ADP, including: doubling time (t_d), specific growth rate (μ), and range of the logarithmic phase, are reported for each type of growth medium.

Media Type	T_d (h)	μ (h^{-1})	Log Phase range (h)
LB	1.54	0.451	0-15
NH_4NO_3	10.2	0.068	0-10
Atrazine/DSMZ (100 mg L^{-1})	15.3	0.045	0-20
DSMZ/Atrazine (50 mg L^{-1})	38.8	0.018	0-22

The midpoint of the logarithmic range is essential to extract as a harvest point of bacterial cells for gene expression experiments for reasons discussed previously. The midpoint of logarithmic phase for LB, ammonium nitrate, DSMZ/atrazine (100 mg L^{-1}), & DSMZ/atrazine (50 mg L^{-1}) are 7.5 h, 5 h, 10 h, 11 h, respectively. As

exemplified, the time at mid-exponential phase does not change drastically between DSMZ medium conditions despite doubling the atrazine concentration. For experiments in gene expression and microscopy, these values will be used as a starting point and reference for bacterial harvest.

Growth curve kinetics have been previously studied for *Pseudomonas* sp. strain ADP, but under different conditions or substrates. Neumann, while studying the phenol and atrazine degradation simultaneously, demonstrated an exponential and stationary phase of P.ADP from 0-10 h and 12-24 h, respectively.[63] Under the highest phenol concentration, the specific growth rate of *Pseudomonas* sp. strain ADP was 0.12 h^{-1}, which corresponded to a doubling time of 5.75 h. Meanwhile, P.ADP substituted with cyanuric acid in place of atrazine contributed a much faster specific growth rate of 0.32 h^{-1}, with a doubling time of 2 h. This demonstrates the great variability in growth rate parameters dependent upon specific medium components and concentrations of C- and N- sources for P.ADP. Garcia-Gonzales additionally demonstrated the effect of a glutamine synthase inhibitor (MSX) on P.ADP growth curves at varying concentrations.[36] The result, similarly, demonstrated a clear log and stationary phase, without a lag nor death phase in the timeframe from 0-25 h. The primary purpose of constructing growth curves under similar conditions with various media serves to give researchers a benchmark for many downstream applications, including PCR gel electrophoresis, ELISA, RNA-Sequencing, plasmid isolation and purification, and microscopy analysis.

The relatively slow growth of P.ADP under minimal medium conditions can be attributed to the absence of rich bioavailable nutrients, in contrast to LB. The bacterial cells have enough carbon and nitrogen sources (via atrazine & glucose or

ammonium nitrate & glucose) to sustain growth and division, but rapid growth is not supported. LB, conversely, contains an abundance of available carbon, nitrogen, and micro-nutrients to support rapid cellular processes and division, resulting in a high optical density over time.

Minor increases and decreases in OD_{600} values, atypical of an ideal growth curve, may be attributed to systematic error. Cells were consistently diluted and OD_{600} was re-calculated based on dilutions to account for the upper limits of detection for the UV-vis spectrophotometer. Each growth curve of P.ADP with minimal medium did not extend enough to capture stationary nor death phases of the bacterial strain. The bacteria were able to sustain slight growth over a longer period on ammonium nitrate or atrazine as a sole nitrogen source. In contrast, LB demonstrated a clear stationary and death phase.

Quality control of RNA following various extraction methods

Following successful optimization of total RNA extraction from *Pseudomonas* sp. strain ADP biofilms and planktonic cells using a Plackett-Burman DOE approach, the total RNA was isolated for each mode of growth for downstream applications.

Quality of RNA following extraction for each mode of growth was assessed by two methods: a) micro-spectrophotometry, and b) capillary gel electrophoresis. The concentration and purity of total RNA from samples are typically estimated by the ratio of the absorbance maxima for nucleic acids and proteins, which fall at 260 and 280 nm. Therefore, the measure of purity is 260/280 nm, with an ideal ratio of 1.8 for “pure” DNA and 2.0 for “pure” RNA. Major deviations from this ratio may be signs of contamination from Trizol, phenol, guanidine HCl, guanidinium isocyanate, or other

chemicals. These residual chemicals produce specific spectra that may be investigated once the ratio has been determined to be impure.[64]

As demonstrated in Table 2.2, the ratio of isolated RNA from planktonic P.ADP cells for each sample averaged 2.09, slightly higher than the pure ratio of 2.0 indicative of pure RNA. The value of 2.09 is well within error and not statistically significantly different than the ideal pure ratio of 2.0. However, the 260/230 ratio, which is expected to be between 2.0-2.2 for pure nucleic acid, fell at 1.09 for sample A and 1.90 for sample B, demonstrating variable purity between samples. The decreased 260/230 in sample A may be a result of residual phenol from nucleic acid extraction. The concentrations, estimated below in Table 2.2, signify the total nucleic acid concentration in each sample, at 82.4 and 94.8 ng/µL. However, this can be confounded with contaminating DNA due to similar absorbance maxima of both nucleic acids. If sample is adequate in purity as designated by the 260/280 ratio, and the reported concentration exceeds 50 ng/µL, the sample was analyzed by capillary gel electrophoresis.

Table 2.2. Micro-spectrophotometric parameters for quality control of RNA following extraction of total RNA using RNeasy Mini Kit. Concentration, absorbance ratios, and multiplication factor are reported above and organized by column.

Sample	Concentration	A260	A280	260/280	260/230	Type	Factor
A	82.4 ng/µL	2.060	0.987	2.09	1.09	RNA	40
B	94.8 ng/µL	2.396	1.136	2.09	1.90	RNA	40

The bioanalyzer detects biomolecules by laser-induced fluorescence.[65] Unlike micro-spectrophotometry, the bioanalyzer is able to distinguish the concentration of RNA by intercalating the RNA with a specific dye during the chip run. The RNA ladder is run with varying fragments from 0.2 to 6.0 kb at a total concentration of 150

ng/μL. The ribosomal RNA peaks and areas of analyzed to evaluate the total RNA concentration and purity.

Eukaryotic chips establish two peaks at 18s and 28s, while prokaryotic chips show 16s and 23s ribosomal peaks. Chips are interchangeable and can be run across both types of organisms. For a pure sample, the height of the larger ribosomal peak should be about twice the height of the smaller peak. Deviation from this can be attributed to degradation by ribonucleases or extraction contamination from chemicals. The other metric of quality is the baseline in the electropherogram. A flat baseline indicates undegraded RNA, while higher background may be indicative of small RNA contamination or partial degradation from ribonucleases.

The RNA integrity number, a measure of the overall quality of RNA from electrophoresis, is calculated from an algorithm within the bioanalyzer based on the electropherogram to consistently and robustly. The range of the RIN is from 0.0 to 10.0, with 10.0 indicating the highest quality as measured by the bioanalyzer. To ensure success of downstream applications, such as RT-qPCR and RNA-Seq, the RIN must be 8.0 or greater to proceed. As indicated in Table 2.3, isolated RNA from planktonic *Pseudomonas* sp. strain ADP cells is of high integrity with Samples A and B having RIN of 9.7 and 9.8, respectively. The RNA concentration was underestimated by spectrophotometry in each case, by a differential of 14.6 ng/μL and 19.2 ng/μL, respectively (Figure 2.6).

In this sample, the prokaryotic chips were used as designated by the 23s and 16s ribosomal peaks and reported ratios. Ideally, the reported ratio would be 2.0 for each sample, however, the height did not fall below 1.0, which would indicate the 16s was higher than the 23s. The baseline in each electropherogram is completely

flat in character, and each peak is sharp, tall, and without jagged edges. This is most likely due to the addition of DNAse treatment methodology that had been implemented in the RNeasy Protocol. No smaller peaks prior to the 16s or 23s are present, which would specify smaller digested RNA fragments. Additionally, no skewed ribosomal peak is present, which would indicate genomic DNA contamination. From these results, we are highly confident to apply our total RNA from planktonic cells in downstream PCR experiments.

The methodology, a combination of Trizol extraction followed by purification of RNA from spin-columns, proves to be a robust method of producing a high quantity of pure total RNA in *Pseudomonas* sp. strain ADP free-cells. Once total RNA is extracted from biofilms, differential gene expression using RT-qPCR may be properly executed.

Table 2.3. Capillary gel electrophoresis parameters for quality control of RNA following extraction of total RNA using RNeasy Mini Kit. Concentration, peak areas, ribosomal ratios, and RNA integrity numbers are reported above and organize by column.

Sample	Concentration	Area	Ratio (23s/16s)	RIN
A	97 ng/μL	233.9	1.3	9.7
B	114 ng/μL	275.6	1.4	9.8

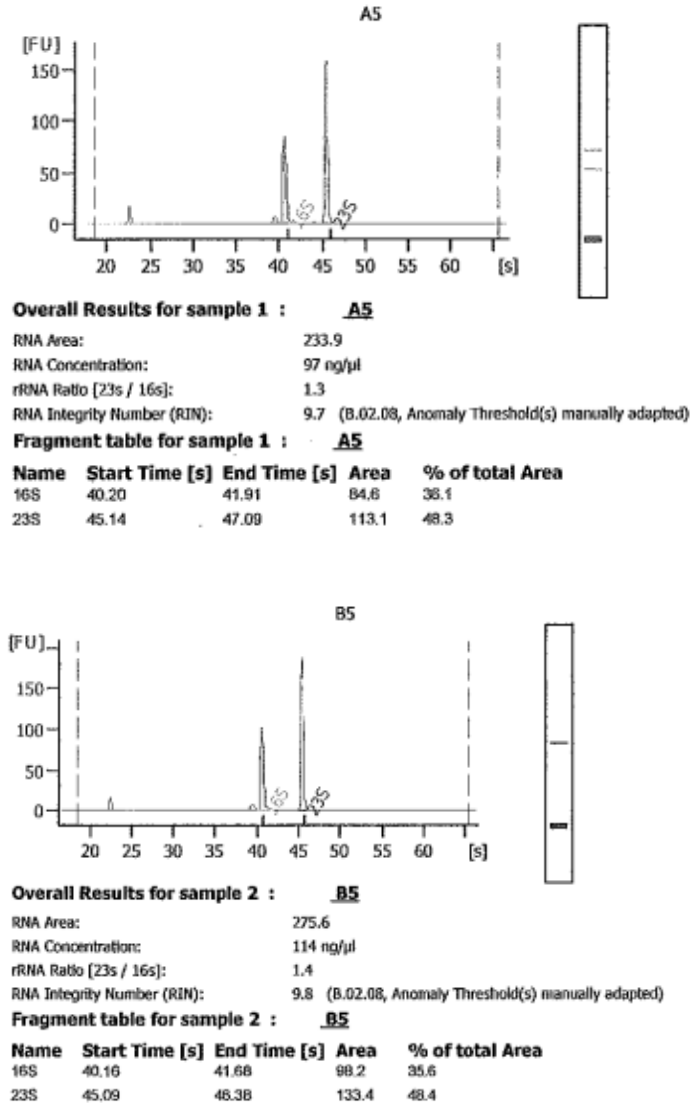

Figure 2.6. Electropherogram of capillary gel electrophoresis, displaying 16s and 23s ribosomal peaks, along with RNA area, concentration, integrity number, and spectra for extraction of RNA from planktonic *Pseudomonas* sp. strain ADP cells. Two samples, AS (top), and BS (bottom), are illustrated, respectively.

Biofilms harvested from the drip-flow reactor are illustrated in Figure 2.7. Biofilms were grown for five-days to maturity and exhibited a physical white film on the surface of the Silane-coated slides.

The absence of EPS was noted in the center of the film, which may have been caused by the area of drip parallel to the each of the needles submerged in the DFR. Each mature biofilm was harvested by scraping with a cell scraper and immersed in a tube, followed by the optimized RNA extraction procedure as described previously.

Figure 2.7. Digital renderings of *Pseudomonas* sp. strain ADP biofilms grown at 30°C for 5-days under a drip-flow reactor with DSMZ media containing atrazine (30 mg L^{-1}). Each image illustrates a mature biofilm, performed in triplicate in drip-flow reactor. Each biofilm is attached to a Silane-coated microscope slide in images above.

Total RNA from biofilms was extracted using the optimized approach of Trizol and RNeasy Spin Columns and have been designated with (TR) in front of each sample. Each sample lacking the combinatory approach is designated with a (S) in front as a prefix. The combinatory method yielded high quantity and quality RNA as indicated by the 260/280 ratios reported in Table 2.4. All 260/280 ratios for TR samples are at or above 2.0, with variable 260/230 ratios. The concentration of RNA extracted from P.ADP biofilms was extremely high, ranging from 225 ng/µL to 320 ng/µL. In contrast, (S) samples, which were extracted solely with Trizol, yielded inconsistently low yields, ranging from 5 ng/µL to 55 ng/µL based on micro-spectrophotometric measurements. This may be attributed to lack of EPS disruption and interference in extraction from biofilm associated components. The bioanalyzer approach was used to attain a more accurate representation of the RNA integrity and quantity extracted from P.ADP biofilms.

Table 2.4. Sample concentrations reported from *Pseudomonas* sp. strain ADP biofilms as measured by micro-spectrophotometry. Absorbance ratios (260/280) and (260/230) are reported, in addition to approximate RNA concentrations from sample.

Sample	Concentration	A260	A280	260/280	260/230	Type	Factor
TRA	224.9 ng/µL	5.623	2.737	2.05	2.02	RNA	40
TRB	321.2 ng/µL	8.029	3.841	2.09	1.46	RNA	40
TRC	271.2 ng/µL	6.779	3.244	2.09	2.16	RNA	40
TRD	264.7 ng/µL	6.617	3.227	2.05	1.90	RNA	40
SRA	5.2 ng/µL	0.13	0.04	3.26	0.02	RNA	40
SRB	54.4 ng/µL	1.361	0.725	1.88	0.14	RNA	40

Based on the micro-spectrophotometric results, five of the six samples had sufficient 260/280 ratios to be submitted for analysis by gel capillary electrophoresis. Sample concentrations were underestimated by the spectrophotometric approach, as illustrated in Table 2.4 and Table 2.5. The bioanalyzer approach contains a dye that specifically intercalates to RNA and is therefore more representative of the "true" concentration of RNA, while the spectrophotometric approach may have skewed concentrations from chemical contaminants, other nucleic acids, or proteins that absorb in the same region. TRA, TRB, TRC, and TRD all passed quality control with RINs in the range of 9.0 to 10.0, while the SRA sample was not of sufficient quality to calculate an integrity number. Additionally, the ratio of 23s to 16s dropped below 1.0, the concentration was extremely low at 2 ng/µL, and no clear peaks could be observed on the electropherogram in Figure 2.8. The other samples distinctively demonstrated clear, sharp 23s to 16s ribosomal peaks at the expected time in the electropherogram. The high concentrations of total RNA extracted from each sample signaled the remaining four are satisfactory for downstream applications.

Figure 2.8 and Figure 2.9 illustrate the quality of the RNA extracted from P.ADP biofilms using the combinatory approach. Each spectrum (TRA, TRB, TRC, and TRD)

has a flat baseline without background noise, clear sharp peaks at the designated ribosomal regions for prokaryotic organisms, and a noticeably absent genomic DNA peak around each peak.

Table 2.5. Sample concentrations reported from *Pseudomonas* sp. strain ADP biofilms as measured by gel capillary electrophoresis. Area, ribosomal ratio, and RNA integrity number are reported in addition to approximate RNA concentrations from sample.

Sample	Concentration	Area	Ratio (23s/16s)	RIN
TRA	262 ng/μL	761.9	1.3	9.6
SRA	2 ng/μL	5.1	0.8	---
TRB	424 ng/μL	1,069.6	1.3	9.2
TRC	343 ng/μL	866.6	1.3	9.3
TRD	343 ng/μL	866.5	1.4	9.5

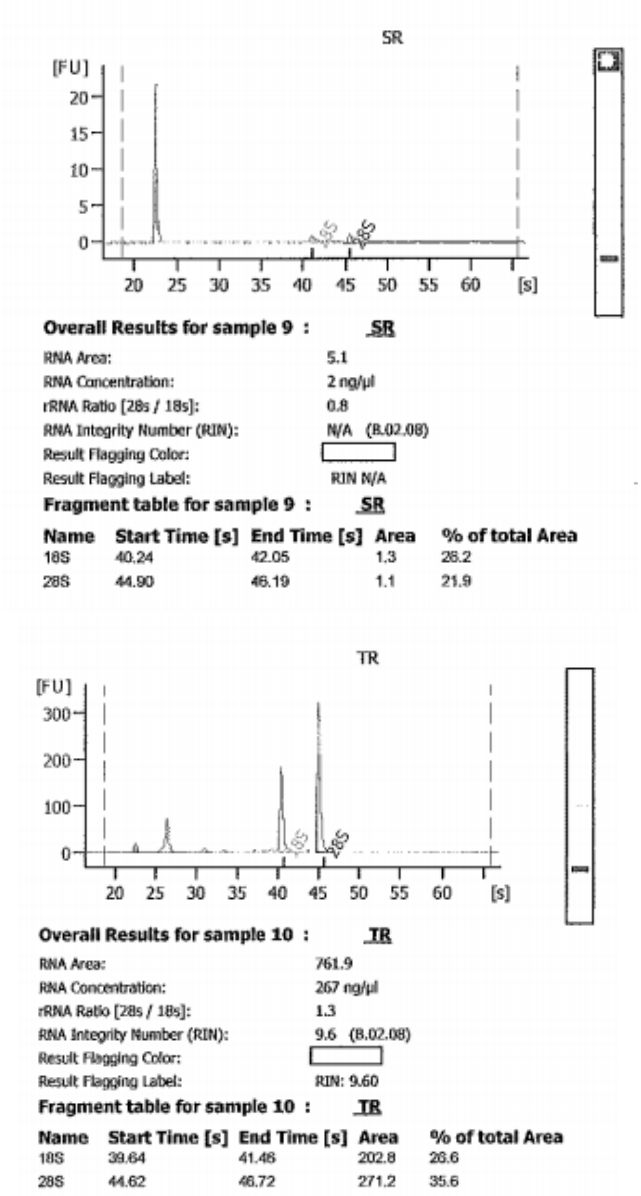

Figure 2.8. Electropherogram of capillary gel electrophoresis, displaying 16s and 23s ribosomal peaks, along with RNA area, concentration, integrity number, and spectra for extraction of RNA from biofilm *Pseudomonas* sp. strain ADP cells. Two samples, SR (top), and TR (bottom), are illustrated, respectively.

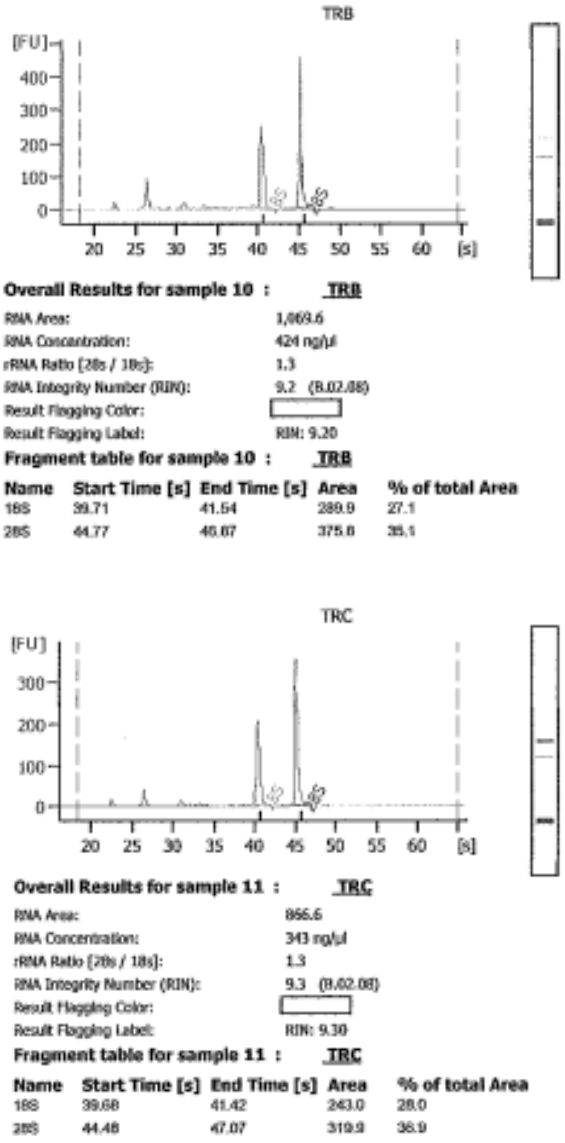

Figure 2.9. Electropherogram of capillary gel electrophoresis, displaying 16s and 23s ribosomal peaks, along with RNA area, concentration, integrity number, and spectra for extraction of RNA from biofilm *Pseudomonas* sp. strain ADP cells. Three samples (TRB), (TRC), and (TRD), are illustrated above at top, middle, and bottom respectively.

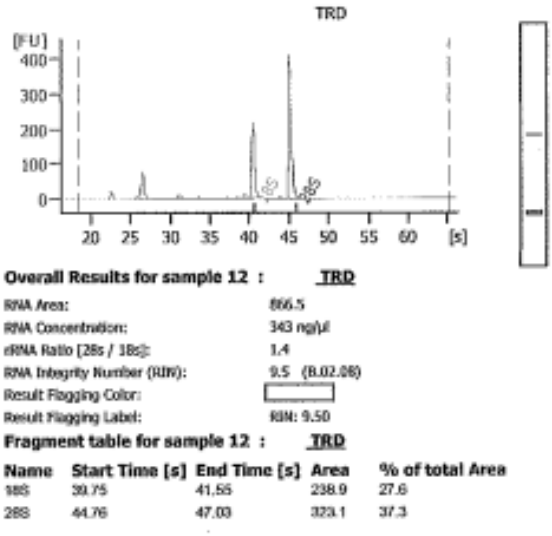

Figure 2.9. – Continued

Characterization: MS and NMR analysis for atrazine synthesis

Atrazine was synthesized by the methods as previously described.[66] The crude product was characterized by mass spectrometry (TOF-MS-EI+) and proton nuclear magnetic resonance (^{1}H4-NMR). The time of flight mass spectrometry electron ionization (TOF MS EI+) spectra displayed peaks at 10.39, 10.67, and 10.39, designating the formation of three compounds in varying abundance levels in Figure 2.10. The compounds, as exhibited in Figure 2.11, are 1,3,5-Triazine-2,4-diamine, 6-chloro-N-N'-bis(1-methylethyl), s-Triazine, 2-chloro-4,6-bis(ethylamino), and 1-chloro-3-ethylamino-5-isopropylamino-2,4,6-triazine (atrazine).

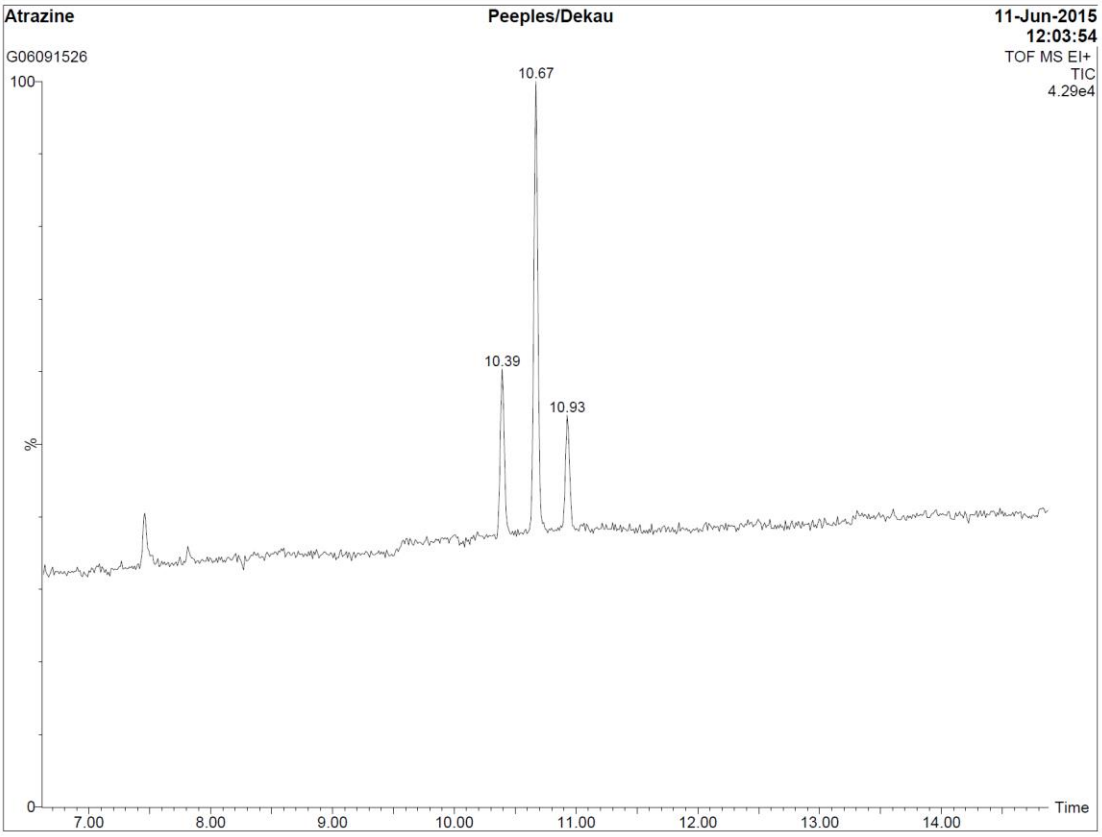

Figure 2.10. Spectrum from TOF MS EI+ designating three peaks, representing the mixture of three compounds synthesized from cyanuric chloride. The compounds appeared at 10.39 s, 10.67 s, and 10.93 s.

The mass spectra (Figure 2.11) illustrate the fingerprint of each hit in different abundances for each compound detected. The fragment patterns are based on each specific chemical. As demonstrated, the mass spectrum most consistent with atrazine, the peak at 215 grams per mole represents our synthesized compound of interest. The reported abundance of 1.58×10^4 is relative to the abundance of the other two compounds. Therefore, the percent of atrazine in the total crude product is approximately 64.6%. The relative yield of the other two compounds 1,3,5-Triazine-2,4-diamine, 6-chloro-N-N'-bis(1-methylethyl) and s-Triazine, 2-chloro-4,6-bis(ethylamino), are 13.5% and 22.0%, respectively.

Based on MS spectra, atrazine was able to be efficiently synthesized with a 64.6% product yield. However, due to the difficulty of separating compounds of similar molar mass and structure, the environmental synthesis of atrazine proves unsuitable for a larger scaling to use in bioremediation experiments. Despite this shortcoming, it has been confirmed the herbicide is able to be crudely synthesized in a relatively short method.

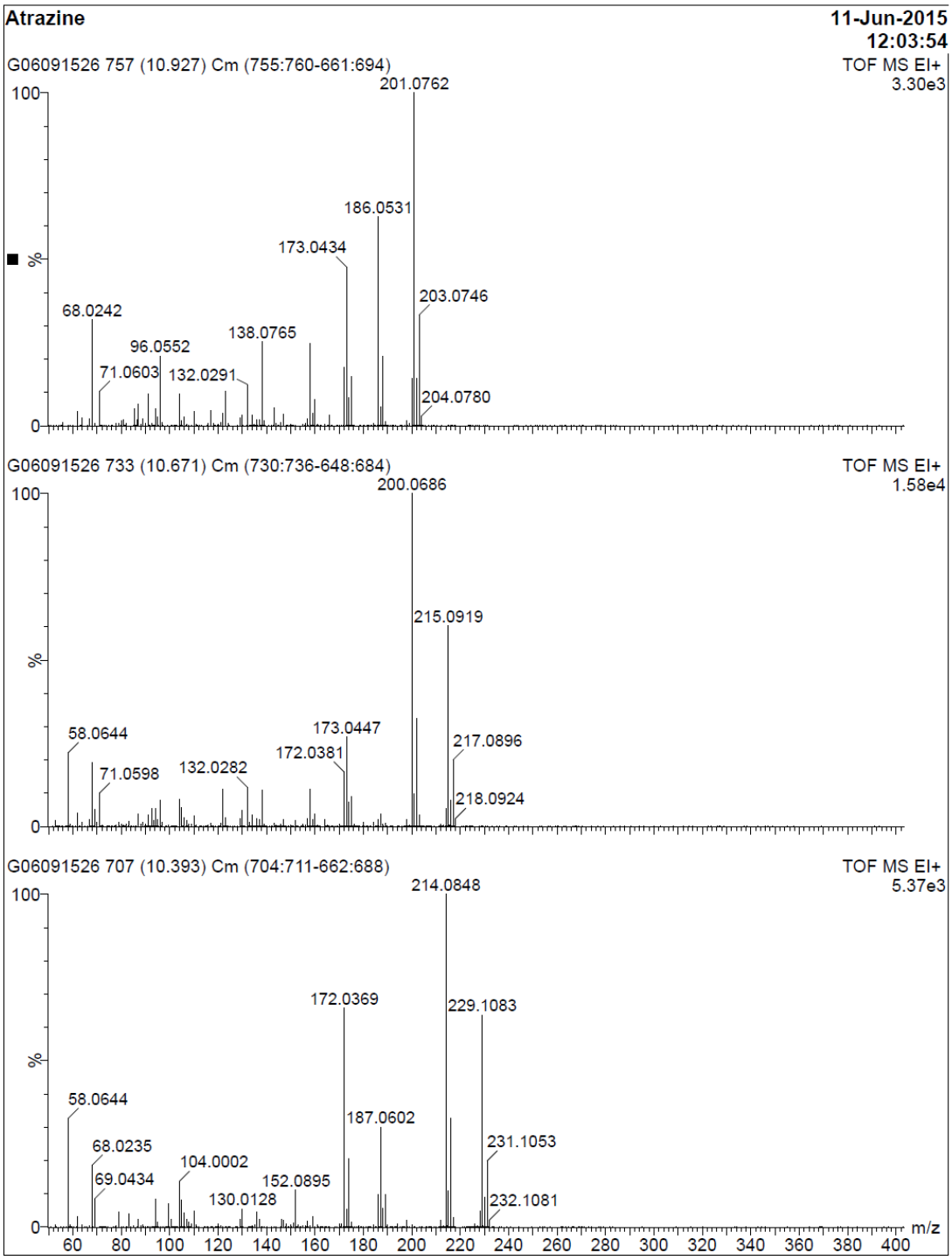

Figure 2.11. Mass spectra from TOF MS EI+ displaying the fingerprint for each of the three compounds detected in varying abundances: 1,3,5-Triazine-2,4-diamine, 6-chloro-N-N'-bis(1-methylethyl), s-Triazine, 1-chloro-3-ethylamino-5-isopropylamino-2,4,6-triazine (atrazine), and 2-chloro-4,6-bis(ethylamino). The abscissa displays the mass to charge ratio and the ordinate displays the relative abundance of each molecular fragment from time of flight mass spectrometry electron ionization (TOF MS EI+).

Previously published ^{1}H-NMR (400 MHz) spectrum of pure atrazine contributes peaks at 1.193, 1.212, 1.22, 1.236, 3.44, 3.456, 3.474, 4.173, 5.403, and 6.297 mg L^{-1} with TMS as a chemical shift reference and $CDCl_3$ as the solvent (National Institute of Advanced Industrial Science and Technology). As exemplified in Figure 2.12, the crude ^{1}H-NMR exhibits peaks at 1.20, 1.41, 1.43, 3.44, 4.14, 4.16, 5.30, 5.95, and 7.26 mg L^{-1}. The peaks and splitting appear to be similar in both spectra, despite chemical shifts downstream in the experimental spectrum from our atrazine synthesis. As confirmed by mass spectrometry, the crude product is impure and contains two other compounds similar in molecular weight and structure. The alternate chemicals may cause the peaks in the crude NMR to shift (mg L^{-1}) from the NIST published standard spectrum for atrazine. It substantiates the impurities found in the crude product synthesized from cyanuric chloride. The similarity in molecular weight, polarity, and structure of the other triazine compounds prevent ease of separation by chromatographic methods. The mixed crude product, containing a high abundance of atrazine, may have potential use in downstream bioremediation experiments despite the presence of impurities. It is not known whether P.ADP is able to metabolize the similar products as a source of nitrogen, or if the alternate products in the impure sample are stimulatory or inhibitory to atrazine catabolic processes.

A yield of 64.6% atrazine resulted from the synthesized product using cyanuric chloride as a starting reagent. The interest in an organic synthesis of atrazine stems from the prohibitive cost of pure atrazine from chemical companies, and the unwillingness of agricultural corporations, including Syngenta and Monsanto, to provide such chemicals for studies in bioremediation in an academic environment. In

future work involving the synthesis of atrazine, alternative methods will be heavily explored.

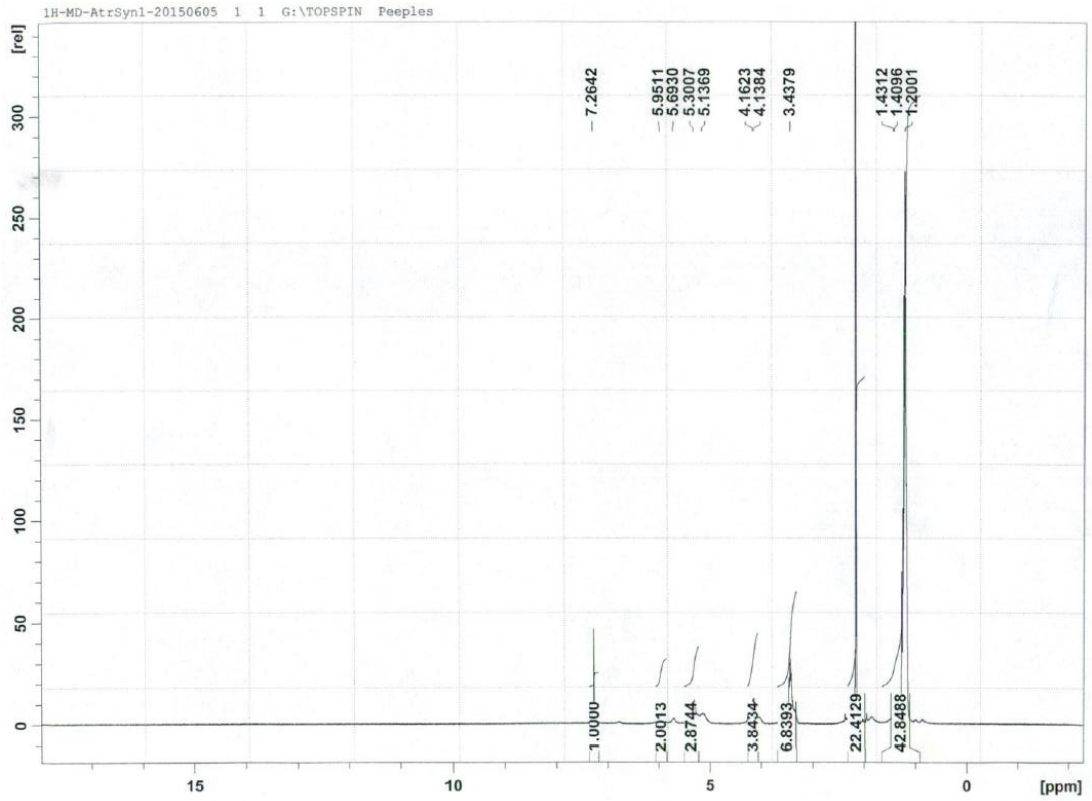

Figure 2.12. Crude ^{1}H-NMR spectrum of synthesized atrazine from cyanuric chloride.

Conclusion

In this chapter, growth curves of *Pseudomonas* sp. strain ADP were established by growth media, with necessary parameters extracted. Our results allowed us to visualize the pattern of bacterial growth and the strains' dependence on type of medium. Next, RNA was extracted from free-cells prior to experimenting with biofilm-based nucleic extractions. Several factors, including the presence of phase-lock tubes, sonication, and phenol-based extraction, were tested in a DOE-approach to evaluate the optimal extraction of RNA in P.ADP biofilms. This proved difficult due to the presence of interfering extracellular polymeric substances, which

may be trapped in spin columns and prevent a pure, clean, isolation of ribonucleic acids.

Once methods were established, RNA was extracted and checked for quality with two methods: a) micro-spectrophotometry, and b) capillary gel electrophoresis. Samples exceeded RNA integrity numbers (RIN) of 8.0 were stored for downstream applications. This step was essential for experiments set out in Chapter 3, Chapter 4, and Chapter 5 involving gene expression and microscopy. Ultimately, validating growth of P.ADP and optimizing nucleic extraction aid in providing necessary information and results for consistency in the bulk of remaining experiments.

Finally, due to the excessive cost of pure atrazine, an environmentally-conscious organic synthesis was attempted to attain atrazine. A mixture of three products, including 64.5% atrazine, was obtained as confirmed by MS and NMR characterization. The product could not be purified, due to the similarity in polarity, structure, and molecular weight of the mixed compounds. Despite ostensibly synthesizing an impure, crude product, the synthesis provides helpful information in future efforts for a cleaner synthesis of atrazine.

In Chapter 3, the atrazine-degrading genes on pADP-1 are differentiated based on expression using RT-qPCR based on mode of growth. The atrazine-degrading genes are further differentiated in relative gene expression experiments by temperature of biofilm growth and maturation. In real-world applications, the presence of alternate nitrogen sources are often available and may hinder the remediation efficiency of *Pseudomonas* sp. strain ADP. This potential issue in engineering biofilms for remediation is addressed by examining the growth of P.ADP under various nitrogen sources and evaluating the expression of atrazine-degrading

genes. Chapter 3 addresses the gap in knowledge of genetics in *Pseudomonas* sp. strain ADP biofilms. Atrazine-degrading genes present in the biofilm mode of growth are evaluated in-depth to fulfill a broader goal of applying biofilm systems to environmental remediation and biotechnology.

CHAPTER 3: EXPRESSION OF ATRAZINE-DEGRADING GENES IN *PSEUDOMONAS* SP. ADP BIOFILMS

Introduction

Bacterium *Pseudomonas* sp. strain ADP degrades atrazine in six catabolic steps as outlined previously.[3] These six genes are central to the catabolic properties of P.ADP in the field of environmental biotechnology, due to their elevated potential for remediation of a recalcitrant compound. By understanding the expression of atrazine degrading genes in metabolically active cells, the real-time remediation potential and efficiency is realized from a genetic standpoint.

Chemical analysis is a powerful tool used to quantitatively determine the amount of pollutant, atrazine, remaining over a timescale but lacks the capabilities of evaluating the mechanism of action. Genetic tools, such as RT-qPCR, provide insight beyond the apparent occurrence of degradation. If cells are not metabolically active, and no atrazine is detected, the other mechanisms may be more plausible than a stream of continuous degradation. By addition of the complexity of bacterial biofilms which contain a matrix composed of extracellular polymeric substances (EPS), entrapment and active degradation could contribute to the overall removal of atrazine. Conversely, in planktonic cells, the metabolic process and degradation are relatively more transparent. Previous literature suggests a first-order kinetic degradation of atrazine by various strains capable of metabolizing the parent compound.[3]

Gene expression is a vital component to analyze in the field of bioremediation. By analyzing the differential gene expression in biofilms and free-cells, the genes associated with the degradation of atrazine may exhibit higher or lower activity based

on mRNA levels. Differential expression of biofilms and free-cells have been previously studied in *Escherichia coli* and *Pseudomonas* aeruginosa systems.[67–69] In the latter, 0.5% of global genes were upregulated and 0.5% were downregulated in biofilms compared to planktonic cells, with a great amount of sensitivity in response to antibiotics.[68] Several notable differences in expression were observed and quantified with microarrays in *Escherichia coli*, including induction of genes in oxygen and nutrient limiting conditions and genes associated with enhanced heavy metal resistance. The consequence of upregulated expression for heavy metal resistance may increase uptake of metal pollutants in biofilm systems for bioremediation efforts. Additionally, the induction of genes by other stressors such as nutrient limitation may be important in bioremediation as natural systems may undergo prolonged periods of little substrates for metabolism. The biofilm, however, would have increased odds of surviving due to induction of genes in stressful conditions.

Initially our studies involved differentiating the expression of atrazine-degrading genes in *Pseudomonas* sp. strain ADP biofilms compared to planktonic cells. These studies contrast previously published literature based on purposefully sharpening our focus to six-genes rather than a global expression system on biofilm and planktonic associated genes. Furthermore, this is a monospecies lab-grown biofilm, which contrasts studies on gene transfer in heterogeneous biofilms found in the environment. Despite the shortcoming of the unrealistic nature of monospecies biofilms found in nature, the process allows us to better understand gene expression and transfer from a very fundamental level prior to movement and studies of more complex biofilm systems.

Metabolic genes may be upregulated or downregulated in monospecies biofilms based on several factors. Previous, sulfur metabolism was upregulated while genes relating to motility were downregulated in early and late stage of *Achromobacter* species biofilms.[70] It has been shown that biofilms increase the rate of horizontal gene transfer (HGT) via conjugation of mobile plasmids in both mono and multi-species biofilms compared to cells grown in the planktonic state. The explanation behind this phenomenon is projected to be the expedited spread of mobile genetic elements (MGE) that are found in biofilm communities.[71] Essentially, plasmids induce for the formation of biofilms while HGT is facilitated from biofilms. It is reported that HGT through conjugation occurs frequently in mono-species and multi-species biofilms which results in novel genetic combinations and facilitates the creation of new genotypes.[72] This forms the basis for our first objective: differentiating the expression of metabolic pathway genes in *Pseudomonas* sp. strain ADP, in two modes of growth: biofilm and planktonic.

In addition, we have studied the expression of atrazine-degrading genes in biofilms grown at various temperatures to simulate environmental conditions that change seasonally in areas of high atrazine use and contamination. Furthermore, the gene expression results may be applied to the use of biofilm reactors in bioremediation systems in the environment, in which case the controlled temperature of the reactor may be optimized. This has been performed on bioremediation systems for the anaerobic treatment of chemical wastewater, using the Taguchi Dynamic DOE methodology. Temperature, along with pH, sulfate concentration, and alkalinity, were analyzed at two levels to optimize treatment using a biofilm reactor.[73] In terms of seasonal variation, it has been demonstrated seasonal differences affecting

temperature are consequential to nutrient limitations and biofilm formation of microbes in the natural environment.[74]

Downstream metabolites and alternate nitrogen sources are initially tested in *Pseudomonas* sp. strain ADP planktonic cells prior to future experiments in biofilms. Due to the transient availability of numerous nitrogen sources in soil, groundwater, and drinking water other than atrazine, these are added as sole and dual nitrogen sources to our system to analyze growth and gene expression. Previous studies have focused on gene regulation of P.ADP growth on cyanuric acid and the *atzDEF* operon, and have evaluated the effect of nitrogen limitation on the activator AtzR.[43] A transport system for cyanuric acid was also explored in depth by Platero et al.[55] Despite this, the expression of the atrazine-degrading genes of P.ADP have not been analyzed with respect to growth on the parent compound compared to alternate nitrogen sources and metabolites. The expression of the primary three genes, which encode for the biotransformation from atrazine to cyanuric acid, are studied under nitrogen sources including urea, cyanuric acid, and atrazine. The purpose is to evaluate the biodegradation capabilities at the genetic level of P.ADP in the presence of more bioavailable nitrogen sources. If the bacterial strain metabolizes simpler structures such as urea and cyanuric acid, then the role of P.ADP in bioremediation may also require genetic engineering to uptake the parent compound atrazine as an increased rate.

In addition to genetics, chemical analysis will aid in our understanding of the potential of *Pseudomonas* sp. strain ADP biofilms in the field of environmental biotechnology and bioremediation. The catabolic activity of P.ADP, based on the six genes located on the pADP-1 plasmid, demonstrates the possible mechanisms of

remediation by biofilms, including entrapment by the EPS matrix, sustained metabolic degradation, or release of innocuous metabolites from the parent compound. The complete workflow from cell growth to expression analysis for qPCR is examined in Figure 3.1.

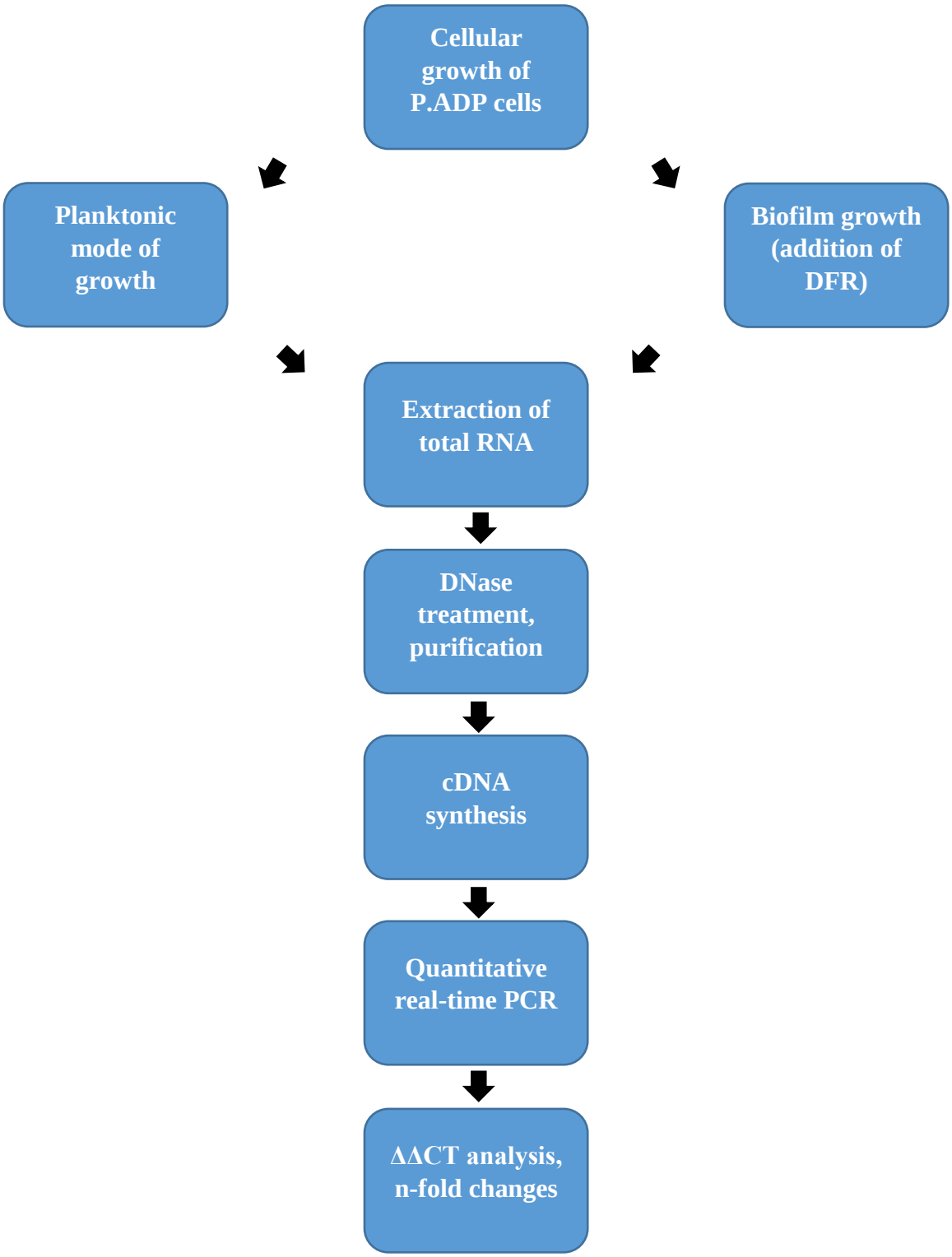

Figure 3.1. RT-qPCR workflow consisted of initial cellular growth, followed by extraction of total ribonucleic acid, DNase treatment, purification, cDNA synthesis, qPCR, and analysis. Each experiment involving gene expression involved the use of the above RT-qPCR schematic.

Materials and Methods

Bacterial strain, cultivation medium, and culture conditions

A frozen glycerol stock of *Pseudomonas* sp. strain ADP (DSM 11735) was streaked onto an agar plate containing mineral medium with 1000 mg L^{-1} atrazine (3.50 g L^{-1} $Na_2HPO_4 \cdot 2H_2O$, 1.00 g L^{-1} KH_2PO_4, 0.10 g L^{-1} $MgCl_2 \cdot 6H_2O$, 0.05 g L^{-1} $CaCl_2$, 1 g L^{-1} d-glucose, 1.00 mL L^{-1} (v/v) trace element solution, 15 g L^{-1} noble agar, pH 7.25). The streak plate was incubated overnight (30°C) and a single colony was inoculated in a liquid mineral medium containing 30 mg L^{-1} atrazine (3.50 g L^{-1} Na_2HPO_4 x $2H_2O$, 1.00 g L^{-1} KH_2PO_4, 0.10 g L^{-1} $MgCl_2$ x $6H_2O$, 0.05 g L^{-1} $CaCl_2$, 1 g L^{-1} d-glucose, 1.00 mL L^{-1} (v/v) trace element solution, pH 7.25) in shake flasks (125 mL) at 30°C. The agitation rate was maintained at 250 rpm. After 12 h, cell growth was measured indirectly using spectrophotometry detailed in the proceeding section. If growth was sufficient in the pre-inoculum (OD_{600} > 0.1), then the culture was passed to fresh medium (50 mL) in a larger flask (250 mL) while maintaining a 10% (v/v) inoculum.

Growth of P.ADP planktonic cells

Cellular growth of the inoculum was measured indirectly using spectrophotometry (Thermo Spectronic BioMate, Waltham, MA). Optical density measurements (OD_{600}) were taken once per hour for 100 h from second pass of cells. Samples were then diluted ten-fold when OD_{600} > 0.3 to remain within the instrument's limit of detection. The growth curve was used to determine the doubling time, specific growth rate, and time to reach exponential phase. Overnight cells were passed to a larger inoculum and samples were collected at previously determined

exponential phase (t = 30 h) for consistency during RNA extraction and microscopy experiments.

Drip-flow reactor for P.ADP biofilm growth

Biofilms were grown by the method of Tolker-Nielsen in a drip-flow reactor with minor modifications. A four-channel Teflon Drip Flow Reactor (10 cm × 2.5 cm × 2 cm) was used to grow *Pseudomonas* sp. strain ADP biofilms. Briefly, cell cultures in exponential phase (OD_{600} > 0.2) from shake flasks were harvested by centrifugation (6000 x g, 10 min, 4^{o}C) and re-suspended in mineral medium (10 mL) containing atrazine (30 mg L^{-1}). Re-suspended cells were dispersed on Silane-coated microscope slides and incubated at 30^{o}C for 6-8 h in batch mode to allow for bacterial attachment. Mineral medium containing atrazine (30 mg L^{-1}) was transmitted by peristaltic pumps (rate of 0.8 mL min^{-1}) to flow over the slide surface with adhered bacteria until the biofilm reaches maturation (five days).

Temperature dependence and mode of growth

Biofilms were grown in the drip-flow reactor during continuous phase at three temperatures (25^{o}C, 30^{o}C, 37^{o}C) in a controlled incubator to determine the effect of temperature on mRNA levels of atrazine-degrading genes using RT-qPCR. Congruently, bacterial biofilms were harvested at full maturation (5 days) and planktonic cultures were harvested at exponential phase (30 h) and subjected to an RT-qPCR workflow to determine the effect of mode of growth on mRNA levels of atrazine-degrading genes.

RNA extraction and quantification

Optimization of extraction for RNA biofilms was achieved by modifications of two established methods. Both suspended cells and biofilms were subjected to the same extraction method to achieve consistency. Briefly, biofilms were scraped from each slide into centrifuge tubes (50 mL) containing Trizol reagent (2 mL). Biofilm suspensions and planktonic samples were vortexed briefly, then sonicated using a sterile probe for 10 s at medium-high output (pulse: 4/10 power, Sonic Dismembrator 550, Fisher Scientific, Waltham, MA). The insoluble material of each sample was removed by centrifugation (6,000 × g, 10 min, 4°C). The supernatant containing the RNA was extracted with the remaining Trizol according to the manufacturer's instructions. RNA precipitated from the isolation procedure was purified and DNase-treated using spin column purification (Qiagen RNeasy Mini Kit, Germany) and on-column enzyme treatment (Qiagen DNase-set, Germany), respectively. Bacterial RNA was quantified and measured for integrity using micro-spectrophotometry (Thermo NanoDrop, Waltham, MA) and capillary electrophoresis (Agilent Bioanalyzer, Santa Clara, CA). Samples containing RNA greater than 50 ng μL^{-1} and an RNA integrity number above 8.0 were used for reverse transcription reactions.

Reverse transcription (cDNA synthesis)

RNA samples were diluted to approximately 50 ng μL^{-1} before proceeding with reverse transcription. Samples were reverse transcribed using a high-capacity reverse transcription kit (Thermo Fisher, Waltham, MA). Briefly, 2 × RT master mix (10 µL) and the RNA sample (10 µL) were added to PCR tubes, mixed, and placed in a thermal cycler under the following conditions: 10 min at 25°C, 120 min at 37°C,

and 5 min at 85°C. Complementary DNA was stored at -20°C until quantitative PCR step. Samples containing kit components in the absence of the enzyme were used as negative controls.

Validation of primers

Prior to qPCR, validation of primer pairs was necessary for proper relative expression results derived from the ΔΔCt method. One target gene (*AtzA*) and an endogenous control (16s rRNA) were chosen to evaluate the efficiencies of the two PCR reactions. Complementary DNA (cDNA) was distributed in a 96-well plate, along with no template controls (NTC), no reverse-transcriptase controls (NRT), and concentrations of each primer pair (16s rRNA forward, 16s rRNA reverse, *AtzA* forward, *AtzA* reverse) spanning a range from 100 ng to 0.1 ng, three logarithmic, as illustrated in Table 3.1. Each lyophilized primer pair was re-suspended in RNase-free DNase-free water prior to each plate addition. The primer and probe concentrations were prepared at the recommended levels as indicated by applied biosystems.[75] Once cDNA samples were aliquoted with appropriate probes and primers on each plate, qPCR was run at conditions specified below and results were analyzed for amplification efficiencies. Each run was performed separately for RNA extracted from biofilms and planktonic *Pseudomonas* sp. strain ADP cells. Six replicates were performed for each standard-curve point.

Table 3.1. Sample 96-well plate for qPCR containing log-range span of endogenous control primer pair and experiment primer pair to evaluate amplification efficiencies. No template controls (NTC) and no reverse-transcriptase controls (NRT) are negative controls used for the qPCR validation experiment. Each (X) represents a well without cDNA or other qPCR components. Each numeric value represents the amount of cDNA in nanograms.

Plate Wells (96-well)												
	1	2	3	4	5	6	7	8	9	10	11	12
A	X	100	20	4	1	0.1	X	NTC	X	NRT	X	X
B	X	100	20	4	1	0.1	X	NTC	X	NRT	X	X
C	X	100	20	4	1	0.1	X	NTC	X	NRT	X	X
D	X	100	20	4	1	0.1	X	NTC	X	NRT	X	X
E	X	100	20	4	1	0.1	X	NTC	X	NRT	X	X
F	X	100	20	4	1	0.1	X	NTC	X	NRT	X	X
G	X	X	X	X	X	X	X	NTC	X	NRT	X	X
H	X	X	X	X	X	X	X	NTC	X	NRT	X	X

Quantitative PCR

Relative quantification RT-qPCR was chosen for the methodology to determine fold changes in expression within groups of temperature dependence and mode of growth. Validation experiments were performed for each primer pair of the target and reference gene to ensure efficiencies are approximately equal. The qPCR assays were the method of Devers et al. with minor modifications. For qPCR, 25 µL reactions were prepared in 96-well plates containing: 12.5 µL Power SYBR Green Master Mix (Thermo Fisher, Waltham, MA), 2.0 µL forward primer (10 µM), 2.0 µL reverse primer (10 µM), 5-fold diluted cDNA sample (12.5 ng), and nuclease-free water. No template controls were added to each plate. Each biological replicate (3×), reverse transcription replicates (2×), and technical replicates (3×) were run under the following qPCR conditions: 10 min at 95°C for enzyme activation, and 40 cycles of 15 s at 95°C, 15°C at optimal hybridization temperature, and 15 s at 72°C. Dissociation curves were performed for all qPCR assays. All RT-qPCR analysis was performed using ABI software. (Applied Biosystems ABI SDS version 2.4.1)

The ΔΔCt method was used to calculate the fold-difference between the calibration samples and experimental samples. In the temperature dependence group, the central temperature condition 30°C was chosen as the calibration sample. In the mode of growth group, the suspended cells were chosen as the calibration sample. The ΔCt values were calculated between the reference gene (16s *rDNA*) and the gene of interest (*AtzA, AtzB, AtzC, AtzD, AtzE, AtzF)*. All calibration samples were normalized to -1 and +1 to calculate the relative fold change in test conditions.

Growth of cyanuric acid as a sole-nitrogen source

To evaluate the growth of *Pseudomonas* sp. strain ADP on an alternate nitrogen source and metabolite, cyanuric acid was substituted in DSMZ medium in place of atrazine. The concentration of nitrogen in each source was kept constant to prevent confounding variables in growth rate comparison. Once growth on cyanuric acid as a sole nitrogen source on plates containing solid media was confirmed, P.ADP was grown in DSMZ liquid medium in a pre-inoculum overnight. The overnight culture was transferred to an Erlenmeyer flask (250 mL) with 50 mL of fresh medium. Cells were diluted to an OD_{600} of 0.05 using DSMZ containing cyanuric acid (30 mg L^{-1}). Measurements (OD_{600}) were taken each hour for the first 24 h, and then every 2-8 h for approximately 250 h. If cells exceeded an optical density of 0.4, culture was diluted, and the optical density was re-calculated according to the serial dilution. Cells were grown at 30°C and shaken at 250 pm in a shaker-incubator. Samples were taken in triplicate. Cyanuric acid in DSMZ was sonicated in prior to use for 60 s for increasing solubility and preventing erroneous spectrophotometric results.

Expression of AtzDEF in response to cyanuric acid

Cells grown on cyanuric acid as a sole nitrogen source and atrazine as a sole nitrogen source were harvested for nucleic acid extraction, cDNA synthesis, and qPCR. The expression of three atrazine-degrading genes in cyanuric acid grown cells was compared to the expression of three atrazine-degrading genes in atrazine grown cells as a baseline using the ΔΔCt method. Genes encoding for enzymes involved in the biotransformation of cyanuric acid to the remainder of the mineralization pathway were analyzed in triplicate using RT-qPCR. Growth conditions, nucleic acid extraction, reverse transcription procedure, and set up for qPCR are as described previously.

Growth of P.ADP under nitrogen sources

Growth of P.ADP was tested under the following as sole or dual nitrogen sources: urea, urea + atrazine, cyanuric acid, cyanuric acid + atrazine, and atrazine for a period of 66 h. Cell growth was measured spectrophotometrically with an OD_{600} assay as described previously. To prevent possible interference during spectrophotometric measurements due to low solubility of nitrogen sources, each source was sonicated until clear in medium. If optical density exceeded 0.5, cell culture was diluted 1:10 with blank medium. Growth medium consisted of DSMZ, which was autoclaved prior to the addition of glucose (1 g L^{-1}) and each of the five nitrogen sources (30 mg L^{-1}).

UV-Vis degradation assay under various nitrogen sources

Atrazine concentration was measured with UV-vis spectrophotometry at a wavelength of 225 nm, the absorbance maxima of pure atrazine (A_{225} assay) based on previously published literature with slight modifications.[36] Cell culture sample was centrifuged briefly to pellet cells, and the absorbance of the supernatant was

measured a single wavelength of 225 nm. This was performed in triplicate using quartz cuvettes to attain an accurate absorbance in the ultraviolet range. DSMZ medium containing atrazine, urea + atrazine, and cyanuric acid + atrazine was measured to evaluate the effect of additional nitrogen sources on atrazine degradation in planktonic P.ADP cells. The previously reported extinction coefficient for atrazine in DSMZ medium is 2.71×10^4 liter cm^{-1} mol^{-1}.[36]

Expression of atzABC by nitrogen source

To quantify gene expression of *atzABC*, the primary three genes involved in the biotransformation of atrazine to cyanuric acid, total RNA was extracted followed by cDNA synthesis and qPCR as in conditions described previously. The choice of nitrogen sources are based on previously published literature by Garcia-Gonzalez et al.[36] *Pseudomonas* sp. strain ADP cells grown on atrazine as sole nitrogen source were used a control and baseline for relative expression experiments. The control was measured quantitatively with reference to four conditions involving DSMZ with alternate nitrogen sources or combinations of nitrogen sources: urea, urea + atrazine, cyanuric acid, and cyanuric acid + atrazine. The concentration of nitrogen remained constant to allow for proper comparison of quantitative PCR data.

Statistical analysis

Following ΔΔCt analysis of RT-qPCR results, the relative fold-changes in expression underwent statistical treatment to evaluate significance of data. Experiments analyzing the expression of atrazine-degrading genes in *Pseudomonas* sp. strain ADP planktonic cells and biofilms, temperature dependent biofilm growth, and planktonic P.ADP growth on various nitrogen sources were analyzed for significance based on a Student's t-test at a level of $\alpha = 0.05$. Due to the use of

logarithmic scales in fold changes for qPCR analysis, error bars representing the 95% confidence intervals are adjusted and calculated as appropriate. Sample sizes in experiments are to be assumed n = 3 unless otherwise stated. No other statistical analyses were performed for gene expression results.

Results and Discussion

No difference in expression by mode of growth

The relative gene expression marginally decreased in biofilm cells compared to cells in the planktonic mode of growth for gene *AtzA*. The raw data showed what appeared to be an increase in expression levels of the biofilm mode of growth relative to planktonic cells over 2.0-fold for genes *AtzB* and *AtzC*. The remainder of the genes assayed, *AtzD*, *AtzE*, and *AtzF*, demonstrated moderate expression between 1.0 and 2.0-fold in biofilm mode of growth compared to the control planktonic condition of *Pseudomonas* sp. APD cells (Figure 3.2). The control condition is designated by a normalized expression of (+/-) 1.0 relative to increases (above abscissa) or decreases (below abscissa). Results and error under abscissa were calculated by taking the (-) inverse of the n-fold change to visually equate the represented bars. Overall, the expression of atrazine-degrading genes in biofilms relative to planktonic *Pseudomonas* sp. strain ADP cells were not found to be significantly different at a statistical p-value of 0.05 ($p = 0.2197$).

We chose to employ relative expression instead of quantitative expression as we are interested in comparing two modes of growth. This type of experiment has been performed to examine differences in gene expression between *Salmonella typhimurium* and *Staphylococcus aureus*, which aided in elucidating expression patterns of antibiotic-resistant pathogens. A method previously developed and

optimized by Devers regarding reverse transcription quantitative real-time PCR (RT-qPCR) for *Pseudomonas* sp. strain ADP cells was used for these studies. The negligible decrease in the expression of *atzA* in biofilms relative to free cells does not establish any novel insight. There is no sufficient evidence to suggest that there are significant changes in expression of atrazine-degrading genes and consequently increased or decreased catabolic activity of biofilm-associated cells with regards to contaminant degradation. The efficiency of our microbe of interest demonstrates similar catabolic activity in both biofilm and planktonic modes of growth based on mRNA levels alone.

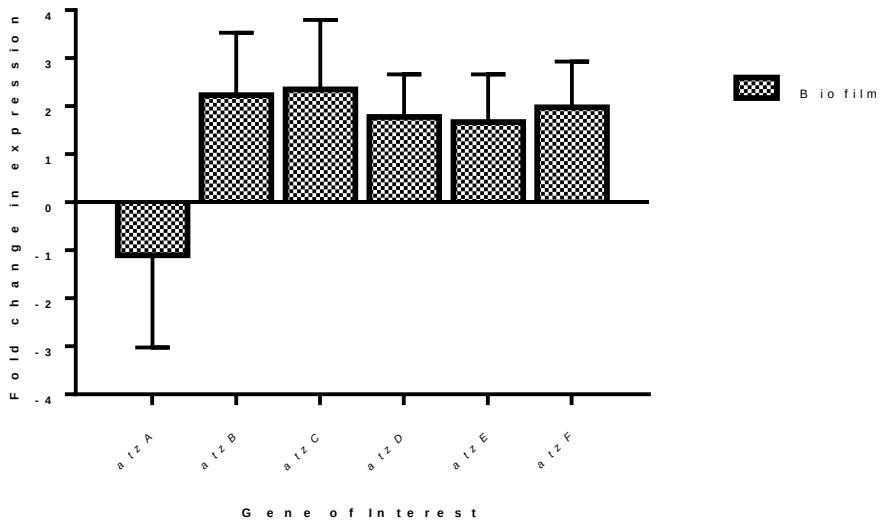

Figure 3.2. Expression of atrazine-degrading genes in *Pseudomonas* sp. strain ADP cells grown in biofilm mode of growth (experimental) relative to suspended planktonic mode of growth reported as n-fold changes. Error bars represent 95% confidence intervals. Baseline is represented by (+1/-1) dependent upon upregulation and downregulation of expression, respectively.

Regulation dependence on biofilm growth temperature

The atrazine-degrading genes assayed for *Pseudomonas* sp. strain ADP biofilms under varied temperature conditions (25°C, 30°C, and 37°C) demonstrated differential expression as illustrated in Figure 3.3.

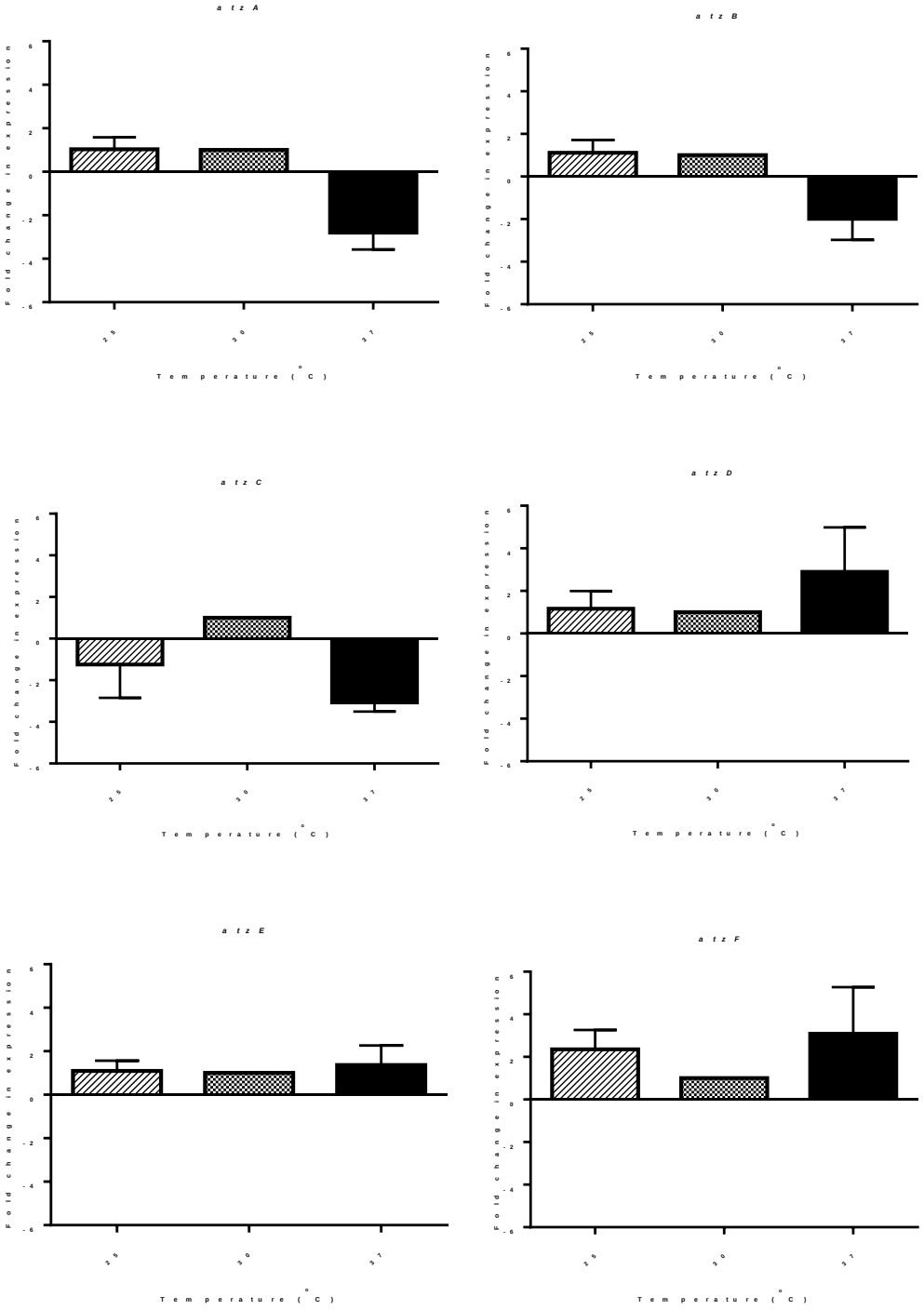

Figure 3.3. Expression of atrazine-degrading genes in *Pseudomonas* sp. strain ADP biofilms measured by growth temperature. Temperature of 30°C (control)was used a baseline for relative expression experiments to temperatures 25°C and 37°C (experimental). Error bars represent 95% confidence intervals for non-control conditions. Baseline temperature is set at a fold change of 1, downregulation is designated as bars below 0, and upregulation is designated as bars above 0-fold-change.

For the first two atrazine-degrading genes, *AtzA* and *AtzB*, expression was decreased considerably for biofilms grown at 37°C relative to the control condition (30°C). *Pseudomonas* sp. strain ADP biofilms grown at 25°C, however, demonstrated relatively negligible changes in expression. Gene *AtzC* decreased in expression for both experimental temperature conditions, but more noticeably for 37°C grown biofilms. The three remaining genes, *AtzD*, *AtzE*, and *AtzF*, exhibited approximately 3.0-fold, 1.5-fold, and 3.0-fold increases in expression for biofilms grown at 37°C relative to the control condition, respectively. Minor increases in expression were also observed for 25°C for genes *AtzD* and *AtzE*, however, *AtzF* revealed over a 2.0-fold increase for the same growth temperature. The difference in expression of atrazine-degrading genes in *Pseudomonas* sp. strain ADP biofilms was not significantly different between biofilms grown at 25°C and 30°C at a p-value of 0.05 ($p = 0.8717$), nor between biofilms grown at 37°C and 30°C ($p = 0.3748$).

In the natural environment, temperature is varied according to season, and for industrial systems, the temperature of biofilm reactors can be controlled. Previously, it has been reported that for every rise in 10°C, the rate of degradation of the pollutant toluene increased nearly 2-fold in soil and water.[76,77] In *Pseudomonas* sp. strain ADP biofilms, decreasing the temperature from 30°C to 25°C resulted in no differential expression and from a genetic perspective, has no increase or decrease in functional gene products that may exhibit higher or lower catabolic potential. After increasing the temperature of biofilm growth to 37°C, the decreased expression of the initial 3 genes (*AtzA*, *AtzB*, and *AtzC*) could point toward either I) a decrease in catabolic activity of transformations of atrazine to cyanuric acid II) loss of genes *AtzA*, *AtzB*, and *AtzC* as they have greater instability on the plasmid pADP-1 compared to

the latter genes in the pathway, or III) increased temperature causes pathway regulatory elements for the initial three genes to decrease in overall mRNA levels. Interestingly, the increase in expression of the remaining three genes (*AtzD*, *AtzE*, and *AtzF*) could help elucidate the regulation of the catabolic pathway with regards the cyanuric acid degradation. If the temperature of biofilm growth is increased to 37°C, this could ensure stability of the operon-like gene set *AtzDEF* on the plasmid, pADP-1 and degrading the intermediates from cyanuric acid to allophanate at increased rates from higher enzymatic activity. This assumption is partly speculative as relative mRNA levels do not perfectly correlate to the production of functional enzymes, and rates of metabolic degradation.

After monitoring atrazine degradation, for 30°C, the control, and 37°C, in *Pseudomonas* sp. strain ADP biofilms, after a period of five days both resulted in the disappearance of atrazine to 12 mg L^{-1} (30°C) and 5 mg L^{-1} (37°C). The characteristic increase in the higher temperature condition, like the previous biofilm degradation curve, may be a result of atrazine trapped within the extracellular polymeric substances, followed by degradation and release. At the end of monitoring period and growth of the biofilms, a greater proportion of atrazine was not detectable by GC/MS for the biofilm grown at 37°C. This phenomenon could be the basis for design of reactor systems with temperature-controlled remediation. Furthermore, in the state of Iowa and Illinois where atrazine contamination is prevalent, biofilms forming the surrounding community that include *Pseudomonas* sp. strain ADP may be able to more effectively degrade atrazine in seasons where the local temperature of the microenvironment increases to 37°C. This may occur, for example, in Iowa where

near-surface soil conditions can reach average temperatures from 25°C to 33°C in mid-summer.

Growth and expression of P.ADP on CYA as sole nitrogen source

Cyanuric acid, a metabolite of atrazine degradation, was used as an alternative sole nitrogen source for *Pseudomonas* sp. strain ADP growth and metabolism. Once growth was validated via streak plates of bacterial cells on plates containing mineral medium (500 mg L^{-1} cyanuric acid) with evident clearing zones and microbe proliferation, a similar growth curve was conducted (Figure 3.4a) over a period of approximately 100 h. A short lag phase, log phase, and beginning of stationary phase are demonstrated from the origin to end. The growth rate of *Pseudomonas* sp. strain *ADP* cells in liquid mineral medium containing cyanuric acid (30 mg L^{-1}) is approximately one-half the growth of rate of cells in medium containing atrazine (30 mg L^{-1}) in exponential phase.

In our studies, *Pseudomonas* sp. strain ADP cells followed a prototypical growth curve when grown on atrazine or cyanuric acid as their sole nitrogen source. It has been previously reported that *Pseudomonas* sp. strain ADP could utilize a metabolite of its catabolic pathway, cyanuric acid, as source for growth and survival. The bacterial isolate has also demonstrated growth on the synthetic herbicide, atrazine. Our results demonstrate the relative growth rates of *Pseudomonas* sp. strain ADP on each nitrogen source, with the exponential phase on atrazine (OD_{600} of 0.18 at t = 20 h) reaching almost double the rate of growth on cyanuric acid (OD_{600} of 0.10 at t = 20 h) using the same concentrations of each substrate. This may demonstrate the plasmid, pADP-1, containing the genes encoding for the catabolic

enzymes, is more efficient for cellular growth when the cells are able to utilize the initial substrates on the regulated pathway.

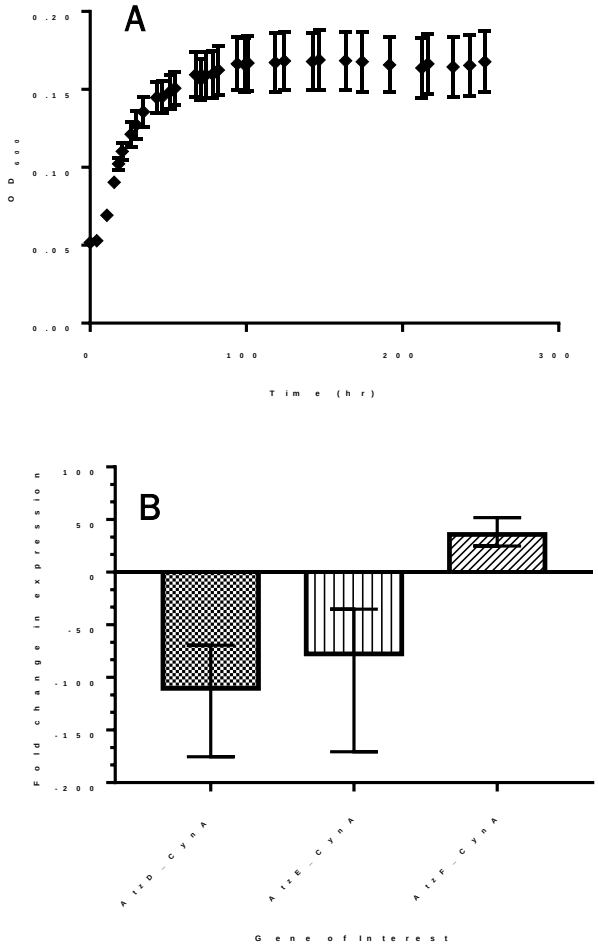

Figure 3.4. Figure a (top) represents the growth curve of *Pseudomonas* sp. strain ADP on cyanuric acid as a sole nitrogen source over a period of approximately 250 h. Error associated is represented as positive and negative bars representing 95% confidence intervals, with n = 3. Figure b (bottom) displays the n-fold changes in expression of atrazine-degrading genes *AtzDEF* in *Pseudomonas* sp. strain ADP planktonic cells grown on cyanuric acid relative to cells grown on atrazine at 30 mg L^{-1} as a sole nitrogen source. Error bars represent 95% confidence intervals. Baseline is at zero (atrazine) with each bar representing the change for cyanuric acid-grown cells.

The expression of genes on the operon *AtzDEF* were subjected to RT-qPCR in *Pseudomonas* sp. strain ADP cells grown with atrazine and cyanuric acid as their sole nitrogen sources. Atrazine as a sole nitrogen source was set as the control condition relative to the expression of cells grown on cyanuric acid as sole nitrogen source

(Figure 3.4b). Genes *AtzD* and *AtzE* were heavily downregulated (110-fold downregulation in *AtzD* and 76-fold downregulation in *AtzE*), but with large variability between samples (n = 3). No significant difference was determined in the expression of genes *AtzD* and *AtzE* in cyanuric acid grown cells relative to atrazine grown cells. Conversely, 25-fold upregulation was quantified in gene *AtzF* in cyanuric acid grown cells, which was found to be statistically significant in the relative expression experiments according to Student's t-test with at $\alpha = 0.05$.

The operon *AtzDEF* encodes for the enzymes completing the biotransformation from cyanuric acid to carbon dioxide and ammonia. No statistically significant difference in regulation of *AtzD* and *AtzE* from RT-qPCR results suggest the substrate cyanuric acid enters the same pathway as the metabolite from the atrazine degradation pathway. The gene *AtzF,* which encodes for the biotransformation from allophanate to the final mineral components carbon dioxide and ammonia.

Downregulation of *AtzD* and *AtzE* in cyanuric acid grown cells relative to atrazine grown cells may signal increased accumulation and conversion of cyanuric acid to allophanate (*AtzD*) and allophonate to biuret (*AtzE*) in the main atrazine-degradation pathway compared to the separate addition of cyanuric acid. However, the results for these two genes are not statistically significant to demonstrate a decrease, which may indicate no difference between the expression of *AtzD* and *AtzE* for planktonic cells grown on atrazine compared to cells grown on cyanuric acid as a sole nitrogen source. This suggests the addition of cyanuric acid as substrate may enter the same degradation pathway as atrazine at a downstream location on the *AtzDEF* operon, rather than a separately utilized pathway. A separate pathway for cyanuric acid degradation activity would produce statistically significant

downregulation in all three genes, as each metabolite would be subsequently transformed outside of the pADP-1 plasmid.

In contrast, the 35-fold increase in expression for gene *AtzF* in cyanuric acid grown cells compared to atrazine grown cells is statistically significant due. The biotransformation encoded by this gene involves the conversion of biuret to carbon dioxide and ammonia. A plausible explanation for the increase in expression for cyanuric acid-grown cells is an accumulation of biuret from the addition of cyanuric acid substrate from increased stoichiometric amounts of compound compared to the initial addition of atrazine. Alternatively, the catabolic activity of *AtzF* may have decreased for atrazine-grown cells from an upstream chemical inhibitor that could form from metabolites upstream of cyanuric acid. These may cause a decrease in the activity of the final enzyme as a feedback-inhibition mechanism for the degradation pathway.

Genes *AtzD* and *AtzE* are regulated differently than *AtzF* as suggested by the great amount of variance in gene expression in either case. *AtzD* and *AtzE*, which encode for the enzymes transforming from cyanuric acid to biuret, and biuret to allophanate, respectively are located on the same operon as *AtzF*, which regulates the biotransformation from allophanate to carbon dioxide and ammonia. However, the addition of extraneous cyanuric acid may cause an increase in the conversion of allophanate to mineral components and slow down catabolic activity of the former two conversions (*AtzD* and *AtzE*). It is unclear why there may be a mechanism of regulation in P.ADP to increase catabolic activity in the last step, but alternate pathways may be available within the cell to utilize cyanuric acid as sole nitrogen source that do not have to rely on *AtzD* and *AtzE*. A homologous *AtzF* gene may be

located outside the plasmid, pADP-1, and increase the conversion of allophanate to carbon dioxide and ammonia to a small degree compared to atrazine degradation.

In soil and water, there are often many bioavailable sources of nitrogen for bacteria to uptake and use for their primary growth substrate. In bioremediation, this could potentially lessen the effectiveness of *Pseudomonas* sp. strain ADP as a degradation agent if the bacterium is using alternate sources of nitrogen, such as urea or ammonium nitrate, as a source for growth and metabolism, rather than the target pollutant atrazine. The growth of *Pseudomonas* sp. strain ADP on various sole and dual nitrogen sources is displayed over a span of 66 h by an indirect method of spectrophotometry at 600 nm. (Figure 3.5)

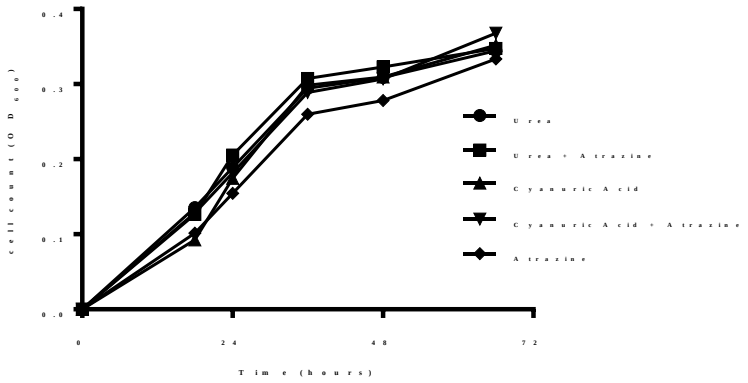

Figure 3.5. Growth curves of *Pseudomonas* sp. strain ADP under the following sole or dual nitrogen sources: urea (●), urea + atrazine (■), cyanuric acid (▲), cyanuric acid + atrazine (▼), and atrazine (♦). Measurements up to 66 h, ranging from an optical density (OD_{600}) 0.05 to 0.4.

The growth of *Pseudomonas* sp. strain ADP demonstrates a clear logarithmic phase and the beginning of stabilization to a stationary phase. The cells were pre-inoculated with the nitrogen sources at an indicated concentration, which had effectively eliminated any sign of a lag phase in the growth curve. Sole and dual nitrogen sources were tested to evaluate the growth rate of P.ADP under both richer

sources of nitrogen for the cells to uptake along with the pollutant of interest. Previous data demonstrates increased rate of growth on richer nitrogen sources, such as urea and ammonium nitrate.[36] LB, for example and as previously noted, supports rich growth for P.ADP well above both ammonium nitrate and atrazine. Over a period of 66 h, the growth of P.ADP on each sole and dual nitrogen source is relatively unchanged. Atrazine as a sole nitrogen source demonstrates a slightly lower rate of growth overall. The cause of this phenomenon may be the result of atrazine's complex structure and the most difficult source of nitrogen for P.ADP to uptake compared to cyanuric acid and urea, which may be a result of atrazine's lower bioavailability compared to alternate nitrogen sources and defined media. The dual nitrogen source conditions with atrazine, conversely, have the availability of urea and cyanuric acid as a source for P.ADP to support growth outside of the degradation pathway.

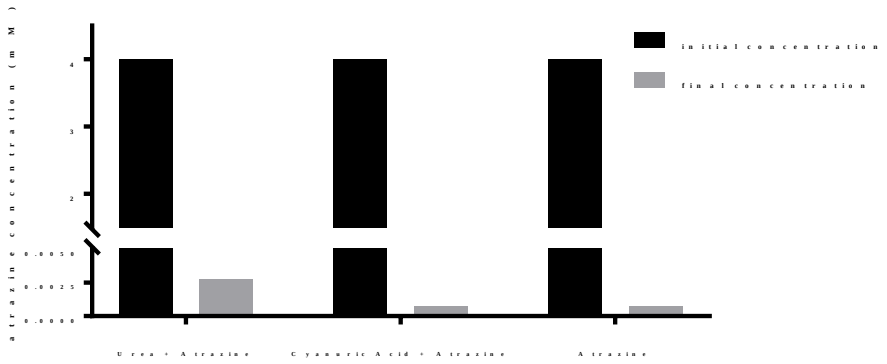

Figure 3.6. Spectrophotometric determination of atrazine remaining after *Pseudomonas* sp. strain ADP planktonic cells (A_{225}) growing on one of the following sole or dual nitrogen sources: urea + atrazine, cyanuric + atrazine, and atrazine. After 66 h, the final concentration was reported as above in each bar (grey) compared to the initial concentrations represented in each bar (black).

Complementary A_{225} data was collected to measure atrazine degradation by *Pseudomonas* sp. strain ADP in a cell assay by spectrophotometry (Figure 3.6). Atrazine possesses a high amount of conjugation due to its physical heterocyclic

structure and demonstrates an absorbance in the UV range at 225 nanometers. Therefore, to measure the presence of atrazine in a sample, the absorbance at 225 nm is recorded and related to concentration of the herbicide by a previously determined extinction coefficient ($\varepsilon = 2.71 \times 10^{-4}$ L^{-1} mol cm^{-1}) and pathlength of the cell (b = 10 mm). Quartz cuvettes were used in this experiment due to the compound of interest falling in the ultraviolet range of light.

In this experiment, substantial amounts of atrazine (4 mM) were used in the 66 h period to evaluate degradation in the presence of other nitrogenous compounds and in the condition with solely atrazine as source of nitrogen. As displayed in Figure 3.6, in the growth medium containing both urea and atrazine, atrazine concentration decreased to 0.0025 mM after 66 h. Meanwhile, in the growth condition with medium containing both cyanuric acid and urea as a nitrogen source, the concentration of atrazine decreased to a negligible amount. In the same manner, a negligible amount of atrazine was detected by the A_{225} assay in the condition of P.ADP cells grown on DSMZ medium with atrazine (4 mM) only. Normally, in non-competing nitrogen sources, it is expected after 66 h for atrazine would be undetected in all conditions.

Previous studies indicate P.ADP grown in similar conditions with the same concentration of atrazine was able to degrade atrazine completely in 24 h.[35,36] The growth rate and degradation of atrazine in the presence of cyanuric acid is a special case, where most atrazine was degraded despite the additional nitrogen source. This observation is speculated to be due to the specific positive effect exerted by cyanuric acid on the atrazine degradation pathway followed by *Pseudomonas* sp. strain ADP.[78] Atrazine as a sole-nitrogen source and as a dual nitrogen source with cyanuric acid, is

metabolized by P.ADP in 66 h as indicated by the spectrophotometric assay. Urea, conversely, appeared to have an inhibitory effect on the degradation of atrazine when used as a dual nitrogen source. Despite comparable growth rates of urea + atrazine to other conditions, the urea case only metabolized atrazine to approximately 0.0025 M. This suggests urea may be a rich, and more bioavailable source of nitrogen to P.ADP for growth and metabolism even in the presence of atrazine. The atrazine degradation pathway is repressed in the presence of more bioavailable source of nitrogen the cells can uptake readily. Cyanuric acid, and possibly other downstream metabolites in the pathway, may have a net neutral or positive effect on atrazine degradation due to upregulation of the main six atrazine-degrading genes.

Similar experiments to this have been performed in soil with many alternate nitrogen sources but failed to provide data of atrazine degradation in water.[43,53,78,79] This is a key component as atrazine may be transported to groundwater and drinking water in the presence of these nitrogenous compounds. To further explore these phenomena, expression data regarding the primary three atrazine degrading genes in the pathway was obtained for each nitrogen source as displayed in the Figure 3.7. The latter three genes on an operon, *AtzDEF*, have been previously studied by Garcia-Gonzalez.[36,43,82]

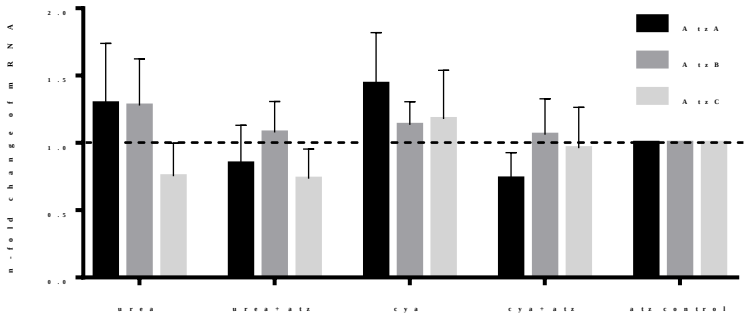

Figure 3.7. Expression of atrazine-degrading genes in *Pseudomonas* sp. strain ADP planktonic cells on various sole or dual nitrogen sources (urea, urea + atrazine, cyanuric acid, cyanuric acid + atrazine) relative to atrazine as a sole nitrogen source. Error bars represent 95% confidence intervals. Atrazine is illustrated with a baseline of 1-fold change as the control condition, with other nitrogen sources reported as upregulation (values greater than 1) and downregulation (values less than 1).

The strongly regulated gene set *AtzDEF* have been thoroughly researched with regards to their cyanuric acid transport system, nitrogen regulation, and putative elements of Lys-R type regulator.[3,42,79,80] Conversely, under the same conditions, the constitutively expressed *AtzA*, *AtzB*, and *AtzC* have been relatively unexplored. In the figure above (Figure 3.7), the expression of *AtzABC* was evaluated for cells grown on atrazine (baseline control) to cells grown on alternate nitrogen conditions. The expression data complement the A_{225} assay and growth curves of P.ADP under various sources of nitrogen containing compounds. As such, the concentration of atrazine remained at an increased level of 4 mM. This concentration allowed for an abundance of total mRNA to be extracted from cells and allowed for adequate comparison of expression and growth data from previously published literature.

The expression data represents the n-fold changes in expression from atrazine degrading genes *AtzABC* in a normalized relative experiment with 16s rRNA as the housekeeping gene. The primary three genes encode for the biotransformation of atrazine to hydroxyatrazine (*AtzA*), hydroxyatrazine to n-ispropylammelide (*AtzB*), and

n-isopropylammelide to cyanuric acid (*AtzC*). Atrazine is illustrated with a baseline of 1-fold change as the control condition, with other nitrogen sources reported as upregulation (values greater than 1) and downregulation (values less than 1). Error bars larger than the n-fold change in expression of the baseline are negligible and considered to not have any statistical significance.

The fold change in expression of atrazine-degrading genes in P.ADP grown with a sole nitrogen source of urea relative to a sole nitrogen source of atrazine is the same, as the up- and downregulation are not statistically significant when error is factored in the results. This may be due to the small sample size (n = 3) or may be interpreted as effectively no change in expression. If we take the latter conclusion, we may interpret the results. Cyanuric acid does not enter the degradation pathway until gene *AtzD*, which is downstream of any of the genes analyzed.[81,82] It would be expected for *AtzABC* to all be significantly downregulated in the presence of cyanuric acid compared to the control condition of atrazine. The enzymes would not have any atrazine to degrade, and therefore no catabolic activity should be present when cyanuric acid is the sole nitrogen source. To rationalize this result, the unchanged expression must be since the primary three genes have been demonstrated to be expressed in a constitutive manner. This means genes *AtzA*, *AtzB*, and *AtzC* are transcribed at a relatively constant level regardless of the cell conditions and substrates present for metabolism. Despite this fact, the endeavor is not futile as expression is able to increase beyond the baseline constitutive level as verified by Devers by the addition of an increased concentration of atrazine.[3] In the expression of atrazine-degrading genes in planktonic cells, Devers suggested genes *AtzA*, *AtzB*, and *AtzC* are constitutively expressed whereas *AtzD*, *AtzE*, and *AtzF* are expressed in

response to atrazine treatment. In the experiments performed, the expression of genes *AtzA*, *AtzB*, and *AtzC* were analyzed under alternate nitrogen sources (to solely atrazine) for growth.[3]

Expression of *AtzA*, *AtzB*, and *AtzC* did not change in response to the use of urea as a source of nitrogen relative to cells grown on atrazine. The degradation pathway does not contain genes that encode for enzymes capable of performing a biotransformation on urea.[44] Rather, urea is an alternate nitrogen source that can be used outside of the genes located on plasmid pADP-1. The unchanged expression suggests a constitutive level of expression may be occurring, just as was occurring in the cyanuric acid grown cells.

Two specific cases resulted in n-fold changes of significance. Gene *AtzC* was downregulated in urea + atrazine grown cells relative to atrazine grown cells (0.75-fold change), and gene *AtzA* was downregulated in cyanuric acid + atrazine grown cells relative to atrazine grown cells (0.60-fold change). Since *AtzC* encodes for the enzyme that aids in the biotransformation of n-isoproylammelide to form cyanuric acid, urea may interfere with catabolic activity of atrazine degradation. Urea and atrazine are being metabolized as sources of nitrogen, and therefore a certain amount of atrazine is not metabolized compared to the condition where atrazine is the sole nitrogen source. This is supported by the A_{225} data in which atrazine Is present at 0.0025 mM in the case of dual nitrogen sources (urea + atrazine). Constitutive expression of *AtzC*, along with a small amount of repression from the addition of urea, may be happening. The expression of genes *AtzA* and *AtzB* may result from active catabolic activity occurring prior to uptake of urea. This suggests

urea may not be used as a nitrogen source as readily until atrazine is transformed to cyanuric acid.

The latter case, downregulation of *AtzA* in cells grown on cyanuric acid and atrazine compared to solely atrazine, may be a result of complex nitrogen regulation and constitutive expression. The gene *AtzA*, which encodes for the initial transformation of atrazine to hydroxyatrazine, is also constitutively expressed. In this case, the cells may express *AtzA* at a lower level when atrazine and cyanuric acid are provided as dual sources of nitrogen. This may be due to the activity of *AtzD* inhibiting the pathway as type of feedback inhibition from the additional cyanuric acid added to the growth medium. Consequently, this would cause a slower rate of conversion of atrazine to hydroxyatrazine when dual sources are used which include a metabolite from the degradation pathway. This phenomenon may also affect *AtzB* and *AtzC*, but to a lesser extent and not to a level of statistical significance with a small pool of samples.

Conclusion

Expression of atrazine-degrading genes has been a relatively unexplored area in *Pseudomonas* sp. APD biofilms, and to a lesser extent, planktonic cells. The expression of atrazine-degrading genes did not change significantly by altering the mode of growth (biofilm and planktonic) of P.ADP. This suggests the catabolic activity of the strain does not change whether it is grown as a biofilm or as planktonic cells. However, efficiency of biodegradation and contaminant removal is not fully understood until analytical chemical methods are employed.

Additionally, it was determined that growing P.ADP biofilms at higher temperatures has a significant effect on changing catabolic activity. For the primary three genes, encoding for the degradation from atrazine to cyanuric acid, metabolism is downregulated at elevated temperatures. Conversely, the genes encoding for the downstream degradation of cyanuric acid to ammonia and carbon dioxide, metabolism is upregulated with an increase in biofilm growth temperature. These results will aid in bioreactor design with specific temperature control for optimization for *ex situ* bioremediation applications.

Several additional experiments on gene expression have been performed regarding *Pseudomonas* sp. strain ADP in its planktonic form. P.ADP grew at approximately the same rate, regardless of nitrogen source identity and duality. However, nitrogen sources not part of the atrazine-degradation pathway demonstrated an inhibitory effect on the metabolism of the model pollutant to a moderate extent. Due to constitutive expression of the primary three genes, it was difficult to obtain remarkable results concerning genes *AtzA*, *AtzB*, and *AtzC* in response to cells grown on various sole and dual sources of nitrogen. In Chapter 4, we establish confocal laser scanning microscopy and scanning electron microscopy as powerful tools to aid us in further characterizing *Pseudomonas* sp. strain ADP biofilms and planktonic cells.

CHAPTER 4: MICROSCOPY TO CHARACTERIZE *PSEUDOMONAS* SP. ADP BIOFILMS

Introduction

Microscopy is a powerful tool in characterization of novel bacteria and evaluating their metabolic properties via means of gene expression.[83–85] By using simpler surface methodologies such as scanning electron microscopy (SEM), one can further understand biofilm physiology and evaluate surface and physical characteristics not possible to visualize by destructive techniques. Some strains in the biofilm mode of growth, such as *Streptococcus mutans* and *Pseudomonas fluorescens*, have been successfully visualized with SEM. The latter strain was further characterized by closely examining the three-dimensional organization consisting of stratified, morphologically-distinct layers of extracellular material.[86,87] In addition, microscopy has been used as a genetic tool to understand mechanisms such as biofilm maturation and dispersion in remediation and pollutant relevant strains. Starvation-induced dispersion in *Pseudomonas putida* biofilms, capable of toluene degradation, was discovered to be dependent upon the gene PP0164 and the *LapG* gene product.[88]

Despite the rapid success of such discoveries, it is of utmost importance to develop a method for visualizing the expression of genes in planktonic cells and biofilms for a variety of possible applications. Real-time confocal laser scanning microscopy combined with a gene expression technique would allow for pollutant monitoring in real-time for chemical engineers. Furthermore, the method could be extended past bioremediation applications, and have a purpose in biofilms relevant in the medical and dental industries. Biofilms frequently attach to medical implants and may be manifested as plaque. Monitoring the expression of genes responsible

for biofilm formation, biofilm dispersion and proliferation would aid in further understanding of the genetics and physiology of model biofilm organisms. A novel approach to exploring the expression of genes in biofilms using a microscopic approach is deemed In Situ Reverse Transcription (ISRT).

This methodology has been implemented sparingly in a variety of areas in biomedical and environmental research, but has profound potential once optimized as evidenced by previous published work.[59,89,90] Traditional In Situ Hybridization approaches (ISH) are often unreliable because they rely on multiple targets in the bacterium to provide a detectable signal above noise and are hindered by the small number of rRNA molecules in naturally-grown bacteria.[59] Similarly, in situ PCR has been developed, however this only allows for detection of gene presence, unlike protocols that involve a reverse transcription step. In Situ Reverse Transcription, conversely, does not rely on increasing signal by amplification, but rather from using labeled nucleotides. A single primer binds to RNA and the primer is extended by reverse transcriptase in the presence of fluorescently labeled nucleotides. This provides an advantage for even bacteria that have a low copy number for RNA.[59]

Previous published literature has utilized methods such as competitive quantitative PCR and oligonucleotide microarrays to monitor bioremediation of benzene, toluene, naphthalene, and biphenyl.[91,92] In our approach, we have initially attempted to optimize an ISRT-based technique for planktonic *Pseudomonas* sp. strain ADP cells and biofilms. Other methods explored for evaluating the expression of atrazine-degrading genes in P.ADP were red/green fluorescent protein fusions, and DIG-antibody labeling for increasing signal strength. A potential disadvantage to development and adaptation of a method for monitoring gene expression lies at the

base of our strain P.ADP. Specific model strains, including *Escherichia coli* , *Pseudomonas aeruginosa*, and *Pseudomonas putida*, have optimized methodologies and sequencing at disposal due to intensive research previously performed. The former strains mentioned have robust DIG-antibody protocols and GFP approaches that are simplistic to implement for visual expression results.

Scanning Electron Microscopy (SEM) and Confocal Laser Scanning Microscopy (CLSM) are two microscopy approaches that may be used to further characterize strain *Pseudomonas* sp. ADP biofilms and their role in bioremediation. Biofilms and free cells may be differentiated from each other on a physiological, surface level using SEM. Whereas planktonic cells lack an extracellular matrix and polymeric substances altogether, biofilms are characterized by a complex structure and network on monosaccharides, polysaccharides, nucleic acids, proteins, water, and other substances secreted by bacteria once surface attachment has been established.

Previous SEM data on P.ADP biofilms correlated to Raman data have provided a baseline for characterization, however, more analysis at a deeper level will aid us in understanding the behavior and peculiar properties of the pollutant-degrading strain in the natural environment.[9] To our knowledge, the distribution of monosaccharides in P.ADP biofilms when grown on medium containing atrazine and a nutrient rich medium has been previously studied. Fluorescent lectin binding analysis (FLBA) has been employed in a variety of biofilm-forming organisms, including lotic biofilms and cyanobacteria-dominated films (tufa-associated).[93,94] Using FLBA with various glyco-conjugates of dyes capable of binding to specific monosaccharides, sugar composition and distribution was able to be determined. Increasing the number of

lectins screened to evaluate the sugar composition allowed for deconvolution of data, since few lectins can bind to a single sugar, such as fucose. In addition, the use of multiple dyes may provide more channels for simultaneous lectin binding for added specificity. Qualitative and quantitative determination is a small subset of biofilm characterization, but nonetheless provides researchers with a deeper understanding of their potential for bioremediation in the field of environmental biotechnology.

To complement non-visual gene expression and growth data attained, microscopy is applied to *Pseudomonas* sp. strain ADP for further characterization and contribution of the extracellular polymeric matrix to remediation of atrazine is carefully considered and evaluated. Development and optimization of a method to visualize the expression of atrazine-degrading genes in real-time using confocal laser scanning microscopy is the primary goal. This is done to aid in the development of future environmental monitoring applications and estimate the distribution and timescale of the expression within the biofilm using a visual technique.

Alternate gene expression methods, including qPCR, DNA microarrays, and RNA-seq, provide useful and quantitative data but are destructive and deficient in visualization. Visualizing *Pseudomonas* sp. strain ADP on the surface via SEM, the expression of genes and presence of specific monosaccharides via confocal laser scanning microscopy, assist in the overarching goal of genetic and physical characterization of our strain for differentiation in the biofilm and planktonic mode of growth. Once gene expression data in non-visual quantitative and visual qualitative forms is gathered, analytical chemistry methodologies may be used to assist in

evaluating the overall biodegradation efficiency of *Pseudomonas* sp. strain ADP biofilms.

Materials and Methods

Optimization of ISRT

Materials and methods for the following protocol are divided into subsections adapted from Chen et al.[59] A schematic of the protocol, with modifications, is illustrated below in Figure 4.1

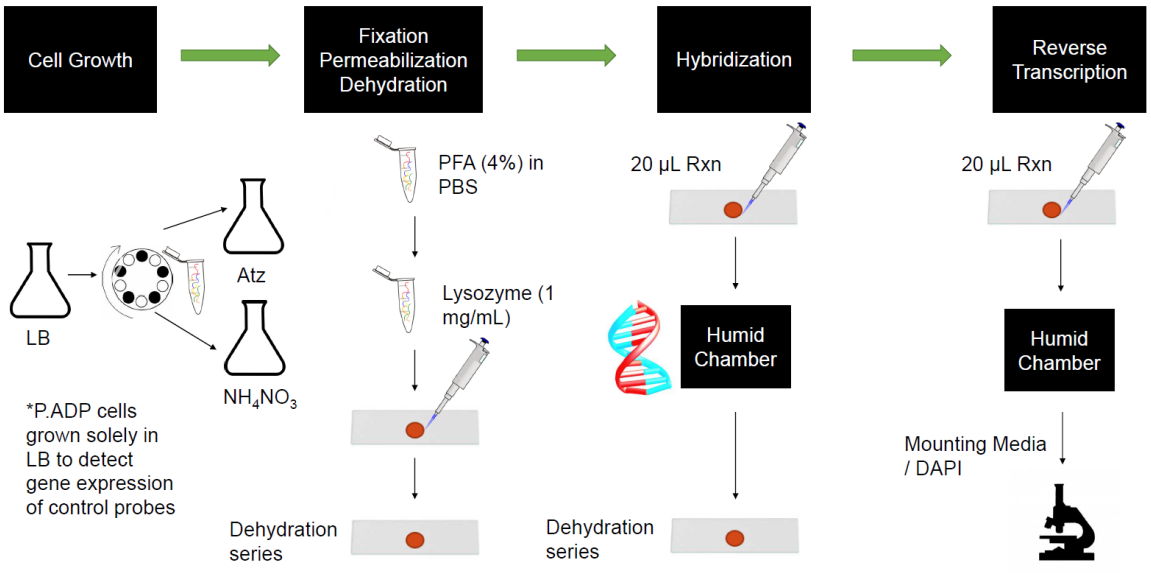

Figure 4.1. A schematic of In Situ Reverse Transcription (ISRT), from initial cell culture of *Pseudomonas* sp. strain ADP cells and *Escherichia coli* DH5α in LB medium.

Prior work for RNA preparation for ISRT

Due to the fastidious nature and insurmountable instability of ribonucleic acid, proper precautions were used prior to the start of In Situ Reverse Transcription as recommended by previously published guidelines.[75,95] All water used in the following experiments was either purchased as DNAse RNAase Nuclease and Pyrogen Free Water from Thermo Fischer Scientific (Waltham, Massachusetts), or was treated with diethyl pyrocarbonate (DEPC). All glassware was thoroughly rinsed and baked in an

oven at 240°C overnight. Alternatively, time permitting, glassware was treated with diethyl pyrocarbonate. All plasticware and plastic tools used protocols were purchased unopened and sterile. Biosafety fume hood was repeatedly washed with RNAse Away Decontamination Reagent, purchased from Thermo Fisher Scientific (Waltham, Massachusetts). Sterile nitrile gloves were used prior to handling samples containing RNA and were frequently changed during protocols. All chemicals used in RNA isolation and analysis were kept in separate areas from chemicals not used in RNA procedures. All pipettors were thoroughly washed with RNAse Away Decontamination Reagent and used with sterile aerosol-free pipette tips.

Atrazine-degrading system and growth of planktonic cells

Frozen stock of *Pseudomonas* sp. strain ADP and model strain *Escherichia coli* DH5α were thawed and streaked onto plates containing LB medium to achieve sufficient growth. Single colonies were picked from respective plates and inoculated into 10 mL of LB medium in two separate Erlenmeyer flasks (125 mL). Each condition was performed in triplicate. Cell cultures were grown overnight at 37°C and 250 rpm. Once OD_{600} was measured at a density between 0.5-1.0 following appropriate dilutions, cells were passed to fresh LB medium. Bacterial cultures were further grown for 6-12 h, or until reaching mid-exponential phase. Cell cultures were centrifuged at 6,000 x g for 10 min at room temperature. To maintain\ osmotic balance between internal and external environment of the cells, phosphate-buffered saline (PBS) was used to wash cells, twice, in 1 mL aliquots. The supernatant containing phosphate-buffered saline was removed, leaving only the cellular pellet. The cell pellet was then re-suspended in PBS (1 mL) and spun in vortex for 30 s to dislodge cell pellet. A small aliquot (10 µL) was removed from the suspension and

inoculated in one of four conditions: A) *Pseudomonas* sp. strain ADP cells in LB medium, B) *Pseudomonas* sp. strain ADP cells in ammonium nitrate medium, C) *Pseudomonas* sp. strain ADP cells in DSMZ medium containing atrazine, and D) *Escherichia coli* DH5α cells in LB medium. In each case (A-D), cell cultures were incubated at 37°C and spun at 250 rpm for 48 h.

Fixation

Cell growth was monitored spectrophotometrically. Cell cultures were removed from incubation at an OD_{600} above 0.5, indicating sufficient growth for fixation to occur. Bacteria were centrifuged at 6000 x g for 10 min at room temperature. Supernatant was removed, and cells were washed twice with PBS (1 mL). Cells in each condition were fixed in paraformaldehyde solution for three h at room temperature. Following fixation, fixative was removed by decanting and subsequent pipetting. Cell pellets were washed twice with PBS (1 mL), and remaining PBS was discarded leaving the cellular pellets. Pellets were re-suspended in ethanol (50% in PBS). Samples were aliquoted in 100 µL portions and stored at -20°C.

Paraformaldehyde solution (4% in PBS)

Paraformaldehyde solution for fixation was prepared as previously described by Cold Spring Harbor.[96] Briefly, EM grade paraformaldehyde (4 g) was added to deionized distilled water (50 mL). Approximately 1 mL of NaOH (1 molar) was slowly added to paraformaldehyde solution, which was placed on a hot plate at ~60°C until dissolution occurred. PBS (10x, 10 mL) was added to the solution and the mixture was cooled to room temperature. The pH was adjusted to 7.4 with hydrochloric acid (1 M), and the final volume was adjusted to 100 mL with the addition of deionized

distilled water. The final solution was filtered through a 0.45 µm membrane filter to remove undissolved matter.

Permeabilization

Frozen cells were thawed in biosafety fume hood until cells cooled to room temperature. Cells were centrifuged at 6000 x g for 10 min at room temperature, and subsequently washed with PBS, twice (1 mL). Remaining PBS was discarded, leaving the cellular pellet. Pellets were re-suspended in 200 µL of lysozyme buffer. Lysozyme buffer consisted of 100 mM Tris, 50 mM EDTA at a pH of 8.0. Treatment with lysozyme, specifically concentration and incubation time, must be optimized for the bacterial strain of interest. Varying concentrations and incubation times were tested for optimization. Optimized incubation times and concentrations of lysozyme for sample strains are listed below in Table 4.1 The cells were treated with 0.5 mg mL^{-1} of lysozyme for 30 min at room temperature. Cells were washed three times with PBS (1 mL). The supernatant was removed, and cellular pellets were re-suspended in 200 µL of PBS.

Table 4.1. Model bacterial strains permeabilized with optimized concentrations and incubations.

Bacterial Strain	Concentration (mg mL^{-1})	Incubation Time (h)
Pseudomonas putida	0.5	0.25
Pseudomonas aeruginosa	0.5	0.5
Synechoccus sp. 046156	1	0.25

Dehydration

Silane-coated slides purchased from Sigma-Aldrich (St. Louis, Missouri) and cover slips were pretreated with RNase Away. Approximately 5 µL of cell solution was spotted onto pretreated slides and allowed to dry at room temperature. Cell spots were dehydrated sequentially in a series with varying concentrations of ethanol as

outlined in Table 4.2. Once dehydration of cell spots was performed, hybridization and reverse transcription immediately followed prior to viewing under a confocal microscope.

Table 4.2. Ethanol dehydration series with an increasing amount of ethanol in each of the following steps.

Chemical identity	(% Ethanol)	Incubation time (min)
Ethanol in PBS	50	3
Ethanol in PBS	80	3
Ethanol in PBS	98	3

Hybridization

Hybridization solution was prepared in advance according to previously published literature with modifications.[59,97] Hybridization solution consisted of sodium chloride (900 mM), Tris (20 mM), and sodium dodecyl sulfate (0.01%) prepared at a final pH of 7.2. Prior to testing of probes associated with atrazine-degrading genes, model probes for hybridization were used for optimization purposes in planktonic cell conditions. Approximately 900 ng of primers were used for hybridization for each of the following conditions. The following probes were tested for signal: EUB338 (a general eubacterial probe), GAM42a (a specific gamma-bacterial probe), and GADPHf (forward model housekeeping probe encoding for metabolic processes in bacteria), and absence of probe (negative control condition). The probes were re-suspended in nuclease free water and diluted prior to addition to hybridization solution. Alex Fluor 488 dye, purchased from Thermo Fisher Scientific (Waltham, Massachusetts) was used as the primary hybridization dye for the probes. Hybridization solution (20 µL) containing the Alexa-Fluor 488 labeled nucleotide probe (100 ng) was placed on each cell spot of the Silane-coated slides. Slides were incubated for 2 h at 45°C in a constructed humidity chamber. Unbound primers were

washed off twice with Saline-sodium citrate buffer (0.5x, pH 7.0) for 10 min at 45°C with the aid of Coplin jars.

Construction of humidity chamber for hybridization

To construct similar conditions of a humidity chamber, modifications to an incubator were made with the slides. Slides were covered with No. 2 cover glasses and placed in a covered plastic petri dish containing tissues pre-dampened with DEPC-treated water. To maintain moist conditions, the petri dishes were kept inside sealed plastic bags containing a pre-dampened paper towel. The bag and contents were incubated for 2 h at 45°C

Reverse transcription

Cell spots were dehydrated as described previously. Ethanol was wicked off prior to the following step in the ethanol dehydration series. Cell spots on slides were air dried, and then covered with 20 µL of reverse transcriptase mixture (RT mixture) containing the enzyme for reverse transcription to occur. Slides were incubated at 60°C for one hour in a constructed humidity chamber. Slides were subsequently washed twice with SCC (0.5x) at 45°C for 10 min with the aid of Coplin jars.

Confocal laser scanning microscopy

Cell spots on slides were treated with DAPI (100 µL) as a counterstain at a concentration of 0.5 µg mL^{-1} for five min. Slides were washed once with distilled deionized water and air dried. All samples were viewed under a Zeiss LSM710 Confocal microscope, graciously provided by the Central Microscopy Research Facility at The University of Iowa.

SEM to differentiate biofilms and planktonic cells

Pseudomonas sp. strain ADP cells were grown as previously described in planktonic and biofilm modes of growth. Biofilms harvested after five days at full maturation and planktonic cells were harvested at mid-exponential phase on mineral medium containing atrazine were prepared for scanning electron microscopy. *Pseudomonas* sp. strain ADP cells were additionally grown on LB medium and ammonium nitrate medium. Biofilms were grown on microscopic cover slips, while cells in suspension were transferred to microcentrifuge tubes. In both conditions, cells were fixed in 2.5% glutaraldehyde, rinsed with cacodylate buffer thrice in an h (3 × 20 min). Subsequently, cells were subjected to 1% osmium tetroxide in buffer for two h, followed by another rinse in cacodylate buffer thrice in an hour (3× 20 min). Cells were rinsed with deionized water and subjected to an ethanol dehydration series (15-30 min in each solution of 25%, 50%, 75%, 95%, and 100% ethanol). Hexamethyldisilane was used as a substitute for critical point drying. Biofilms and suspended cells were then mounted on stubs, sputter coated, and examined in the Hitachi S-4800 & Hitachi S-3400N Scanning Electron Microscope.

Antibiotic testing on P.ADP for GFP Constructs

Minimum inhibitory concentrations for three antibiotic(s): tetracycline, gentamicin, and carbenicillin, were evaluated by spectrophotometric methods. A pure culture of *Pseudomonas* sp. strain ADP cells was inoculated in LB medium (10 mL) overnight at 37^{o}C. Cell counts (CFUs) were calibrated to OD_{600} measurements for P.ADP cells in LB using methods described previously. Antibiotics tetracycline and gentamicin were serially diluted from initial stock concentrations of 100 µg mL^{-1} to 3.125 µg mL^{-1}, and carbenicillin was serially diluted from an initial stock

concentration of 400 μg mL^{-1} to 12.5 μg mL^{-1}. Each dilution level for all three antibiotics were added to overnight cultures of P.ADP in LB. The series of dilution vessels were observed for microbial growth indirectly via spectrophotometry. OD_{600} measurements were taken for all dilution levels for each antibiotic to determine the minimum inhibitory concentration (MIC) for tetracycline, gentamicin, and carbenicillin.

FLBA for monosaccharide analysis

Fluorescent lectin binding analysis (FLBA) was performed as described by previously published literature with additional modifications.[109] *Pseudomonas* sp. strain ADP biofilms were grown as described previously in one of two media: a) LB medium, and b) DSMZ medium containing 30 mg L^{-1} atrazine. Biofilms were grown on Silane-coated slides in the drip-flow reactor, and subsequently harvested for FLBA. Samples were washed with deionized, distilled water and incubated with each of the following rhodamine-bound lectins: Concanavalin A (ConA), Dolichos Biflorus Agglutinin (DBA), Peanut Agglutinin (PNA), Ricinus Communis Agglutinin I (RCA I), Soybean Agglutinin (SBA), Ulex Europaeus Agglutinin (UEA I), Wheat germ agglutinin (WGA) at a concentration of 0.1 mg mL^{-1} for 30 min at room temperature. The specificity for each lectin is detailed in Table 4.3. Samples stained with dye-bound glycoconjugates were washed four times with distilled, deionized water to remove unbound lectins. DAPI was added to samples in an incubator in the absence of light for five min to provide a counterstain.

Table 4.3. Monosaccharide specificities for rhodamine-bound lectins.

Lectin	Sugar specificity
ConA	α-mannose, α-glucose
DBA	α-N-acetylgalactosamine
PNA	Gal-β(1-3)-GalNAc
SBA	α or β-N-acetylgalactosamine
UEA I	α-fucose
RCA I	Galactose
WGA	N-acetylglucosamine

Samples were observed under a Zeiss LSM710 Confocal microscope, graciously provided by the Central Microscopy Research Facility at The University of Iowa. All microscopic samples were performed in triplicate for statistical treatment. IMARIS was used to calculate Mean Intensity Ratio (MIR) for each lectin to evaluate the distribution and identity of monosaccharides in LB-grown and DSMZ-grown P.ADP biofilms. Furthermore, IMARIS was used to capture images and visualize DAPI, rhodamine-bound lectins, and combination of counterstained, lectin-stained samples.

Results and Discussion

Differentiation of surface properties by mode of growth

Previous work by Henry et al. was further explored using scanning electron microscopy (SEM) as a tool to differentiate surface characteristics of planktonic *Pseudomonas* sp. strain ADP cells from *Pseudomonas* sp. strain ADP cells in the biofilm mode of growth.[9] As displayed in Figure 4.2, the panel illustrates surface characteristics extremely specific to cells grown as biofilms not present in free cells. The close, mutual relationship of cells is exemplified in Panel (A) (10 kV, 8.1 mm, 400x), while at an increased magnification in Panel (B) (13.0 kV 8.2 mm, 15,000x) the aggregate of cells and mesh-like webbing can be seen, which is characteristic of

the EPS only present in biofilm mediated cell structures. This mesh-like webbing from the extracellular polymeric substances and matrix has also been documented in *Listeria monocytogenes* biofilms in previously published literature.[98]

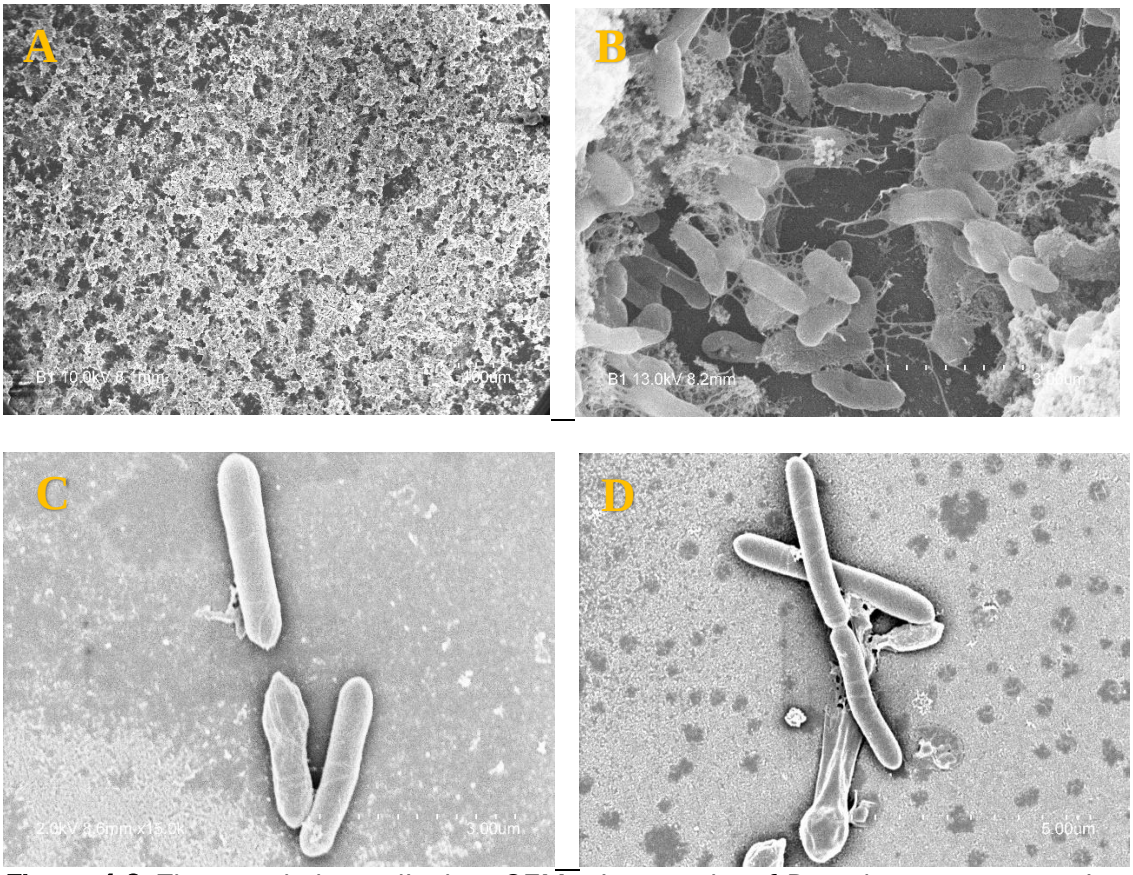

Figure 4.2. The panel above displays SEM micrographs of *Pseudomonas* sp. strain ADP cells grown as a mature five-day biofilm under DSMZ medium containing atrazine (A-B), and SEM micrographs of *Pseudomonas* sp. strain ADP free-cells under DSMZ medium containing atrazine (C-D).

Even more so, at a high magnification (15,000x), the rod-shaped structure unique to *Pseudomonas* species can be readily observed in Panel(B). Panels(C) (2.0 kV, 8.6 mm, 15,000x) and (D) (2.0 kV, 8.6 mm, 11,000x) are SEM micrographs of *Pseudomonas* sp. strain ADP planktonic cells grown in shake flasks with DSMZ medium containing 100 mg L^{-1} of atrazine. It is clear, as displayed in Figure 4.2, there is a noticeable absence of any EPS designated by mesh-like webbing and no

entangled structures. Cells dividing in the logarithmic phase, as were harvested below, are often compared to slowly growing cells in the stationary phase for biofilm mediated cells.[98] Therefore, it was essential to harvest the cells in the planktonic and biofilm in the aforementioned states to make an apt SEM comparison of surface morphologies. In the planktonic cells, the cells can be observed dividing, and the sparseness characteristic of free-floating bacteria can be detected in Figure 4.2. The cell density and dependence on growth media can be qualitatively observed in SEM micrographs, as illustrated in the next subsection.

Qualitative measure of cell density by media using SEM

To complement *Pseudomonas* sp. strain ADP cell growth data, SEM micrographs were obtained for cells in mid-exponential phase grown in diverse types of medium. Cells were grown and harvested from LB, ammonium nitrate, and DSMZ (containing 100 mg L^{-1} of atrazine). The former representing a nutrient rich-medium with an expected high cellular density and the latter representing a nutrient poor-medium with an expected lower cellular density. At a specified magnification, the number of visible cells from a surface morphology perspective should increase in more nutrient-rich growth media.

Planktonic *Pseudomonas* sp. strain ADP cells grown in DSMZ containing atrazine (100 mg L^{-1}) displayed in Panel A of Figure 4.3 shows a low density of cells (2.0 kV, 8.6 mm, 13,000x). Panels (B) and (C), conversely, demonstrate a high cellular density of P.ADP cells grown in LB medium. Panel (B) is at lower relative magnification (2.0 kV, 8.9 mm, 10,000x), whereas Panel (C) is at a higher relative magnification (2.0 kV, 8.9 mm, 11,000x). Despite the discrepancy in magnification

between panels (A) and (C), it is still clear at similar magnifications the cellular density would be higher for cells grown in LB medium, however this only semi-quantitative at best. Panel(D) in Figure 4.3 (4.0 kV, 8.5 mm, 7,000x) is at a lower magnification, but it is apparent the relative cell density falls between that of LB and DSMZ. The goal is not to provide a robust semi-quantitative method of estimating cell density by SEM, as other methods for quantification of cells such as hemocytometry and plate-counting, are highly developed and accurate.

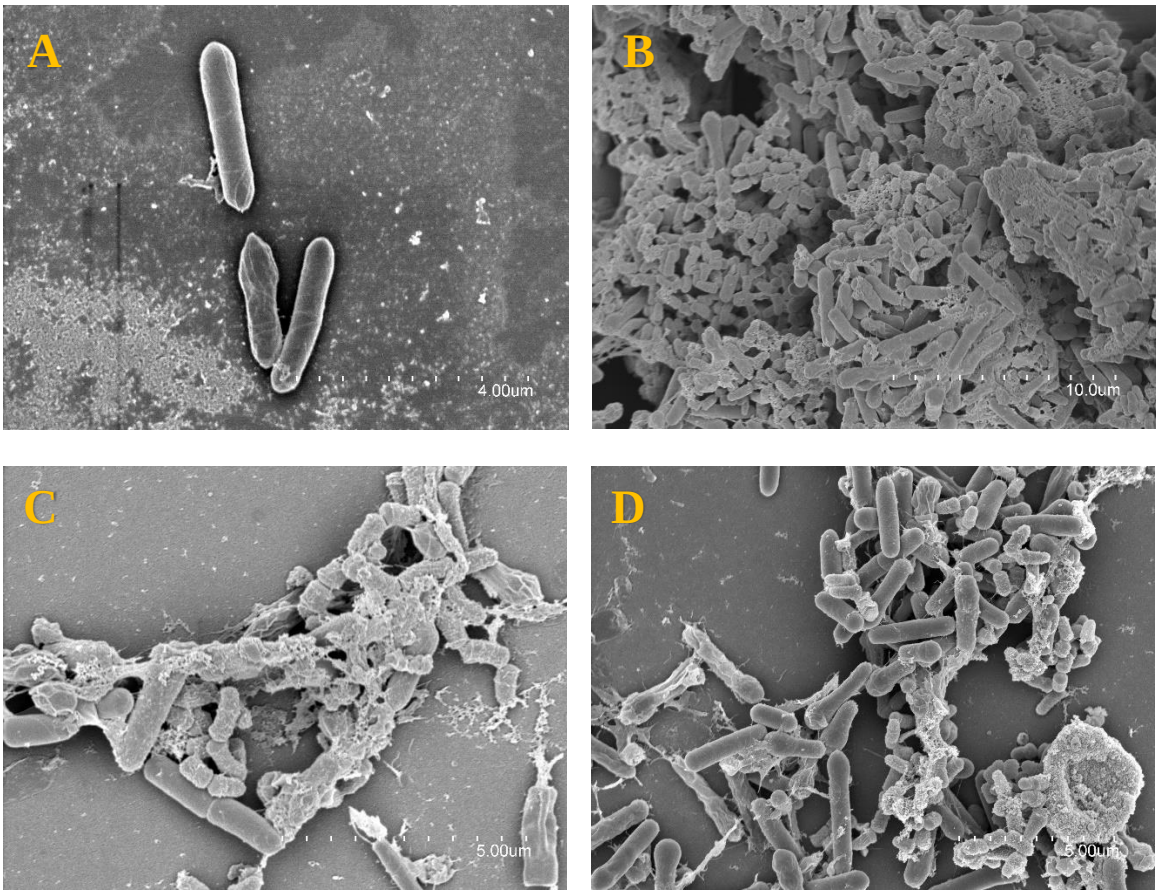

Figure 4.3. The panel above displays SEM micrographs of planktonic *Pseudomonas* sp. strain ADP cells grown in A) DSMZ medium containing 100 mg L^{-1} of atrazine, B) LB medium, C) LB medium (magnified), and D) ammonium nitrate medium.

Optimization of ISRT in planktonic P.ADP for AtzD

Housekeeping genes (GAPDH), eubacterial probes (EUB338), gamma bacteria specific probes (GAM42a), and two atrazine degrading primers (AtzA, AtzD) were used

for planktonic *Pseudomonas* sp. strain ADP cells as detailed in Table 4.4. Initially, Alexa Fluor 488 was tested with AtzD forward and reverse primers as the probes of interest for ISRT as illustrated in Figure 4.4.

Table 4.4. Probes tested in In Situ Reverse Transcription (ISRT) protocol for optimization in *Pseudomonas* sp. strain ADP planktonic cells. Primer, direction, and sequence are listed for each specific probe.

Primer	Orientation	Sequence 5' to 3' Orientation
GAPDH	Forward	TGCACCACCAACTGCTTAGC
GAPDH	Reverse	GGCATGGACTGTGGTCATGAG
AtzA	Forward	ACGGGCGTCAATTCTATGAC
AtzA	Reverse	CACCCACCTCACCATAGACC
AtzD	Forward	TCCCACCTGACATCACAAAC
AtzD	Reverse	GGGTCTCGAGGTTTGATTG
EUB338		GCTGCCTCCCGTAGGAGT
GAM42a		GCCTTCCCACATCGTTT

The DAPI counterstain is used to visualize all cell material from *Pseudomonas* sp. ADP, as it specifically binds to nucleic acid material which is present in each P.ADP cell and therefore makes a proficient counterstain. Cells expressing *AtzD*, the gene encoding for the enzyme for the biotransformation from cyanuric acid to biuret in the atrazine degradation pathway, would theoretically display a green hue under CLSM. As demonstrated in (A) and (C) of Figure 4.4, no green hue is present and therefore mRNA transcripts of *AtzD* are not present.

However, this may not necessarily mean transcription is not taking place and atrazine is not being degraded. Rather, due to the demanding optimization of this protocol, as well as natural low copy numbers without PCR amplification, the signal may not be high enough for detection by CLSM. Perhaps the addition of RT-PCR with an *in situ* approach, the signal-to-noise (SNR) ratio may be higher and detection of

AtzD under confocal would be possible. ISRT was successfully optimized for the *cbbL* gene of chemoautotrophic nitrifying bacteria using CY3 as a label, instead of Alexa Fluor 488 employed in our approach.[97]

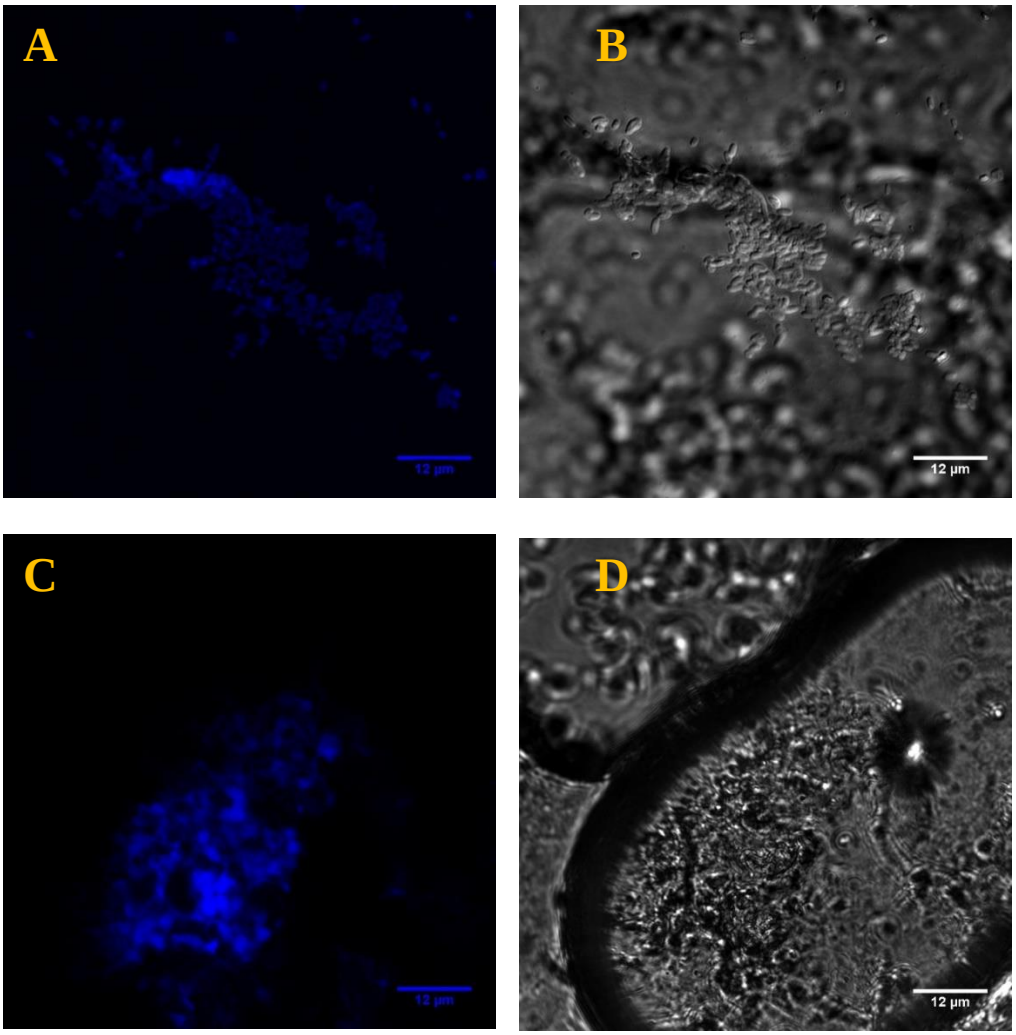

Figure 4.4. Initial ISRT confocal (A, C) and transmission (B, D) micrographs illustrating planktonic *Pseudomonas* sp. strain ADP cells with positive *AtzD* expression with DAPI counterstain and Alexa Fluor 488 conjugated dye (A) and negative *AtzD* expression with DAPI counterstain (blue) and Alexa Fluor 488 conjugated dye (C). [10]

Positive red fluorescence was observed under CLSM for growing chemoautotrophic bacteria by direct incorporation of dye CY3. Background autofluorescence was easily avoided and significantly reduced using aged seawater where phytoplankton were not found. This protocol, however, was not developed by

C.D. Sinigalliano et al. for broad use, which was the goal of our incorporation of ISRT optimization for biofilms and planktonic cells. In (B) and (D) of Figure 4.4, planktonic P.ADP cells appearing as small single micrometer rod shapes in clusters, are visually apparent in the transmission micrographs. This confirms bacterial cell presence in ISRT. The probes evaluated by In Situ Reverse Transcription, including all atrazine-degrading gene probes and a control eubacterial probe, are displayed in Table 4.4.

ISRT optimization of planktonic P.ADP with GADPH

Following the use of primer AtzD (forward and reverse), ISRT was implemented on planktonic P.ADP cells with probe GADPH. Glyceraldehyde 3-phosphate dehydrogenase (GAPDH or G3PDH) is the enzyme that catalyzes an important step of glycolysis, and breaks down glucose for energy and carbon molecules.[99] GADPH is expressed in both prokaryotic and eukaryotic cells, and more generally functions in most metabolic processes involving the breakdown of sugars. The primary role of GADPH as a 'housekeeping gene' is to regulate a stable amount of mRNA produced during transcription, regardless of other processes taking place. Therefore, the expression levels should be stable, despite what is occurring outside of the cell's environment.[100] This model gene used a primer, along with eubacterial probe (EUB338) and gamma bacterial probe (GAM42a), to ensure the ISRT protocol was working correctly, in spite of atrazine degradation processes.

As displayed in Figure 4.5 in panel (A) under the blue channel, the relatively small number of cells can be observed visually using DAPI as a general nucleic acid counterstain for P.ADP. Conversely, the green channel in CLSM which corresponds to the wavelength range for Alexa Fluor 488, there is an extremely low level of fluorescence above background, suggesting no expression of GAPDH in P.ADP

planktonic cells. This interpretation, however, must be scrutinized. All cells, bacterial and mammalian, express the gene GADPH consistently, despite the flux of atrazine utilized by the cells. Transmission micrograph (C) in Figure 4.5 validates the presence of *Pseudomonas* sp. strain ADP cells not clearly shown in CLSM micrographs (A) and (B). This is evident by the rod-shaped structures (~1 µm) densely packed in the grey transmitted image (C).

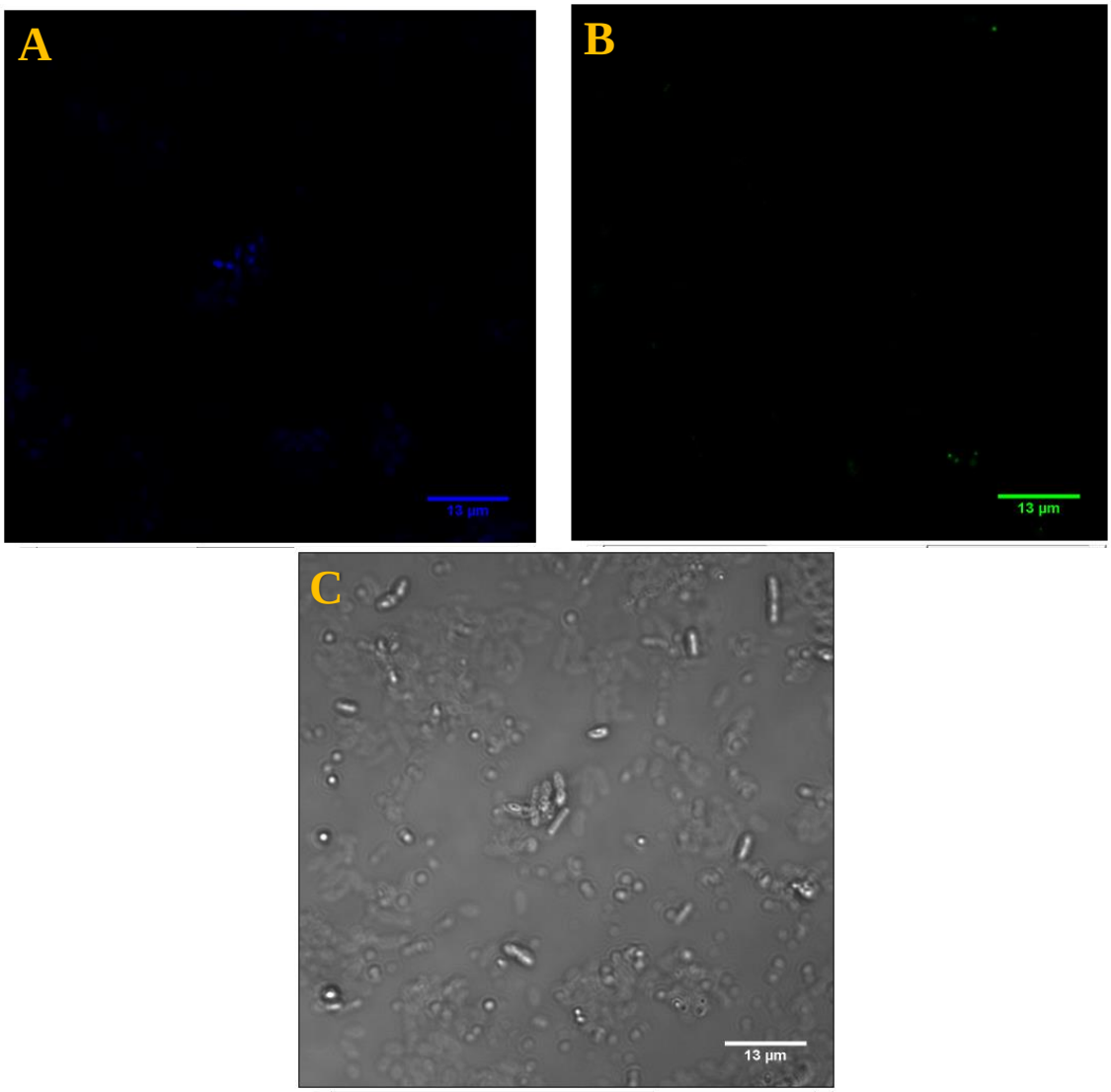

Figure 4.5. ISRT confocal (A, B) and transmission (C) micrographs illustrating planktonic *Pseudomonas* sp. strain ADP cells with positive GAPDH expression with DAPI (blue) counterstain (A) and Alexa Fluor 488 (green) conjugated dye (B).

The conclusion reached is similar to use of Alexa Fluor 488 conjugated to *AtzD*: the signal is far too low by mRNA copy numbers of P.ADP, even for normal metabolic processes which transcribe for the gene product GAPDH. This was an important experiment to implement after use of *AtzD* to rule out the possibility of probe choice. By choosing GAPDH as a normalized expression probe, troubleshooting for optimization of ISRT must lie outside of this factor. This further substantiates that the signal for ISRT must be amplified or tagged to increase the SNR and visualize expression of the gene of interest.

To increase the signal of Alexa Fluor conjugated to the specific probe, alternate approaches must be considered to ISRT. Digoxigenin (DIG) antibody labeling, both primary and secondary, is one possible approach to increase fluorescence signal. Biotin and digoxigenin as labels for light and electron microscopy for in situ hybridization are common in immunohistochemistry.[101] However, due to poor characterization of genes in P.ADP at the this time, no approaches are feasible. This would require the development of primary and secondary antibody DIG labeling for each of the six atrazine-degradation genes present in the esoteric strain *Pseudomonas* sp. ADP. Another alternate approach to visualize each gene in P.ADP is implementation of red/green fluorescent protein fusions.

Effect of select antibiotics on P.ADP

To determine whether protein fusion approaches would be a viable solution for detection of enzymes *AtzA-AtzF* in *Pseudomonas* sp. ADP biofilms and planktonic cells, minimum inhibitory concentration (MIC) procedures were performed using 3 antibiotics: gentamicin, tetracycline, and carbenicillin. In Figure 4.6, minimum inhibitory concentration (MIC data suggests strain *Pseudomonas* sp. ADP is resistant

to carbenicillin at the highest concentration tested (400 μg mL^{-1}) but demonstrates growth at lower antibiotic concentrations as evident from OD_{600} values between 0.1-1.7 AU.

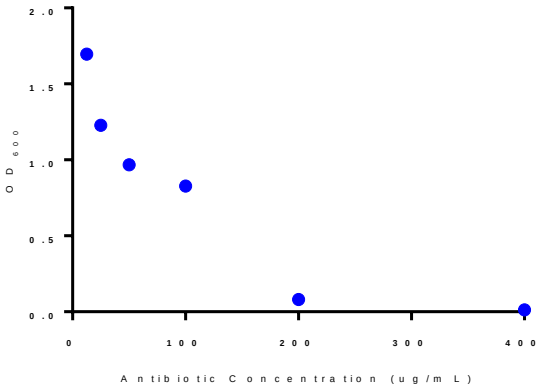

Figure 4.6. Minimum inhibitory concentration (MIC) data for antibiotic carbenicillin on *Pseudomonas* sp. strain ADP cells growing on LB.

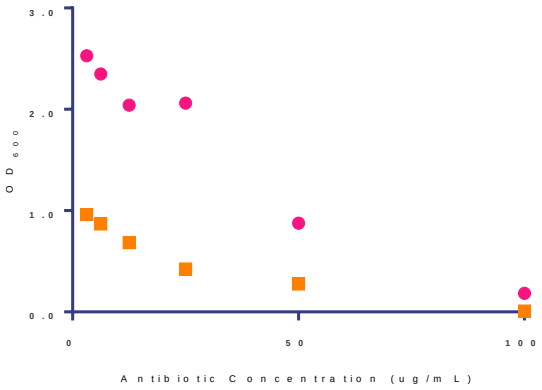

Figure 4.7. Minimum inhibitory concentration (MIC) data for antibiotics gentamicin (●) and tetracycline (■) on *Pseudomonas* sp. strain ADP cells growing on LB.

Antibiotics gentamicin and tetracycline were added to growing cultures of *Pseudomonas* sp. strain ADP for determine their respective MICs. Most growth was inhibited in P.ADP for tetracycline and gentamicin at a concentration of 100 μg mL^{-1}, however even a significant amount of P.ADP growth was inhibited at a lower concentration of 50 μg mL^{-1} of tetracycline as demonstrated in Figure 4.7. As expected for all three antibiotics tested, growth was inhibited in an increasing fashion

for each increased level of antibiotic, as evident from lower OD_{600} values. After the isolate was tested for the ability to transform and resistance patterns were analyzed, *Pseudomonas* sp. strain ADP was deemed unsuitable for current green/red fluorescent protein fusion approaches available. However, the mercury resistance operon on plasmid pADP-1, may be used as a selective marker alternate to antibiotic resistance markers.[2]

Optimization of ISRT in planktonic P.ADP with EUB338

A third probe, EUB388, was analyzed for ISRT incorporation as a housekeeping gene to encode for consistent mRNA in all eubacteria, which is present in P.ADP. Figure 4.8 demonstrates a panel of transmitted P.ADP cells in both a standard view (A) and as a z-stack, which is typical of biofilm micrographs (B). The z-stack representation of P.ADP cells aids in visualization of the cell monolayer in planktonic samples, and how it can be differentiated for *Pseudomonas* sp. ADP biofilms, which is thicker and has a denser layer of cells at varying heights as evident by CLSM. Figure 4.8 also shows panels (C) and (D), which optimally demonstrate conjugation of Alexa Fluor 488 dye to our probe of interest, EUB338.

In this case, the positive control EUB338 (D) demonstrates both the expression of the gene product associated with the probe of interest, EUB338, in addition to non-specific binding. Non-specific binding in (D) is visualized in the dual-channel image due to the presence of a green hue in areas where no DAPI is present. Since DAPI is a counterstain and stains all areas where nucleic acid is present (i.e., presence of P.ADP cells), no EUB338-Alexa Fluor 488 can be expressed where cells are not present. The non-specific binding of Alexa Fluor 488 may be to one of the following factors: A) extensive incubation time in hybridization step, B) high noise and

signal intensity from CLSM settings, i.e., boost of background signal to boost Alexa Fluor 488 signal, C) low signal of DAPI and Alexa Fluor 488, or D) low penetration of DAPI during incubation.

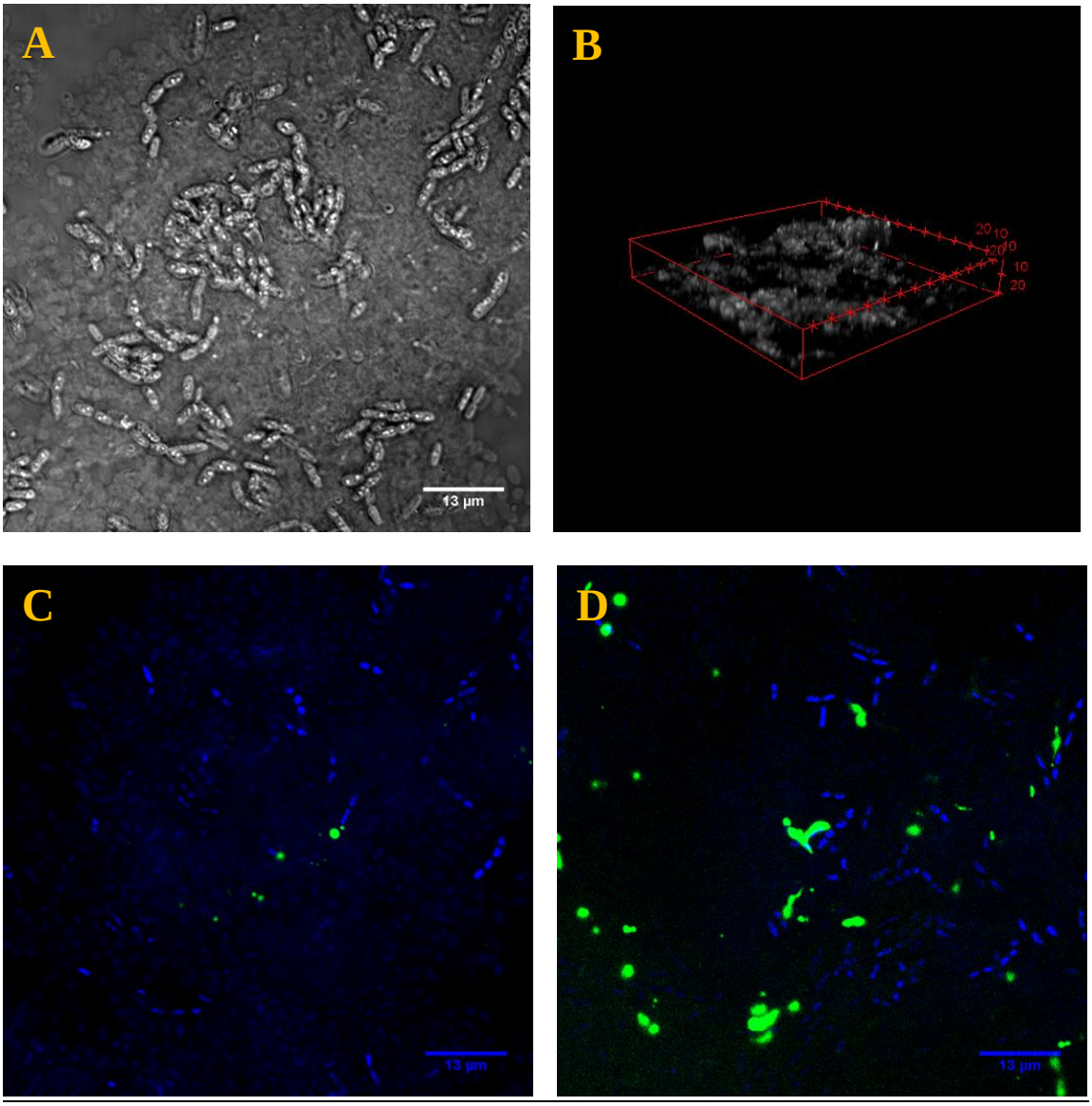

Figure 4.8. Micrographs of ISRT *Pseudomonas* sp. strain ADP cells under confocal laser scanning microscope (C, D) and transmission (A, B) in single-layer (A, C, D) and z-stack (B) conformations. Image in panel (C) is the negative control of DAPI counterstain with no probe containing Alexa Fluor 488 in dual channel mode, and image in panel (D) is DAPI counterstain (blue) with eubacterial probe EUB338 conjugated to Alexa Fluor 488 (green) in dual channel mode.

Figure 4.8 panel (C) suggests the presence of Alexa Fluor 488 despite the absence of probe EUB338. This is not a typical result, and did not occur in either previously published literature concerning the use of bacterial cells for ISRT.[59,97] Blocking agents in immunohistochemistry approaches (DIG), for example, would remediate this issue. Moving forward, ISRT may be modified and first used with model organisms prior to further use in P.ADP, which will aid in future development for use in microbial biofilms.

Confocal laser scanning microscopy was used to create z-stacks of images for monolayer *Pseudomonas* sp. strain ADP cells with both DAPI and Alexa Fluor 488 channels as illustrated in Figure 4.9. As suggested earlier, the presence of a green hue despite the absence of any probes (EUB388) imply Alexa Fluor 488 non-specific binding may have occurred during ISRT. Once ISRT is correctly optimized with a model strain of bacteria such as *Escherichia coli* DH5α or *S. aureus*, the method may be applied to the atrazine-degrading strain, *Pseudomonas* sp. ADP in the biofilm and planktonic mode of growth.

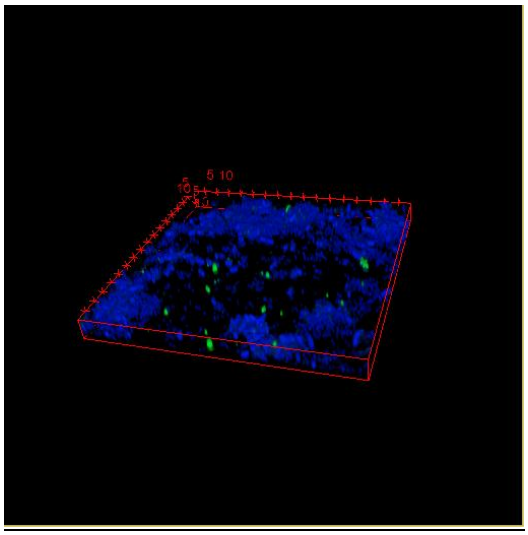

Figure 4.9. Confocal laser scanning micrograph of *Pseudomonas* sp. strain ADP in planktonic mode of growth viewed as a z-stack with DAPI counterstain (blue) and Alexa Flour 488 conjugated to EUB338 probe (green).

Mean intensity ratio of glycoconjugates in P.ADP biofilms

Fluorescent Lectin Binding Analysis (FLBA) was used to evaluate the presence, relative quantity, and distribution of monosaccharides present in *Pseudomonas* sp. strain ADP biofilms. Each lectin bound to rhodamine dye was added to biofilms briefly for incubation, and subsequently washed to remove unbound dye. Each lectin specifically or non-specifically binds to a certain monosaccharaide or set of monosaccharides, and with aid of rhodamine and confocal laser scanning microscopy, the fluorescent dye appears where the lectin is present in *Pseudomonas* sp. ADP biofilm samples. It is important to determine the identify, quantity, and relative distribution of monosaccharides for their potential role in the EPS in regard to bioremediation applications. In its current state, little is known about the extracellular polymeric substances in P.ADP biofilms which may contribute to bioremediation of atrazine via entrapment or other physio-chemical means.

The Mean Intensity Ratio (MIR) was calculated as the ratio of the mean intensity of the active rhodamine signal (rho-lectin) to the mean intensity of the DAPI counterstain signal (DAPI) which corresponds to all cell material. The MIR therefore equates to a normalized ratio of lectin-to-cell material to evaluate the degree of monosaccharaides in a particular biofilm sample. This measure, MIR, is used due to the variance of thickness, cell density, and cell count across biofilm samples. The mean intensity of signal alone from a rhodamine dye, as detected by CLSM, cannot be used as a method of comparison due to an expected increase with an increase in cell mass. Biofilm fluorescent signal data was compiled across several samples and averaged thereafter. Therefore, all results have been adequately normalized to compare MIR values for each lectin and by growth media.

The MIR of each lectin was calculated in the following manner. Each mean intensity for every biofilm sampled was averaged from the rhodamine channel (n = 4). For example, the mean intensity for ConA bound to rhodamine was generated from the CLSM micrograph. The mean intensity for ConA bound to rhodamine in the DAPI channel was also generated from the CLSM micrograph, which corresponds to the relative amount of cell material, i.e., nucleic acid stain. The quotient of the two values for ConA is the MIR.

The significance of the mean intensity ratio is a relative proportion of a specific monosaccharaide or monosaccharides present in *Pseudomonas* sp. strain ADP biofilms. Figure 4.10 illustrates the MIRs for each lectin.

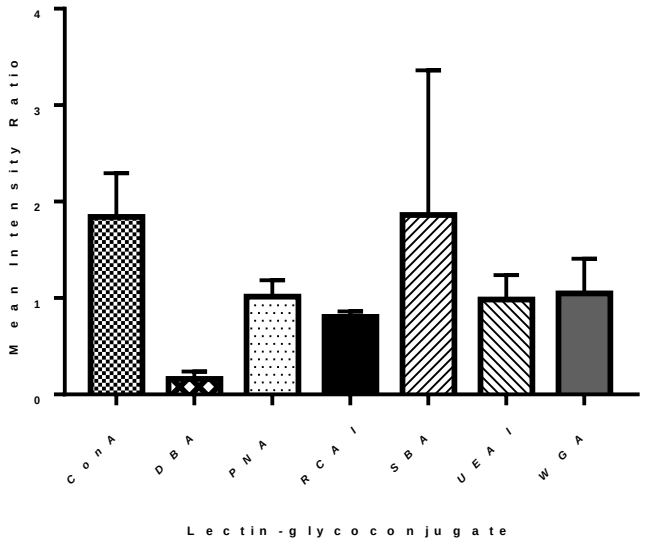

Figure 4.10. Mean Intensity Ratios, the ratio of the mean intensities for rhodamine (red) conjugated to lectins relative to the mean intensities for DAPI (blue), for each lectin was calculated for *Pseudomonas* sp. strain ADP biofilms grown under DSMZ medium (30 mg L^{-1} atrazine). Error bars represent 95% confidence intervals.

The highest MIR in produced in P.ADP biofilms were lectins Concanavalin A (1.9 MIR) and Soy Bean Agglutinin (1.9 MIR). As shown in Table 4.5, these lectins correspond to sugar monomers α-mannose, α-glucose, and α or β-n-

acetylgalactosamine, respectively. However, due to the sparse number of lectins screened, it is not possible to differentiate whether mannose or glucose is present in P.ADP biofilms.

Conversely, it is possible to distinguish the presence of the α vs. β form of n-acetylgalactosamine is present due to the use of Dolichos Biflorus Agglutinin (DBA). Lectin DBA corresponds to the alpha form of n-acetylgalactosamine. Figure 4.10 displays a low MIR for DBA at approximately 0.15, suggesting a relative absence of the monosaccharaide α-n-acetylgalactosamine. Therefore, a high distribution of the beta form of n-acetylgalactosamine is almost certainly present in *Pseudomonas* sp. ADP biofilms. For other lectins, such as PNA, RCA I, UEA I, and WGA, distinction of specific sugars may be less precise. The sugars corresponding to these lectins are present in low to moderate quantities relative to cell material, as suggested by their MIRs between 0.9-1.1. Due to a high amount of variability in the MIR for SBA, the relative quantity of the sugar n-acetylgalactosamine is hard to predict.

A notable disadvantage of using fluorescent lectin binding analysis (FLBA) as a primary source to identify the monosaccharides present in the biofilm in their non-specific nature. For example, as illustrated in Table 4.3, several lectins bind to two or more sugars, and without additional screening to narrow down the precise lectin binding, it is not possible to distinguish the monosaccharides from another (e.g., alpha and beta forms of the same sugar, or mannose and glucose). An additional assay must be used in conjunction to attain more specificity in monosaccharaide identification and quantification.

Table 4.5. Mean Intensity Ratio (MIR), associated error, and indicated presence or absence of specified sugar as demonstrated by fluorescent lectin binding analysis (FLBA) and confocal microscopy (CLSM) for *Pseudomonas* sp. strain ADP biofilms grown in DSMZ medium containing 30 mg L^{-1} atrazine.

Lectin	Sugar Specificity	Mean Intensity Ratio	Error	Presence
ConA	α-mannose, α-glucose	1.840	0.891	(+)
DBA	α-N-acetylgalactosamine	0.173	0.115	(-)
PNA	Gal-β(1,3)-GalNAc	1.1014	1.027	Inconclusive
SBA	α or β-N-acetylgalactosamine	1.861	0.577	(+)
UEA I	α-fucose	0.986	0.590	Inconclusive
RCA I	galactose	0.805	0.344	(-)
WGA	N-acetylglucosamine	1.036	1.289	Inconclusive

Table 4.6. Mean Intensity Ratio (MIR), associated error, and indicated presence or absence of specified sugar as demonstrated by fluorescent lectin binding analysis (FLBA) and confocal microscopy (CLSM) for *Pseudomonas* sp. strain ADP biofilms grown in LB medium.

Lectin	Sugar Specificity	Mean Intensity Ratio	Error	Presence
ConA	α-mannose, α-glucose	1.840	2.533	(+)
DBA	α-N-acetylgalactosamine	0.173	0.441	Inconclusive
PNA	Gal-β(1,3)-GalNAc	1.1014	0.364	(-)
SBA	α or β-N-acetylgalactosamine	1.861	6.955	(+)
UEA I	α-fucose	0.986	2.316	(+)
RCA I	galactose	0.805	1.507	Inconclusive
WGA	N-acetylglucosamine	1.036	0.763	Inconclusive

IMARIS generated images of FLBA for P.ADP biofilms

Generated of IMARIS images from confocal laser scanning data allows for visualization of cell material along with lectins, corresponding to specific sugars. This data provides composition and x-y-z spatial information on where monosaccharides

are in *Pseudomonas* sp. ADP biofilms. In Figure 4.11 the top view (A) and sectional view (B) demonstrate the spatial distribution of cell material, along with the presence of sugars corresponding to lectin DBA. The alpha form of N-acetylgalactosamine, as confirmed by quantitative MIR data, is relatively sparse. This monosaccharide is not present in DSMZ medium used for growth. It is improbable, based on the IMARIS image and quantitative fluorescent data that the EPS secretes α-N-acetylgalacosamine. In bacterial biofilms of *Xyella fastidiosa*, for example, this sugar is not present throughout the wild type organism nor the mutants.[102]

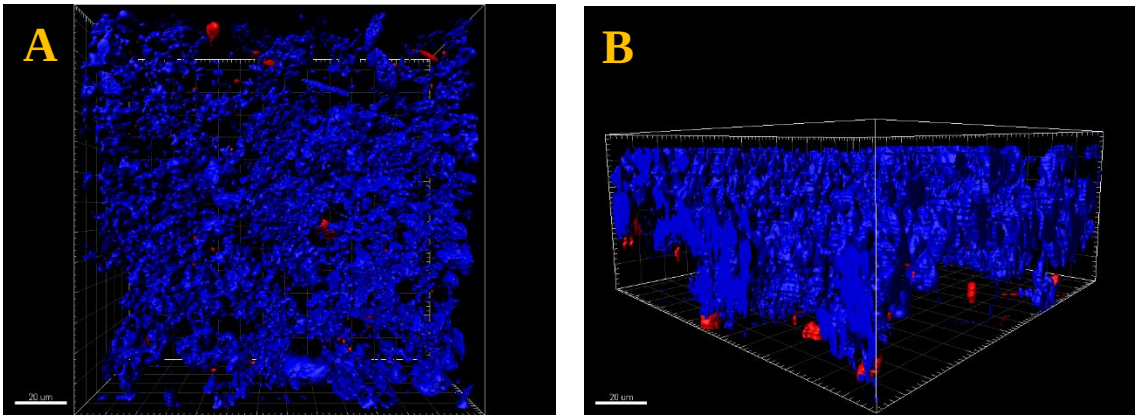

Figure 4.11. IMARIS generated images of *Pseudomonas* sp. strain ADP biofilms with DAPI counterstain (blue) of whole cell population and rhodamine-bound lectins (red) of Dolichos Biflorus Agglutinin (DBA) from a top-view (A) and sectional view (B) with aid of confocal laser scanning microscopy (CLSM).

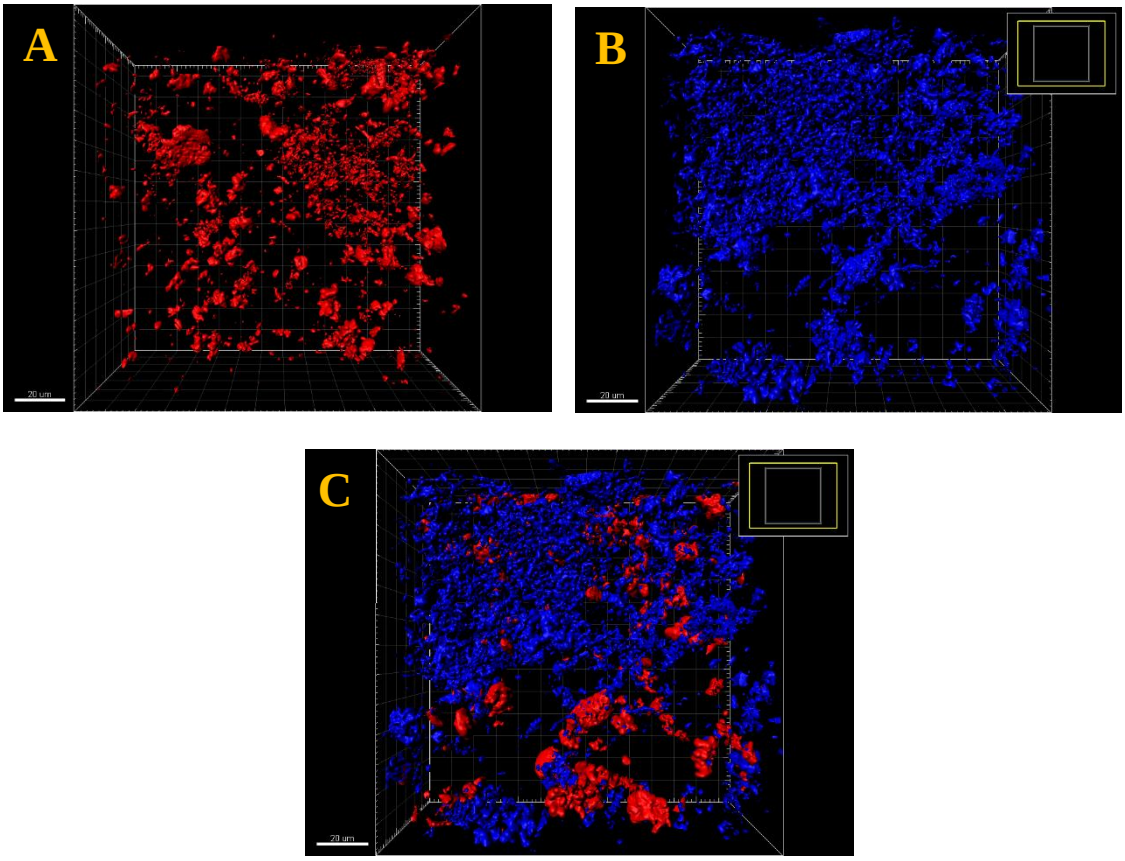

Figure 4.12. IMARIS generated images of *Pseudomonas* sp. strain ADP biofilms with DAPI counterstain (blue) of whole cell population (B), rhodamine-bound lectin (red) of Concanavalin A (ConA) (A), and dual-channels (C) from a top-view with aid of confocal laser scanning microscopy (CLSM).

Lectin Concanavalin A (ConA) is expected to be present in *Pseudomonas* sp. strain ADP biofilms. This is due the presence of glucose in quantities of 1 g L^{-1} in DSMZ growth medium. Despite utilization of glucose by bacterium as a source of carbon, sugar glucose is common monosaccharide present in the extracellular polymeric substances (EPS) of bacterial biofilms.[103] Lectin ConA correlates to both α-mannose and α-glucose specificity as indicated by Tables 4.5 and 4.6. In *Xyella fastidiosa* wild-type and *Rfp* mutants, 0.003 mg mL^{-1} of glucose and 0.141 mg mL^{-1} of glucose in the composition of the EPS was determination from quantification.[102] In Figure 4.12, the separate channels of the IMARIS generated image can be observed with DAPI (B) and rhodamine (A) for the cell material and lectin ConA, respectively.

The superimposition of both channels (C) illustrates the high proportion of α-glucose and/or α-mannose to cellular P.ADP material. This is confirmed by the quantitative mean intensity ratio (MIR) in DSZM medium containing atrazine for lectin ConA, which is 1.840 (± 0.891) as displayed in Table 4.5.

It is clear that biofilms are complex structures with a great amount of heterogeneity both in their structure and in the EPS matrix housing the cells.[104–106] This applies to the spatial heterogeneity of macromolecules, such as monosaccharides and polysaccharides secreted by the EPS. Figure 4.13, panel (A) demonstrates the wide distribution from spatial view of mannose and/or glucose at the bottom, middle, and top layers of the *Pseudomonas* sp. strain ADP biofilms. Panel (B) represents the maximum intensity projection (MIP), of the same biofilm sample. In this view, generated by CLSM, represents compression of the z-stack images, demonstrating both cell material (blue), rhodamine-bound lectins (pink), and the overlay of both (purple).

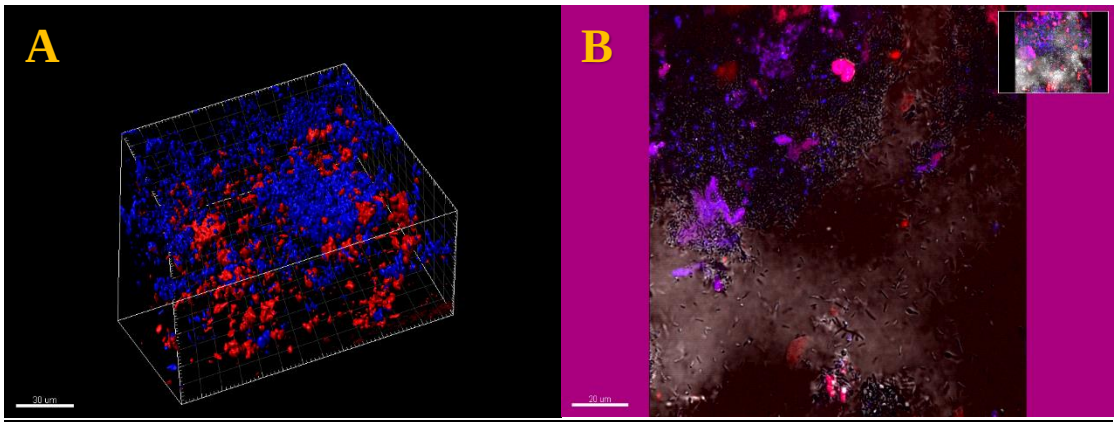

Figure 4.13. IMARIS generated image of *Pseudomonas* sp. strain ADP biofilms with DAPI counterstain (blue) of whole cell population in dual-channel with rhodamine-bound lectin (red) of Concanavalin A (ConA) from a three-dimensional view (A), and Z-stack confocal lasers scanning microscopy (CLSM) superimposed with transmission image (B) displaying DAPI (blue), ConA (pink), and the combination (purple).

The spatial organization and heterogeneity also depends upon the identity of the rhodamine-bound lectin as evidenced by the images in Figure 4.14.

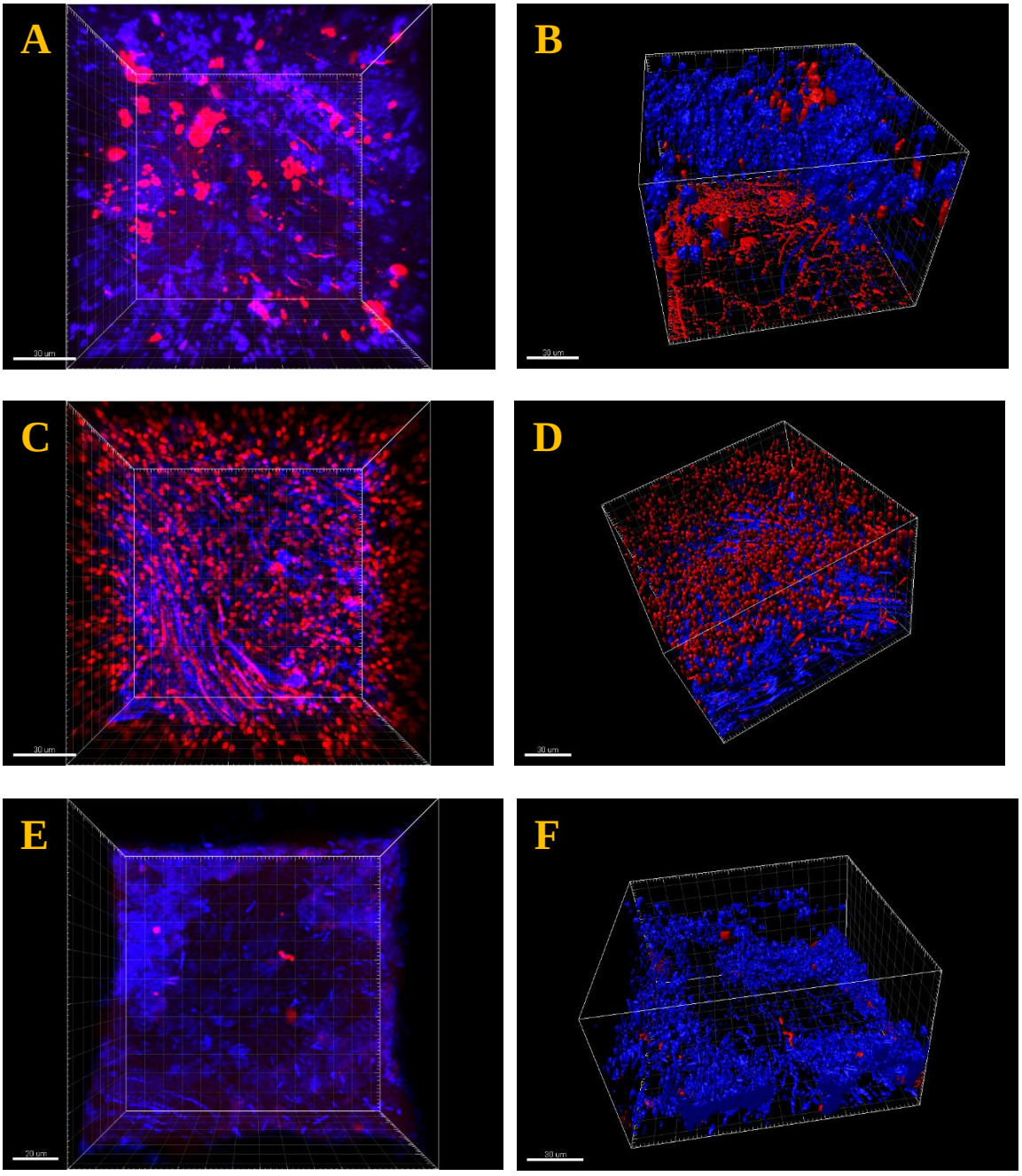

Figure 4.14. Rhodamine-bound Peanut Agglutinin (PNA) (A, B), rhodamine-bound Wheat Germ Agglutinin (WGA) (C, D), rhodamine-bound Ricin Communis Agglutinin (RCA) (E, F) from top-view (A, C, E) and sectional-view (B, D, F). DAPI counterstain (blue) is displayed in all confocal laser scanning (CLSM) micrographs for *Pseudomonas* sp. strain ADP biofilms.

Panels (A), (C), and (E) of Figure 4.14 demonstrate the relative quantity of monosaccharides corresponding to lectins PNA, WGA, and RCA I. For Peanut Agglutinin, corresponding to sugar Gal-β(1,3)-GalNAc, the relative proportion to cell material is high, as confirmed by the MIR values listed in Table 4.5 when grown in DSMZ containing atrazine.

Similarly, Wheat Germ Agglutinin, corresponding to sugar N-acetylglucosamine, is present in moderate quantities but exhibits a different pattern spatially. Small dotted red structures in Figure 4.14 panel (C) represent this specific sugar, but mostly appear at the top layer of the biofilm. This may be the result of active secretion of monosaccharides and polysaccharides emanating from the bacterial cells forming the EPS matrix during the maturation of the *Pseudomonas* sp. ADP biofilm. Since this sugar is not present in the formulated DSMZ medium nor LB medium, it must be formed by the cells. Additionally, as expected, most of the actively dividing cell material with almost no N-acetylglucosamine presence is at the middle and bottom layers of the biofilm sample. In panels (E) and (F) of Figure 4.14, the lectin displayed RCA I corresponds to a sugar specificity of galactose. This sugar is not present in high quantities, unlike glucose/mannose, in *Pseudomonas* sp. ADP biofilms. Visualization of the sparse amount of galactose is confirmed by panels (E) and (F). In other bacterial strains, such as *Bacillus subtillis*, the presence of galactose and metabolism thereof plays a crucial role in biofilm formation. Galactose is used for synthesis of EPS in *Bacillus subtillis* biofilms.[107] In Tufa-associated biofilms, cloud-like EPS glycoconjugates were dominated by galactose, among other amino sugars.[108] *Xylella fastidiosa* biofilms also exhibited the presence of 0.002, 0.002, 0.003 mg mL^{-1} of the sugar galactose, in wild-type, rpfA, and rpfB mutants, respectively.[102] However, as

indicated by IMARIS generated micrographs and CLSM quantifiable MIR values from fluorescence data, a low quantity of galactose may be present in *Pseudomonas* sp. ADP biofilms dependent upon the type of medium.

For comparison purposes of sugar presence and distribution throughout the biofilm, in the absence of cell material, images (A), (B), and (C) in Figure 4.15 are provided.

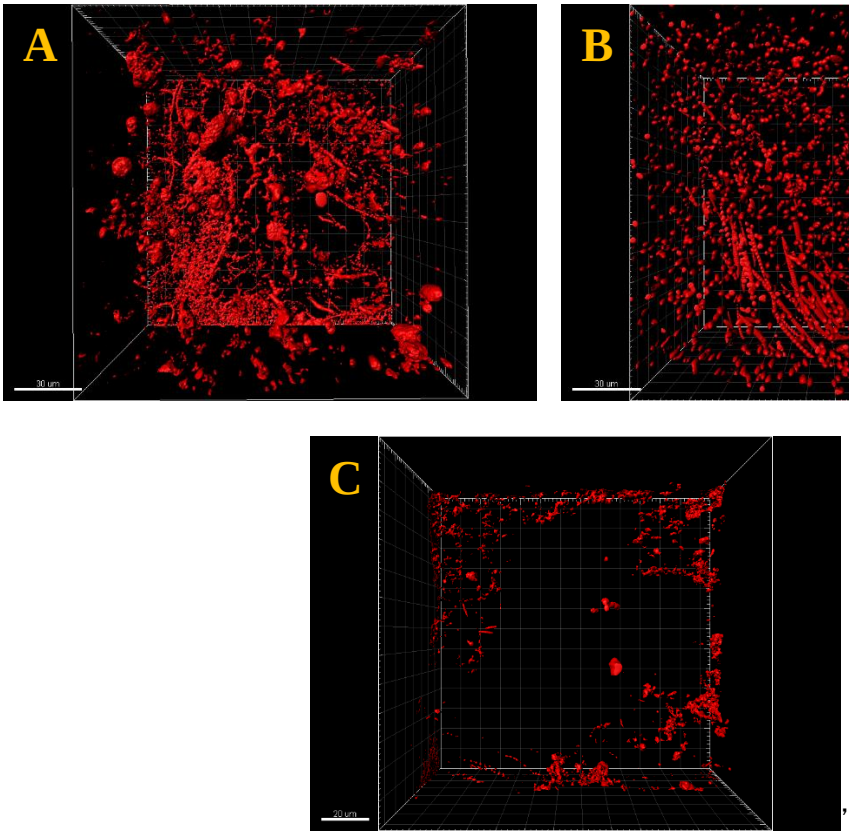

Figure 4.15. IMARIS generated images of *Pseudomonas* sp. strain ADP biofilms viewed under a confocal laser scanning microscope in single-channel mode displaying rhodamine-bound lectins Peanut Agglutinin (PNA) (A), Wheat Germ Agglutinin (WGA) (B), Ricinus Communis Agglutinin (RCA) (C) from a top-view.

It is also clear to visualize the heterogeneity in the shape and size of the glycoconjugates. The lectin distribution for PNA and WGA both demonstrate the presence of sugars throughout all layers of the biofilm, but in different manners. Possibly due to the broad specificity of PNA (two sugars) compared to the single-

specificity of WGA (single-sugar), the shape and size of the lectins bound vary considerably in panel (A), whereas the size and shape of the lectins bound in panel (B) are relatively consistent. N-acetylglucosamine, the sugar corresponding to lectin WGA, appears to be relatively small and circular throughout the layers of the *Pseudomonas* sp. ADP biofilm sample. In panel (C), lectin RCA I is represented without DAPI staining for cell material. As described earlier, the presence of galactose in P.ADP is relatively sparse throughout the entire biofilm. However, the absence of rhodamine-bound lectin may also be due to insufficient incubation time during staining. These images generated by IMARIS showcase heterogeneity of sugars in P.ADP biofilms.

Lectin dependence upon media in P.ADP biofilms

Pseudomonas sp. ADP biofilms were grown under two distinct types of growth media: LB, a nutrient-rich medium, and DSMZ containing 30 mg L^{-1} of atrazine, a relatively nutrient-poor medium. Due to the different nutritional compositions and rate of growth, it was assumed this may affect the distribution of the sugars present in a mature P.ADP biofilm. Seven lectins were screened in each case and displayed a marked change in lectin-binding as evaluated by the mean intensity ratios (MIR) for each case. Figure 4.16 shows the relative amount of each lectin in averaged biofilms by growth medium used. In LB, the amount of Soy Bean Agglutinin, which contains a specificity for α or β-N-acetylgalactosamine, is proportionally much higher (~80%) than in DSMZ (~25%), while conversely ConA demonstrates a vast difference. ConA, specific for a-mannose and a-glucose, is proportionally higher (~25%) in DSMZ medium, while only at (~15%) in a nutrient rich medium (LB). At this stage, there is no suggestive explanation for the specific changes observed in composition by lectin

identity due to the complex nature of biofilms. However, the presence of glucose (1%) added in DSMZ as carbon source to aid as a supplement for biofilm formation may contribute to the high proportion of ConA lectin in the DSMZ condition.

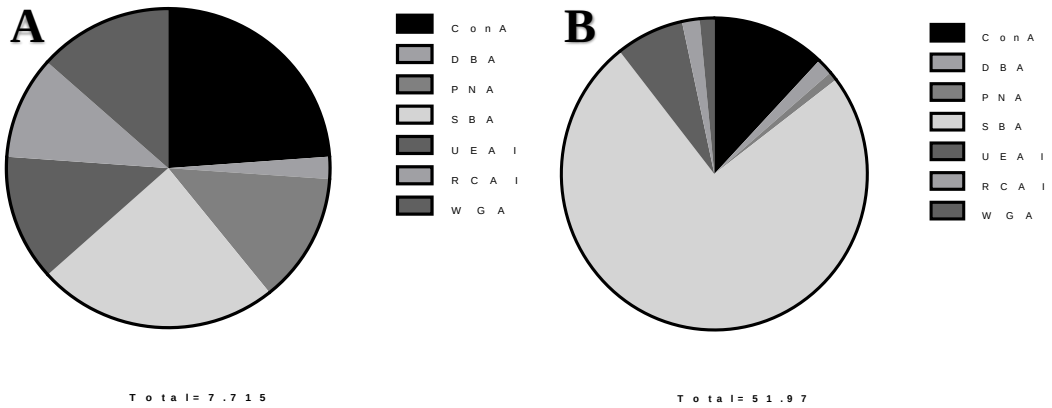

Figure 4.16. Relative distributions of rhodamine-bound lectins normalized to cell material in *Pseudomonas* sp. strain ADP biofilms grown in DSMZ medium (A) and grown in LB medium (B). Total represents fluorescence intensity ratio (arbitrary units).

Contributions of sugars such as galactose and fucose from the generated EPS may play a significant role in biofilm formation processes, originating in the corresponding lectins RCA 1 and UEA 1. The total amount of mean intensity is reported below each chart in Figure 4.16. The sugar specificity for each lectin is outlined in Tables 4.5 and 4.6. Some lectins, as described earlier, have a specificity for multiple sugars (ConA, SBA while other lectins only have a specificity for one sugar (DBA, PNA, UEA I, RCA I, WGA). The mean intensity ratios are reported, along with associated error. As demonstrated in both tables, regardless of media, the criteria for presence of absence of the monosaccharide is dependent upon the following: MIR>>1.0 signifies a positive value (presence), MIR<<1.0 signifies a negative value (absence) while values MIR ~ 1 or with a high amount of error are deemed inconclusive. Due to the sample size for each set of data (n = 4 biofilms), the

variance for a few of the lectins was quite high and no adequate conclusion on the presence or absence of specific sugars could be determined.

The data provides a starting point for the presence and absence of certain monosaccharides in *Pseudomonas* sp. strain ADP biofilms. However, it is necessary to also survey rhamnose sugars, which are key sugars normally bound to fatty acids to build rhamnolipids, which are known to have a role in biofilm formation. Additionally, in strain *Pseudomonas aeruginosa*, a molecule known as LPS is spontaneously released into growth medium which contains glucose, mannose, and N-acetylglucosamine.[109] Tables 4.5 and 4.6 show these would correspond to lectins ConA and WGA, which are present in moderately high quantities, regardless of LB or DSMZ medium for growth. Future research will be focused on screening an increased number of lectins to further characterize the macromolecules present in *Pseudomonas* sp. ADP biofilms. Henry et al. began further characterization of P.ADP biofilms by describing proteins, nucleic acids, and sugars detectable by Raman analysis.[9] It is necessary to evaluate the macromolecules within P.ADP biofilms to further understand biofilm-specific processes such as formation, maturation, dispersion, and secondary colonization. This may aid progress in optimization of conditions for P.ADP in bioreactors at a faster rate for both *ex situ* and *in situ* bioremediation.

Conclusion

The development and optimization of a novel method for detecting the expression of genes in bacterial biofilms with the aid of confocal microscopy (CLSM) has profound implications in the field of environmental biotechnology. Real-time

monitoring of the degradation of priority pollutants, such as the degradation of atrazine by strain *Pseudomonas* sp. ADP, is an application of this specific technology. Furthermore, evaluating the expression of genes in three-dimensional biofilms, including knowledge of the distribution of genes and timescale, may be extended to medical and dental industries whose often aim is to terminate the presence of biofilm-mediated microbes.

Despite attempts to optimize In Situ Reverse Transcription (ISRT) for *Pseudomonas* sp. ADP planktonic cells, the negative controls produced a signal in the absence of eubacterial probes. Furthermore, a high density of non-specific signals was observed in the presence of eubacterial probes bound to dye Alexa Fluor 488. The dual channel, displaying both a DAPI counterstain and Alexa Fluor 488 expression dye, was used to differentiate cells not expressing the gene of interest and the entire population of planktonic *Pseudomonas* sp. strain ADP cells. To move forward, it is essential to amplify the signal prior to proceeding for optimization in P.ADP free-cells and biofilms. This may be done in one of two methods A) DIG-antibody labeling, and b) ISRT in tandem with PCR. Each extension will amplify the signal in diverse ways but may prevent non-specific binding of probes and intensify the signal originating from a bacterial strain that may have a low-copy number of mRNA. Despite the result of no differential expression in atrazine-degrading genes for *Pseudomonas* sp. strain ADP biofilms relative to free cells, it would be of great value to proceed optimizing ISRT for applications of in environmental monitoring and demonstrating the temporal and localization characteristics of expression in a biofilm. Furthermore, applications of ISRT as an *in situ* method for determining gene expression in a visual manner may be extended to microbial biofilms in the fields of

dentistry, medicine, pathology, and bio-corrosion. Transmitted micrographs of *Pseudomonas* sp. strain ADP cells were successfully obtained and appeared to be consistent with cellular morphology of *Pseudomonas* species.

Scanning electron microscopy (SEM) was used to evaluate morphological differences between P.ADP biofilms and planktonic cells. The webbed matrix, contributed by the extracellular polymeric substances characteristic of biofilm-mediated cells, was visually present in mature five-day biofilm micrographs. Conversely, cells grown in shake flasks under constant agitation appeared to have morphological consistent characteristics with planktonic cells. Several rod-shaped cells in less dense clusters were present in SEM micrograph, without the presence of mesh-like webbing and/or matrices.

To further characterize the macromolecules, a non-destructive method was employed. Confocal laser scanning microscopy (CLSM) was successfully used for implementing fluorescent lectin binding analysis (FLBA) to evaluate the monosaccharide composition and distribution in *Pseudomonas* sp. strain ADP biofilms. By screening a high number of lectins, specific identities of monosaccharaides were able to be distinguished. The mean intensity ratios (MIR) of lectin-glycoconjugate to cell population signal were calculated for each lectin assayed. Lectins Concanavalin A (ConA) and Soybean Agglutinin (SBA) demonstrated to have the highest MIR in *Pseudomonas* sp. ADP biofilms, suggestive of α-mannose, α-glucose, and N-acetylgalactosamine presence.

In addition, the monosaccharide dependence upon medium, LB and DSMZ containing atrazine, was assayed. Cells grown in LB has a greater proportion of SBA and a lower proportion of ConA. Screening of more lectins would be necessary for a

comprehensive evaluation of sugar composition and distribution in P.ADP biofilms. However, the seven lectins screened aid demonstrate, to a certain degree of specificity, the monosaccharides present. This data may be correlated to previously collected Raman data on macromolecules in P.ADP biofilms to help further characterize macromolecules secreted in extracellular polymeric substances (EPS) unique to biofilms.

Microscopy is a powerful tool used across chemical engineering, molecular biology, microbiology, medicine, and pharmacology. Here, we have demonstrated the use of confocal laser scanning microscopy and scanning electron microscopy to aid in genetic and physical characterization, respectively, of *Pseudomonas* sp. strain ADP biofilms. The development of novel methods in microscopy is essential for adding to the toolbox of engineers working in bioremediation. Biofilm-based bioreactors for *ex situ* bioremediation and real-time monitoring of recalcitrant pollutants may be successfully realized by furthering the described efforts.

CHAPTER 5: KINETICS OF ATRAZINE DEGRADATION BY ANALYTICAL METHODS

Introduction

Pseudomonas sp. strain ADP is the model strain for atrazine degradation, and the kinetics of the biodegradative process in a planktonic mode of growth has been extensively studied since the strain's initial discovery.[3,10,32,110–112] Devers et al. discovered the strain degrades atrazine following a first-order kinetic model with a steady decrease in atrazine concentration until it is completely metabolized.[3] Furthermore, other researchers were able to define optimal conditions for atrazine-degradation and resulting kinetics, but with the use of mixed microorganisms rather than solely pure ADP using response surface methodologies (RSM).[113] Despite the increasing wealth of knowledge on atrazine-degradation kinetics with shake flask based experiments, relatively little has been researched, to our current knowledge, on atrazine biodegradation as a result of biofilm-based metabolism. Biglione et al. first explored growth of P.ADP in the biofilm mode of growth and determined design and scale-up parameters using a Monod model of kinetics.[10,112] More recently, in 2017, Henry et al. began evaluating the degradation kinetics of atrazine in P.ADP biofilms compared to free-cells using GC-MS based approaches.[5]

The approach of comparing catabolic activities of biodegradative bacterial strains is not original, however the use of P.ADP and atrazine degradation as the model bacterial strain for these experiments is the novelty. For example, planktonic and biofilm cultures of chlorophragm-degrading cultures were found to differ in chlorophragm-degrading activity. Biofilm cultures demonstrated slower chlorophragm removal with less accumulation of 3-chloroaniline (a toxic intermediate). However, once the biofilm architecture was disrupted, the system demonstrated similar

degradation to free cells.[114] Toluene degradation kinetics for planktonic and biofilm cells of *Pseudomonas putida* 54G were also evaluated. The biofilm cells were grown on ceramic rings and removed, then suspended in batch cultures to calculate the degradation rate of toluene. However, the specific activities measured for degradation by planktonic and biofilm-based cells were similar at the same biomass. This may suggest the architecture and matrix formed from biofilm plays an important role in catabolic processes and pollutant removal.[114–116]

In this chapter, we explore the process of atrazine-degradation by a pure culture of *Pseudomonas* sp. ADP cells. In the biofilm mode of growth, the architecture will remain intact. In shake flasks, the cells will be removed at a constant rate. The biofilm effluent was evaluated for atrazine and metabolites and compared to the removal of samples from shake flasks. The challenge, however, is completion of a mass balance for the drip-flow reactor biofilm growth system. The influent medium containing a desired amount of atrazine must be equivalent to the amount of atrazine within the growing and degrading within the biofilm with the atrazine left in the effluent waste. Then, entrapped atrazine contained in the biofilm and degraded atrazine can be evaluated. Furthermore, our goal is to compare the overall biodegradation efficiency, defined as the total amount of atrazine removed over a specified period, of biofilms to planktonic cells. The results will aid in future development of biofilm-based systems used for bioremediation purposes, if they are more efficient than planktonic counterparts.

Lastly, it is worthwhile to determine the concentration of the metabolites of the six-step degradation process over time in each condition. By employing methodologies such as enzyme-linked immunoassay (ELISA), gas chromatography –

mass spectrometry (GC-MS), and high-performance liquid chromatography (HPLC), we can determine concentrations of the parent molecule, atrazine, and its biodegradative metabolites.

Materials and Methods

Sample collection for P.ADP planktonic cells

Strain *Pseudomonas* sp. ADP cells were thawed from frozen -80^{o}C stock, and subsequently inoculated in 10 mL DSZM medium containing atrazine (30 mg L^{-1}). Cell culture was grown for 48 h prior to pre-inoculum transfer to 50 mL of DSMZ medium in an Erlenmeyer Flask (250 mL). Flasks containing cell culture were shaken at 250 rpm and incubated at 30^{o}C in a shaker-incubator, and samples (1 mL) were retrieved in triplicate (biological and technical replicates) every 12-24 h and transferred to a cryogenic vial. Samples were immediately flash frozen with liquid nitrogen and stored at -20^{o}C. Contents in each cryogenic vial were then subjected to one of the following analytical protocol(s): GC-MS, HPLC, ELISA, or UV-Vis spectrophotometry.

Sample collection for P.ADP biofilms

Strain *Pseudomonas* sp. ADP cells were thawed from frozen -80^{o}C stock, and subsequently inoculated in 10 mL DSZM medium containing atrazine (30 mg L^{-1}). Cell culture was grown for 48 h prior to pre-inoculum transfer to 50 mL of DSMZ medium in an Erlenmeyer Flask (250 mL). Flasks containing cell culture were shaken at 250 rpm and incubated at 30^{o}C in a shaker-incubator until mid-exponential phase. Cells (50 mL) were then centrifuged, concentrated and re-suspended as previously described. Bacterial suspensions (10 mL) were then dispersed on Silane-coated slides on the DFR in triplicate and allowed incubated at room temperature in a sterile

environment to allow for bacterial attachment (batch phase) for 6-8 h. DSMZ medium containing 30 mg L^{-1} atrazine was propelled with peristaltic pumps onto the drip-flow reactor to dispense on the slide containing attach P.ADP at a rate of 0.8 mL min^{-1}. Samples (1.0-1.5 mL) were retrieved in triplicate (biological and technical replicates) every 12-24 h and transferred to a cryogenic ail. Samples were immediately flash frozen with liquid nitrogen and stored at -20°C. Contents in each cryogenic vial were then subjected to one of the following analytical protocol(s): GC-MS, HPLC, ELISA, or UV-Vis spectrophotometry.

Mode of growth dependence using GC-MS

Extraction protocol was followed as described by Henry et al.[5] Briefly, atrazine in the biofilm state and planktonic mode of growth was quantified over a period of five days to maturity using gas chromatography mass spectrometry (GC-MS). Liquid-liquid extraction was used to extract atrazine from shake flask samples (1 mL) and biofilm effluent samples (1 mL) every 12-24 h.

Ethyl acetate (0.5 mL) was mixed with either shake flask sample or effluent sample (1 mL), and vortexed. Once the organic phase had clearly separated, as indicated by a clear biphasic solution, the upper layer was drawn off and transferred to a micro tube. The upper phase is characteristic of being the organic phase containing atrazine. Extraction from the lower phase, containing the other components, was repeated with ethyl acetate twice more and all the organic fractions were combined. This was done to remove the highest concentration of atrazine possible.

Next, a benchtop centrifugal evaporator (Savant SDP13DDA SpeedVac Concentrator, Thermo Fisher, Waltham, MA) was used at a high drying rate and

medium speed for 6-8 h, until extracts were completely dry and devoid of an aqueous component. If aqueous components remained, samples were extracted with ethyl acetate until dried. Then, dried extracts were re-suspended in ethyl acetate to a volume of 1mL, vortexed, and transferred to GC-MS glass vials. Samples were stored at -20°C until GS-MS analysis.

Temperature-dependence using GC-MS

Methods described previously with minor modifications were used to analyze the dependence of *Pseudomonas* sp. strain ADP growth temperature on atrazine-degradation. Biofilms were grown at 30°C and 37°C, and the effluent was subjected to GC-MS analysis for samples taken in triplicate every 12-24 h for five-days until biofilm had completely matured, and prior to dispersion. In this protocol, no planktonic cells were sampled.

Atrazine concentration in biofilms using GC-MS

Methods described previously with minor modifications were used to analyze the concentration of atrazine in *Pseudomonas* sp. strain ADP biofilms grown at 30°C. Biofilms were harvested after 10 days from DFR and scraped into 50 mL centrifuge tubes and stored at -20°C prior to extraction. Biofilm samples were thawed and each biological replicate (× 4) were split into two samples. Samples were extracted using methods described previously with modifications. Briefly, each biofilm was split into two tubes and charged with ethyl acetate (2 mL). Samples were vortexed for two minutes, centrifuged, and extracted twice with ethyl acetate. EPS and solid components were discarded following extraction process, and supernatant was subjected to evaporation under reduced pressure and resuspension prior to GC-MS

analysis. Standards ranging from 0 mg L^{-1} to 50 mg L^{-1} of atrazine were prepared in advance, and samples concentrations were analyzed based on a calibration curve of peak area.

HPLC

HPLC was used to quantify and characterize downstream metabolites of atrazine degradation, including cyanuric acid and biuret. Prior to HPLC analysis, samples were collected for biofilm and shake flasks as described previously. To remove cell mass and particulates, the supernatants of samples were filtered through a 0.22-µm filter following centrifugation (6,000 x g, 10 min, 4°C), and transferred to 9 mm threaded S/T amber vials (12 mm x 32 mm, Sigma Aldrich, St. Louis, MO) with R.A.M. 9 mm PTFE/Silicone screw caps. Analysis was performed with an Agilent 1100 High Performance Liquid Chromatograph quarternary pump G1311A system equipped with a diode array detector. To resolve and quantify downstream metabolites (cyanuric acid and biuret) of the parent compound (atrazine), a method was adopted and modified as per Strong et al.[117] An Inertstil 5-µm, (150 x 4.6 mm) phenyl column (GL Sciences, Torrance, CA) was used with guard cartridges (10 mm) and an isocratic mobile phase of sodium octane sulfate in 0.05% H_3PO_4 at pH 2.8 (5 mM). Standards for each metabolite and uninoculated medium were run in HPLC. The theoretical retention times for the compounds of interest are: 2.6 min for cyanuric acid and 2.6 min/3.6 min/4.0 min in three phase segregated peaks for biuret. Concentrations of each compound were evaluated based on peak areas from standard curves.

ELISA

Samples were collected in shake flasks and biofilms as previously described. Samples were stored at -20^{o}C prior to ELISA analysis. An atrazine ELISA kit (ABNOVA, Taipei, Taiwan) was used for the quantitative measurement of atrazine by a competitive binding enzymatic immunoassay mechanism. The concentrations of initial un-diluted samples were expected to be between 0.1-30 mg L^{-1}, which falls above the limit of detection for ELISA. Samples were diluted 1000-fold to ensure the highest sample did not exceed 50 µg L^{-1}. Aliquots of 0.1 mL were retrieved from frozen samples once thawed and transferred to another micro tube and subsequently diluted to fall in the middle of the standard curve.

As per manufacturer's instructions, the kit components were equilibrated at room temperature prior to use. Samples or standards (50 µL) were added to the bottom of each well of a microtiter plate, and ATZ-ALP conjugate (#3) (100 µL) was added to each well thereafter. Mixture was incubated at room temperature for 40 min. Solution was then inverted and shaken, and washed 3x with wash buffer to remove un-bound conjugates. To each well, pNPP substrate (#5) (100 µL) was added and allowed to incubate for 20 min. Approximately 50 µL of Stop Solution (#7) was added to each well, and the strip holder was tapped to ensure proper mixing. The absorbance was read on plate reader at 405 nm. The concentrations of atrazine were determined based on results of the standard curve.

Results and Discussion

Dependence of biodegradation on mode of growth by P.ADP

As measured by GC-MS, the concentration of atrazine decreased from an initial concentration of 50 mg L^{-1} to 18 mg L^{-1} after 24 h. In the next three days, the

amount of atrazine was relatively unchanged and remained at 18 mg L^{-1}. Atrazine decreased slightly from the fourth to fifth day to 16 mg L^{-1}. Overall, atrazine diminished at a slow rate when grown in shake flasks and did not demonstrate any transient increases. The atrazine within a batch mode of growth remains stationary prior to inoculation of P.ADP cells. Once P.ADP begin utilization of atrazine of a source of growth and nitrogen, the concentration rapidly decreases. Devers et al. reported a decrease in atrazine at an initial amount of 45 and 10 mg L^{-1} over a shorter period of 350 min. The amount of atrazine decreased more rapidly in previously published literature.[3] This may be a result of slight modifications in the medium used, as well as different amount of starting cell material. However, both previously published literature and the work presented here are consistent in steady decreases of atrazine in planktonic *Pseudomonas* sp. strain ADP cells. Biofilm based cells grown in a DFR, however, demonstrate differential degradation kinetics as each case is shown in Figure 5.1.

In the biofilm mode of growth, concentration of the effluent rapidly decreased in 48 h from 50 mg L^{-1} to 20 mg L^{-1}. Initially, the rapid decrease in atrazine may likely be due to entrapment of the contaminant within the extracellular polymeric matrix while the substrate is being utilized by biofilm-enclosed cells, as evidenced in previous studies by Henry et al.[9] The increase in atrazine concentration in the biofilm flow system most probabilistically is a result of dispersal of the biofilm-mediated cell release into the effluent after maturation. In this model, atrazine entrapped within the matrix would fall into the effluent when dispersed, and therefore cause a transient apparent increase in atrazine concentration. Following maturation after 5-days, we would expect the biofilm to degrade atrazine at a greater efficiency until no

pollutant remains. To accurately assess the overall biodegradation efficiency of planktonic cells compared to use of biofilms, a longer timescale may be necessary until both conditions reach negligible atrazine by measured by GC-MS.

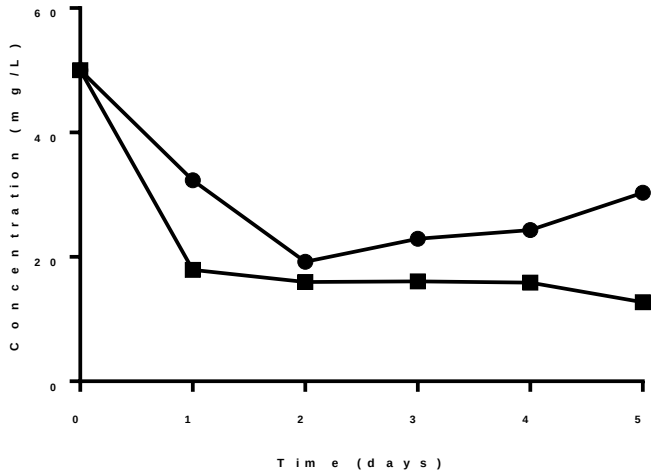

Figure 5.1. Atrazine concentration measured by GC-MS over five days in shake flasks containing a planktonic cell medium (■) and a DFR-grown biofilm containing reactor effluent (●) as a result of microbial degradation.[5]

Interestingly, the ELISA assay implemented demonstrated different results for atrazine degradation in planktonic cells and biofilm effluent compared to GC-MS analysis. Samples were diluted 1000-fold from original concentrations to be in the range of detection. Once the 96-well microtiter plate containing samples was washed to remove non-specifically bound antibodies or proteins, an enzymatic substrate was added to the bound sample, and a colorimetric result was produced. That is, the originally clear solution increased in yellow character over time and was proportional to the amount of atrazine present (Figure 5.2).

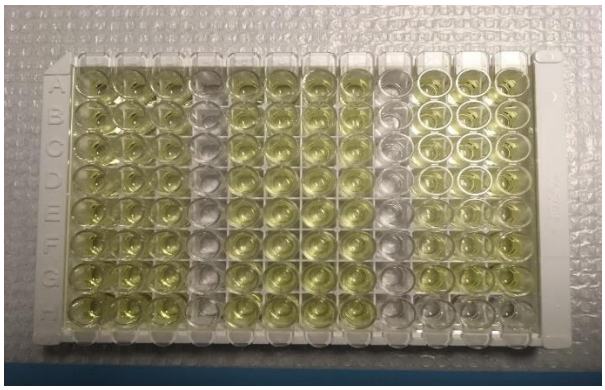

Figure 5.2. 96-well microtiter plate for atrazine-based ELISA assay demonstrating colorimetric change of enzyme-substrate binding.

The concentration of atrazine in biofilm effluent and planktonic cell culture was measured to be 30 mg L^{-1} after accounting for dilutions. The concentration of atrazine substantially decreased to 5 mg L^{-1} after 4 h in planktonic culture, and steadily decreased until undetectable at 20 h. The concentration fell below the limit of detection for the remainder of the 10-day period. This result is consistent with previous data acquired on atrazine degradation in planktonic cells in higher concentrations at approximately 50-100 mg L^{-1}.[1,3] In contrast, the biofilm effluent dropped off considerably in the beginning at 4 h, and then remained relatively constant at 5 mg L^{-1} until 10 days as illustrated in Figure 5.3.

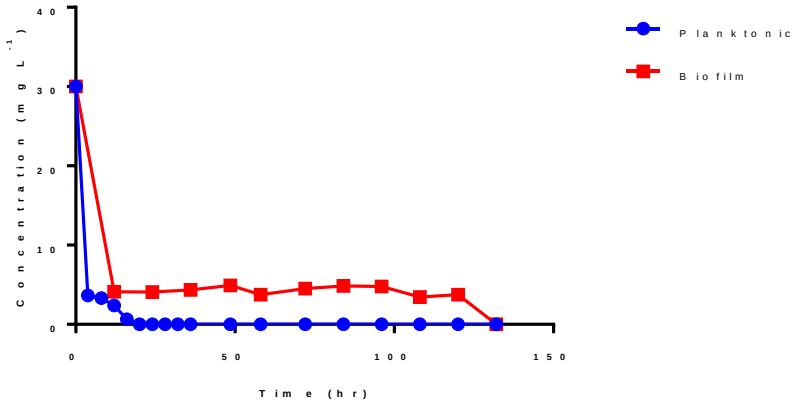

Figure 5.3. ELISA results for tracking atrazine concentration in samples from biofilm effluent and planktonic cell culture. Samples were diluted 1000-fold and inhibition curve was constructed for calibration.

The initial decrease in atrazine concentration from biofilm effluent suggests adsorption of atrazine to the extracellular polymeric substances and active biodegradation processes may be occurring simultaneously to remove atrazine. However, the level of atrazine in the effluent does not decrease from 4 h to 144 h in the remainder of the experiment. This result could suggest that atrazine is within the biofilm undergoing a degradation process and entrapped within the EPS, and continuously removing atrazine at a consistent rate until 144 h.

Regardless of method, the atrazine level decreases and remains at low levels in both GC-MS and ELISA results from the biofilm effluent after 24 h and remains relatively constant. This is likely due to changes in the biofilm which are contributing to an EPS matrix capable of removing atrazine and metabolically active cells using atrazine as a source of nitrogen and growth.

Prior to 10 days, the atrazine level in the effluent decreases to undetectable concentrations. It is necessary to analyze the level of atrazine within the biofilm, and evaluate the presence and quantity of biodegradation metabolites, such as cyanuric acid and biuret to suggest the extent of catabolic activity and physical EPS entrapment processes occurring. We may surmise, however, that the combination of physio-chemical methods of EPS entrapment along with catabolic activity of P.ADP contributes a more comprehensive process for atrazine removal relative to planktonic cells in shake flasks. In addition to analyses based on mode of growth, temperature may also play an important role in the removal of atrazine using P.ADP biofilms.

Dependence of biodegradation on temperature by P.ADP biofilm

Strain *Pseudomonas* sp. ADP biofilms were grown under two temperatures: 30°C and 37°C and monitored for atrazine degradation over a period of five days. (Figure 5.2) Atrazine attained an initial concentration in DSMZ medium between 21-25 mg L^{-1}. In the 30°C condition, the herbicide decreased steadily over a period of 2.5 day until it reached 8 mg L^{-1}. Then, atrazine increased over the next 2.5 days until maturity with a final effluent atrazine level of 14 mg L^{-1}. At 37°C, atrazine transiently increased from 21 mg L^{-1} to 26 mg L^{-1}in the first 2 days, and then sharply dropped at 2.5 days to 12 mg L^{-1}. Then, from 2.5 days to 3.7 days, the level of atrazine remained relatively unchanged. Towards complete biofilm maturation, the herbicide concentration decreased even greater to a final concentration of 5 mg L^{-1}.

Temperature has an effect on the rate of biodegradation from certain microbes, as evidenced previously.[118] However, it is unclear as of writing this the optimum temperature for atrazine degradation by *Pseudomonas* sp. strain ADP free-cells. Even more so, the optimum temperatures for atrazine degradation by P.ADP biofilms are not clear. Despite the absence of research, the kinetic biodegradation profiles reported here provide data on the effect of biofilms as a bioremediation agent for atrazine removal and degradation. Based on the final concentrations of atrazine, it appears P.ADP biofilms grown at 37°C are more efficient degraders than P.ADP biofilms grown at a lower temperature of 30°C. This may suggest that use of biofilm-based bioreactors should increase the reactor growth temperature at the upper end of the mesophilic range to ensure a greater degradation efficiency. Future work should include evaluating the herbicide concentration within the P.ADP biofilm to complete a mass balance for the proposed system. This would allow researchers

to evaluate the mechanism of action for atrazine disappearance more clearly, i.e., whether atrazine is being actively degraded within the film or the contaminant is solely entrapped with poor bioavailability as a substrate to *Pseudomonas* sp. strain ADP cells. The effect of temperature of biofilm growth on biodegradation capacity of atrazine over a period of 5 days is illustrated in Figure 5.4

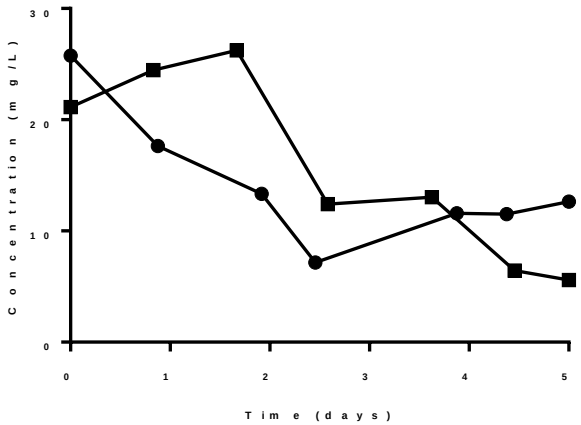

Figure 5.4 Atrazine concentration measured by GC-MS over five days in a DFR-grown biofilm (reactor effluent) at incubation temperatures of 30°C (●) and 37°C (■) as a result of microbial degradation.

Atrazine detection in DFR-grown P.ADP biofilms

Strain *Pseudomonas* sp. ADP biofilms were analyzed for atrazine concentration following analysis of biofilm effluent and influent to complete the total mass balance of the system. Initially a calibration curve was constructed from atrazine concentrations in the range of 1.0-50.0 mg L^{-1} of atrazine to account for possible accumulation higher than 30.0 mg L^{-1} (Figure 5.5). The coefficient of determination was 0.994 as a result of linear regression analysis, suggesting the regression model explains 99.4% of the variability of the response data surrounding the mean values. Total atrazine was extracted from P.ADP biofilms to evaluate the remainder of herbicide within the biofilm not present in the effluent or the influent. A

significant amount of atrazine in the biofilm would suggest physical interactions of the EPS play an influential role in bioremediation of atrazine, compared to catabolic activity. Conversely, negligible amounts of atrazine within the biofilm samples would suggest catabolic activity may play a more significant role in biofilm-based remediation relative to physical EPS entrapment and interactions.

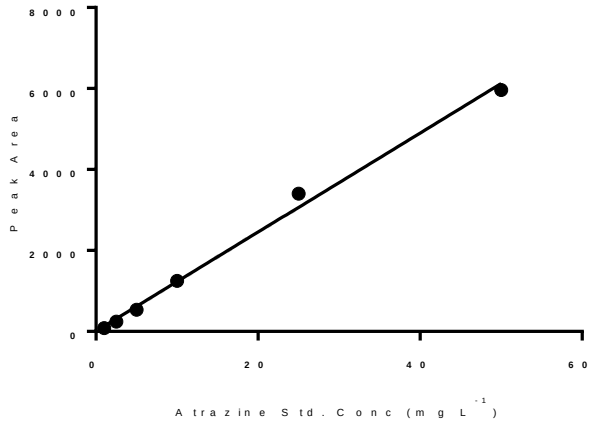

Figure 5.5 Constructed calibration curve of atrazine concentrations ranging from 1.0-50.0 mg L^{-1} and peak area using GC-MS.

However, there may be intracellular atrazine that had not been completely extracted due to the nature of the complex architecture of the extracellular polymeric substances. No atrazine was detectable by GC-MS within the biofilms, nor any biological or technical replicates (n = 4).

This may be a result of inefficient extraction and EPS interference or suggests physical EPS interactions are not influential in atrazine biofilm-based remediation processes. However, it is still possible that atrazine is physically bound to the the EPS, the cells within the biofilm are catabolically active, and downstream metabolites flow to the effluent. To attain a more accurate depiction of the processes and role of P.ADP biofilms in bioremediation, it may be necessary to optimize an extraction

process prior to GC-MS analysis to detect small quantities of entrapped atrazine, or additional intracellular atrazine. It would be beneficial to use Raman spectroscopy or IR to evaluate the concentration of atrazine in the solid component of the EPS. It is conceivable that atrazine is bound to the extracellular polymeric matrix and was not extracted in the process for GC-MS detection. Conversely, solid-state methods such as Raman spectroscopy may be able to detect atrazine and its metabolites within the solid phase components. These results would allow us to deduce the mechanism of action for atrazine disappearance with clarity. Furthermore, harvesting biofilms at various time points would add a necessary temporal component the complete P.ADP drip-flow biofilm system.

Conclusion

It is clear to see that atrazine-degradation kinetics for biofilm-based systems (flow) are more complex than planktonic systems (batch). This is due to the dynamic component of nutrients propelled onto the surface of a culture, and further disposed of in the effluent as waste. In contrast, planktonic cells have a static supply of nutrients and the substrate (atrazine) to use as a source of nitrogen and is expected to have a steady decrease. GC-MS experiments revealed the complexity of biofilms with respect to different temperatures of growth. Based on effluent, biofilms grown at 37^{o}C had a greater biodegradation efficiency in a five-day growth period with a final concentration of 3 mg L^{-1} atrazine, while biofilms grown at 30^{o}C had a lower biodegradation efficiency in a five-day growth period with a final concentration of 12 mg L^{-1} atrazine.

ELISA results demonstrated the concentration of atrazine decreases rapidly to undetectable traces in the first 24 h period. Conversely, the concentration of the

effluent in the biofilm decreases to 5 mg L^{-1} in the first 4 h period, and then remains steady until 144 h. Atrazine concentration within the biofilms were at undetectable amounts following extraction and subsequent analysis by GC-MS. This data suggests biofilm kinetics are increasingly complex compared to atrazine biodegradation in planktonic cells and must be further studied.

When comparing the degradation kinetics for atrazine in *Pseudomonas* sp. strain ADP biofilms to planktonic cells, the degradation efficiency was not clear. Planktonic cells steadily removed atrazine by catabolic degradation, as supported be previously published literature suggesting first-order reaction kinetics. Biofilms, however, decreased concentration of atrazine below 50% in the first two days, and the concentration increased from the third to fifth day. This may suggest atrazine removal via EPS matrix, and the flow system in the DFR contributing to multifaceted kinetics that requires future work.

CHAPTER 6: CONCLUSION AND FUTURE PERSPECTIVES

Thesis Conclusion

The model strain for atrazine degradation is the bacterial strain *Pseudomonas* sp. ADP. This bacterium has been extensively studied in its planktonic, free cell state since its initial discovery. In the work presented, we have furthered characterization of *Pseudomonas* sp. ADP from a genetic, molecular, and chemical level in a biofilm mode of growth. Bacteria often congregate onto a surface, biotic or abiotic, and secrete a myriad of extracellular polymeric substances which serves to protect the microbes in a matrix. These structures are termed biofilms, and they are the dominant form of microbial life in the natural environment

First, to evaluate possible induction of atrazine-degrading genes in the biofilm mode of growth, we utilized genetic tools such as RT-qPCR to compare the fold-changes in expression of each of the six atrazine-degrading genes relative to the strain grown as planktonic cells. There was no statistically significant difference in expression. However, the expression of atrazine-degrading genes in *Pseudomonas* sp. ADP biofilms changed in response to growth temperature. These results, which suggest catabolic activity of P.ADP increases or decreases dependent upon temperature, will aid in future optimization of biofilm-based bioreactors for ex situ bioremediation as well as further our understanding of P.ADP's response to natural environmental temperature changes.

Next, we explored microscopy as a tool for localizing expression and temporal data on atrazine-degrading genes in *Pseudomonas* sp. strain ADP. Our approach using ISRT and green/red fluorescent protein fusion requires more optimization to apply to the bacterial strain and genes of interest. However, a technique suitable for

characterization of macromolecules in biofilms, fluorescent lectin binding analysis, was employed to determine the identity and location of monosaccharides present in P.ADP biofilms. Also, the monosaccharaide type of quantity was affected by changing in medium from a nutrient rich medium (LB) to a nutrient poor medium (DSMZ containing atrazine). Previous data collected on proteins, nucleic acids, and fatty acids based on Raman fingerprints will aid in generating a complete macromolecule profile of P.ADP biofilms.

Lastly, analytical chemistry was used to distinguish atrazine-degradation kinetics of biofilms and planktonic cells. Furthermore, these methods were used to determine the overall biodegradation efficiency of P.ADP biofilms compared to planktonic cells. GC MS results suggested degradation of atrazine by free cells followed first-order kinetics while a flow system using P.ADP biofilms demonstrated more complex reaction kinetics. The identity and quantity of the parent compound, atrazine, and its bacterial metabolites, were determined using ELISA and HPLC, respectively. It is clear degradation kinetics involving biofilms is more complex due to the presence of the EPS matrix and the nature of the real-time flow system for biofilm generation and maturation. Conversely, kinetics for P.ADP free cells and atrazine-degradation, as validated by previous literature, is a well understood process.

The work presented set out to analyze the overall biodegradation efficiency of *Pseudomonas* sp. strain ADP biofilms compared to planktonic cells, but it has been revealed to be more complex and multifaceted than a numerical comparison. Analytical and genetic data suggests that despite similar catabolic activity of P.APD cells in the biofilm and planktonic mode of growth, physio-chemical mechanisms of the EPS may play a significant role in bioremediation processes for P.ADP and

atrazine. GC data revealed no atrazine was present within the biofilm or EPS, which may suggest the process of atrazine removal is mostly catabolic. However, the extraction process prior to GC is liquid based, and fails to quantify atrazine that may be bound to the EPS matrix of the biofilm. This will be analyzed by Raman spectroscopy and IR spectroscopy to evaluate the presence of atrazine in solid components of the P.ADP biofilm. Previous studies on fluorescent lectin binding analysis demonstrated the presence of EPS glycoconjugates produced by cyanobacteria (mostly fucose, amino sugars, and sialic acid).[93] In addition, the presence of these glycoconjugates originating from *Acidianus* sp. DSM 29099 biofilms grown on elemental sulfur (glucose, galactose, mannose, sialic acid, and fucose).[94] Our results in FLBA may demonstrate sugars which may distinguish P.ADP biofilms, but share commonalities with other microbial biofilms. The significant presence of glucose and amino sugars demonstrate similarities of EPS-produced glycoconjugates in previous work, however our biofilms demonstrating an absence of galactose aid in being a unique identifier in *Pseudomonas* sp. strain ADP. Furthermore, screening of specific lectins could demonstrate atrazine removal capacity depending on the sugars biochemical properties. Lectins corresponding to binding of sialic acid were not assayed in our FLBA experiments but may be an aspect of future work to evaluate similar sugars found throughout the extracellular polymeric substances in microbial biofilms.

Overall, *Pseudomonas* sp. ADP biofilms were further characterized using tools in chemical engineering, molecular biology, genetics, microbiology, and biochemistry. Our understanding of P.ADP in a biofilm capacity will aid in bioremediation efforts around the world.

Scientific Impact

The work presented serves to further our understanding of the role of *Pseudomonas* sp. ADP biofilms in the bacterial remediation of the persistent herbicide atrazine. Furthermore, the work serves to develop and optimize methods in microscopy to be used across environmental monitoring and non-environmental biofilm applications in human healthcare. Data collected on the expression of atrazine-degrading genes may aid engineers in optimizing temperature control for efficient degradation of atrazine using biofilm-based bioreactors in *ex situ* bioremediation with strain *Pseudomonas* sp. ADP. In addition, kinetic data gathered may help environmental scientists resolve the use of either biofilm or planktonic based bioremediation approaches. Ideally, a decrease in the amount of atrazine in the environment will then decrease the presence of this specific endocrine-disrupting compound which negatively affects the health of humans and many aquatic organisms.

Future Work

Following the work presented within the thesis, a few important aspects will be extended in the future: 1) Component optimization of *in situ* reverse transcription by employing a design of experiments (DOE) approach, 2) Whole transcriptome analysis of *Pseudomonas* sp. ADP as a biofilm and as free-cells using next generation sequencing (NGS), 3) Detection of atrazine by Raman/IR spectroscopy, and4) Optimization of atrazine-degradation using DFR concerning temperature and acidity/basicity.

Component optimization of ISRT by a DOE approach

As discussed earlier, several potential issues may have arisen for successful detection of atrazine-degrading genes to be detected in real-time with an *In Situ* Reverse Transcription (ISRT) approach. A low-copy number of nucleic acid is a common culprit for low fluorescent signal without the use of further amplification procedures, such as is the case with *in situ* PCR. However, in the cases using *Pseudomonas putida* and de- nitrifying bacteria, neither utilized amplification procedures in order to obtain a detectable signal by reverse transcription and hybridization.[59,60,97] Factors such as permeabilization time and concentration of lysozyme, fixation time, dehydration, and probe choice may all affect the end fluorescence signal for ISRT.

This approach to hybridization experiments aids in determining the optimal step for each part of the entire experiment to ensure signal for low copy number RNA can be reliably detected and observed under a confocal laser scanning microscope. This type of approach was very successful in fluorescent in situ hybridization (FISH) with strain *Aurreobasidium pullulans by* evaluating type of fixative, enzymatic treatment times, digestion of probes, multilabel, and mutant strains. This experiment helped in increasing the signal to noise ratio, decreasing natural autofluorescence of the strain, and avoiding artifacts or losing target cells.[119] A similar DOE approach to this was taken with another strain, and rather than employ ANOVA a response-factor design was utilized.[120] Use of DOE in various ways is useful for troubleshooting experiments due to the fastidious nature of RNA—based methods, such as RT-qPCR, In Situ Hybridization, and cDNA microarrays.[121] In our case, it is recommended to utilize a partial factorial design, such as Plackett-Burman, which would allow multi-

level and multi-factors to be used, without the time and expense of a full-factorial design. Factors the must be tested for ISRT include fixation time, permeabilization time and concentration of lysozyme, amount of probe, as well as hybridization time and temperature. By employing a fractional factorial design, one varies the factors accordingly by Table 6.1, Table 6.2, and Table 6.3 presented below:

Table 6.1. Fixation time factor in DOE approach to ISRT

Fixation time (h)
0.5
1
2
3
4
8

Table 6.2. Permeabilization time and concentration in design-of-experiments approach to ISRT, each concentration and time are independent of each other and factored separately.

Lysozyme Concentration (mg/mL)	Permeabilization Time (h)
0.5	0.25
1.0	0.50
1.5	0.75
2.0	1.00
2.5	1.50
3.0	2.00

Table 6.3. Hybridization time and temperature of probe in design-of-experiments approach to ISRT, each temperature and time are independent and factored separately.

Hybridization time (h)	Hybridization temperature (°C)
0.5	30
1.0	37
2.0	50
4.0	60
8.0	65

By using a statistical methodology, it is our contention that the signal-to-noise ratio will be subsequently increased, and the hybridization of the probe will produce a signal detectable by CLSM.

Whole-transcriptome analysis of P.ADP biofilms and planktonic cells

The work presented in this thesis examines six genes involved in atrazine-degradation, *AtzA-AtzF*, as followed by the catabolic pathway which begins with the catalytic dehydrogenation of atrazine. Real-time quantitative PCR is the model method for analyzing precisely the expression of a small number of genes, and supplanted northern blotting in the twentieth century.[122] However, it is much more useful once a small set of genes has been analyzed to further analysis by employing gene discovery approaches and analyzing a new set of genes with relevant interest. This is difficult to perform on a large scale and without a reference genome by using RT-qPCR. Rather, we must rely on next-generation sequencing (NGS) technologies. Prior to NGS, a large set of genes was analyzed with microarrays, which are often costly and tedious to perform with a complete set. RNA Sequencing, often abbreviated RNA-Seq, is a NGS technology that exploits the dynamic transcriptome.

Gene fusion detection, targeted approaches, small RNA profiling, direct RNA sequencing, and characterization of alternative splicing patterns are a few of the features that can be performed by RNA-Seq.[123,124] Not only is it possible to validate RT-qPCR results using RNA-Seq with a small number of genes, but it is possible to obtain an entire set of transcriptome data for all genes in a particular species of bacterium or fungus.[125] A challenge working with *Pseudomonas* sp. strain ADP comes with lack of sufficient data on the genome, unlike model strains such as *Escherichia*

coli DH5α , *Pseudomonas aeruginosa*, or *Streptococcus mucans*. However, it is possible with RNA-Seq to perform transcriptome analysis without a reference genome with an approach termed "*de novo* assembly" which is specifically used for non-model organisms which do not have a reference genome available.[126] This is the approach that will be used for *Pseudomonas* sp. ADP with the primary goal(s) being: a) obtain novel information on genes induced and inhibited in the biofilm mode of growth, b) discovery of genes not previously recognized by performing a *de novo* transcriptome assembly, and c) validating gathered RT-qPCR data on six genes involved in atrazine-degradation. This method is not limited by prior knowledge of P.ADP, gives a broad dynamic range and high levels of sensitivity for expression levels, and is comparatively cheaper than employing microarrays.[127–129]

RNA-Seq would involve a workflow more complex than RT-qPCR and requires more time and financial obligations. RNA-Seq experiments have provided a wealth of data in differentiation of biofilms and planktonic cells in other bacterial strains and have been successfully performed in various microbes.[130–132] Despite this, the preparation and quality check of RNA in the beginning steps is massively paralleled to the RT-qPCR workflow. The workflow is displayed in Figure 6.1. Once the experiment is designed for P.ADP biofilms and planktonic cells, the RNA may be isolated and purified. The RNA will be checked for quality, and then if it has a RNA RIN greater than 9.0, will undergo rRNA depletion. Once rRNA is depleted, the RNA may be converted to cDNA with addition of sequencing adapters for library preparation. Next, cDNA may be sequenced using an Illumina sequencing platform, and analysis will be performed on the resulting set of data using bioinformatic approaches. Novel data on gene regulation and transcription as a response to changes from planktonic cells to a

biofilm mode of growth will deliver an abundant amount of original information concerning its applicability as a bioremediation strain in the biofilm state. Additionally, our understanding of molecular and genetic characterization of *Pseudomonas* sp. ADP biofilms will further advance.

Detection of atrazine by Raman spectroscopy

A separate effort will be focused on evaluating the mechanism of action for atrazine removal from the environment. In this work, it was determined that cells were metabolically active and degrading atrazine in both biofilms and planktonic cells at a similar extent, but the EPS may have an additional role in the disappearance of atrazine from the resulting effluent. By methods of liquid—liquid extraction and GC-MS analysis, no atrazine was detected within the biofilm itself. However, it is probable atrazine is bound to the EPS of P.ADP biofilms. It is of great interest to use a solid phase detection approach, such as Raman spectroscopy or IR spectroscopy, to detect remaining amounts of herbicide that may be bound to the P.ADP matrix. It is unlikely to be quantified by GC-MS due necessary condition of absent water and particulate matter in prepared samples.

Raman may detect a significant amount of atrazine within the EPS-bound components, and the mass balance of the DFR may be completed. We may then conclude that the EPS matrix of P.ADP biofilms plays a key role in bioremediation of atrazine, as opposed to purely catabolic activity. However, these two mechanisms may both play a significant role in the removal of atrazine from the environment and consequently lead to implementation of biofilm-based bioreactors for remediation purposes of atrazine.

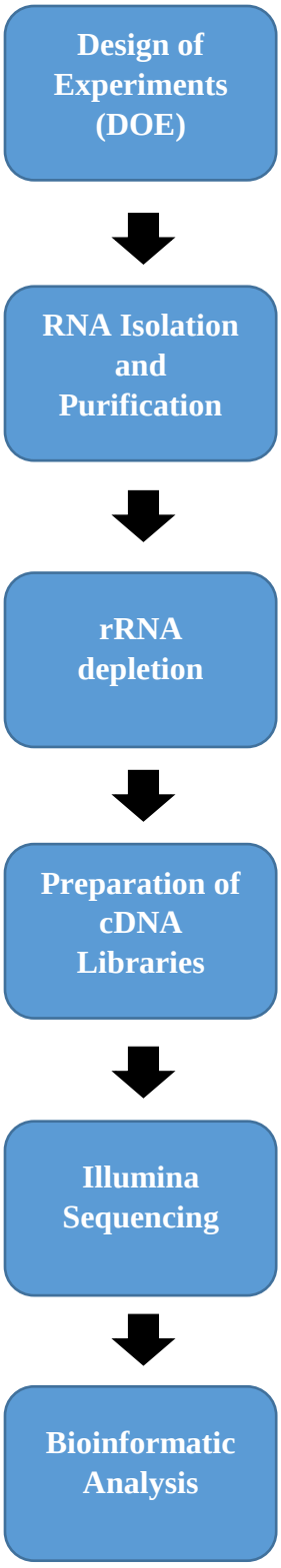

Figure 6.1. RNA-Seq workflow for *de novo* transcriptome assembly of *Pseudomonas* sp. strain ADP biofilms and planktonic cells.

Optimization of atrazine-degradation for P.ADP biofilms

Moving forward from biofilm-based experiments with *Pseudomonas* sp. strain ADP, it is essential to determine the optimal conditions for biodegradation processes once implemented in bioreactors for remediation purposes. Gene expression and analytical data on atrazine catabolism and degradation from the thesis presented provides the necessary groundwork to evaluate optimizing the temperature and pH of a bioreactor-based system to grow biofilms for remediation. There are several examples from previously published literature on bioremediation efforts on methods of optimizing biodegradation processes in a variety of environments using a variety of remediation agents.

Carbon and nitrogen content, for example, was evaluated optimal for biodegradation of creosote-contaminated soil with variation of the pH, moisture content, and nutrient concentration. All of these factors played a significant role in utilization of creosote in soil.[133] In other studies, design-of-experiments methodologies played a huge role in evaluating the optimal degradation. The commercial strain of fungus *Pleurtus ostraetus*, capable of degrading lindane, was evaluated with optimization parameters such as pH, temperature, nitrogen content, and initial lindane concentration. This was successfully performed using a central composite design.[134] Similarly, an orthogonal design was used for determining the optimal conditions (sediment type, inoculums, salinities, presence of other PAHs) for the biodegradation of the polyaromatic hydrocarbon phenanthrene.[115] A pH of 8.0 and temperature of 30^{o}C was noted at the optimal conditions for PAH degradation with use of a mixed inoculum of biodegrading anaerobic cultures. However, for aerobic mixed cultures, the optimal conditions changed to a pH of 7.0 and

temperature of 30°C. In both of these studies, some of the PAHs involved were phenanthrene, anthracene, fluorene, acenaphthene, and pyrene.[116,135]

Despite extensive research on PAHs, these methods can also be extended to bioremediation pollutants more common in water or soil, such as oily seawater and pesticides such as atrazine. Zahed et al. determined, using a five level three-factor central composite design, that, nitrogen content, phosphorous content, and time of day all affected crude oil removal by oil-degrading microbes.[136] Similarly, bacterial strain *Pseudomonas putida* KP-T202, capable of degrading 2,4,6-Trinitrotoluene (TNT), was optimally configured to be most efficient at a pH of 7.0, 30°C, and the addition of corn steep liquor (CSL) and Tween. This produced a reaction rate constant of 0.348 h^{-1} .[137]

Optimal conditions for biodegradation of a certain polymeric dye using a pulsed bed bioreactor by immobilized *Phanerochaete chrysosporium* was evaluated, and it was determined that conditions at 37°C, use of oxygen, and Mn^{2+} concentrations between 33 and 330 μM resulted in the most efficient biodegradation.[138] Each of these are methods that may be extended for use in atrazine remediation with *Pseudomonas* sp. strain ADP grown as a biofilm. To move forward, the temperature of biofilm growth must be varied (25, 30, 37, 42, 50°C) along with pH of growth medium (pH 6.0, 7.0, 8.0) and the degradation rate of atrazine must be quantified using HPLC. Other factors such as nutrient limitation, initial concentration of atrazine, initial concentration of cells, and oxygen content will be added to the conditions tested. Using a DOE approach, such as a central composite design (CCD), the optimal conditions for atrazine biodegradation with *Pseudomonas* sp. strain ADP biofilms will be determined.

APPENDIX A: RNA GEL ELECTROPHORESIS

RNA quality and quantity were checked after isolation with electrophoresis using a denaturing gel. Since RNA forms numerous secondary structures by intramolecular base pairing, a denaturing system is vital. The gel was prepared according to manufacturers' instructions (Thermo Fisher, Waltham, MA). Briefly, the gel was prepared by heating agarose (1 g) in water (72 mL), with the addition of 10X MOPS (10 mL) and 37% formaldehyde (12.3 M, 18 mL). The gel was cooled to 60^{o}C. Once the RNA sample was prepared from previously described methods, 1-3 µg was added to 0.5-3X volume of the formaldehyde loading dye. The denatured samples were heated at 65-70^{o}C for 5-15 min. Because a Northern blot was not done, our samples were only heated for a brief period of 5 min. The gel was loaded and electrophoresed at 5 V/cm until the blue dye (bromophenol) traveled 2/3 of the length of the gel. The dye was visualized under UV light. High, medium, and low concentrations of RNA were tested, along with and without proper DNAse treatment. The characteristic 16S and 23S rRNA bands of prokaryotic RNA are vaguely present in non-DNAse treated samples as presented in Figure A.1. However, due to the un-quantitative nature of this method, micro-spectrophotometry and capillary gel were used as the primary methods for RNA quality and quantity validation.

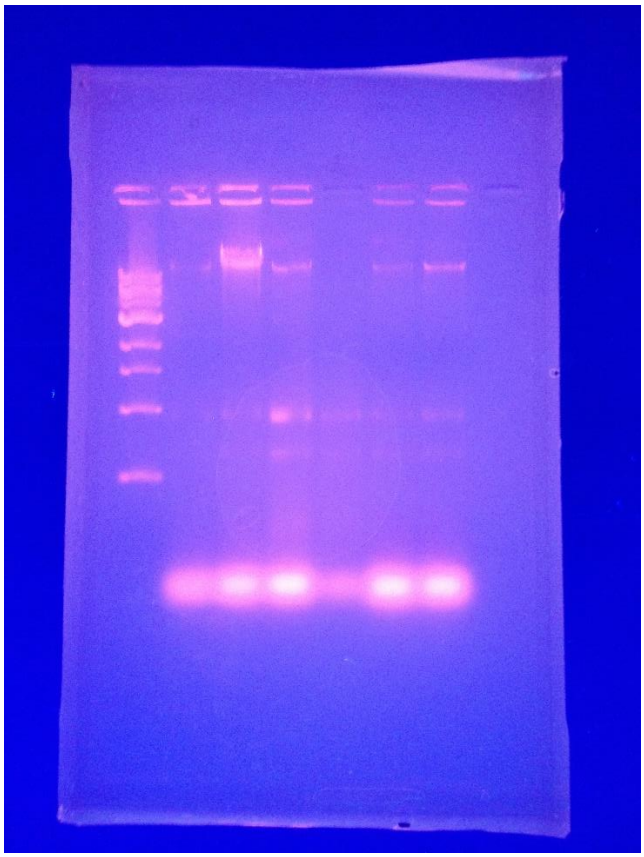

Figure A.1. RNA denaturing gel electrophoresis. RNA ladder (L) is the left-most band. Bands 2,4, and 6 are not DNase treated while bands 1,2, and 3 are DNase treated.

APPENDIX B: CALIBRATION CURVES

Spectrophotometry at 600 nm was used as an indirect method to measure bacterial growth. However, the optical density at 600 nm (OD_{600}) alone does not quantify the number of bacterial cells in a given solution. Using petri dishes and serial dilutions of P.ADP bacteria on two types of rich media: A) LB and B) TY, a calibration curve was constructed to correlate the number of colony forming units per mL (CFU mL^{-1}) of *Pseudomonas* sp. strain ADP bacteria to an OD_{600} value. Below, in Figure B.1 and Figure B.2, the calibration curves for LB and TY medium are presented, respectively.

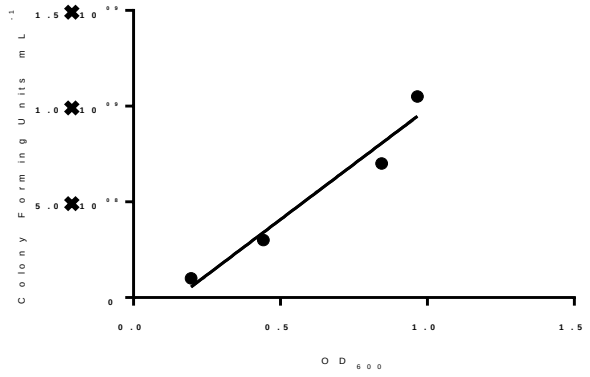

Figure B.1. Calibration curve for P.ADP bacterial growth for LB medium using Colony Forming Units per mL and optical density at 600 nm.

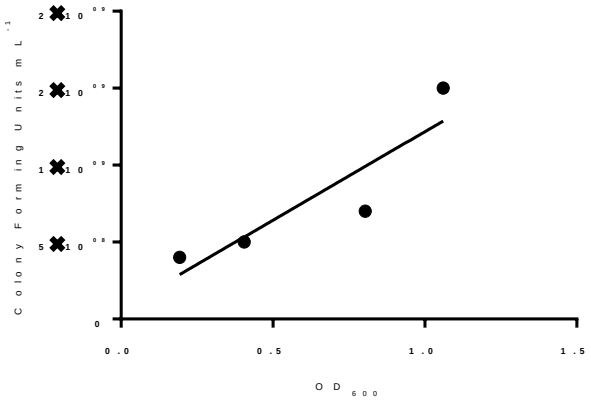

Figure B.2. Calibration curve for P.ADP bacterial growth for LB medium using Colony Forming Units per mL and optical density at 600 nm.

APPENDIX C: NANODROP RNA QUALITY ANALYSIS

The A260/230 and A260/280 ratios indicate the quality of an RNA sample. The maximum absorbance for nucleic acids is 260 nm, due to the presence of heterocyclic rings in the nucleotides. The sugar phosphate backbone does not contribute to the absorption. Therefore, a sharp peak at 260 nm and smoothness and low absorption in the rest of the spectrum indicate a high quality, pure sample of nucleic acid. However, the Nanodrop cannot distinguish between RNA and DNA since both absorb in the same range. To validate and substantiate the A260/2330 and A260/280 ratios reported in this work, an example of the corresponding spectra are displayed below in Figure C.1. The figure below represents the absorbance spectra for four different total RNA samples originating from *Pseudomonas* sp. strain ADP biofilms. No contamination is present, which would manifest as peaks at 220 nm and 270 nm. In this case, the samples would need to be re-purified on a spin column from the RNeasy Mini Kit. Furthermore, the peaks at 260 nm are high and sharp, indicating high concentration and purity, respectively. Samples with low concentration characteristically have a flat line with no visible peaks, or only small peaks in the 240-280 nm range. The A260/230 and A260/280 values should be assessed with the absorbance spectra, followed by use of a bioanalyzer capillary gel electrophoresis assay prior to using RNA for downstream applications.

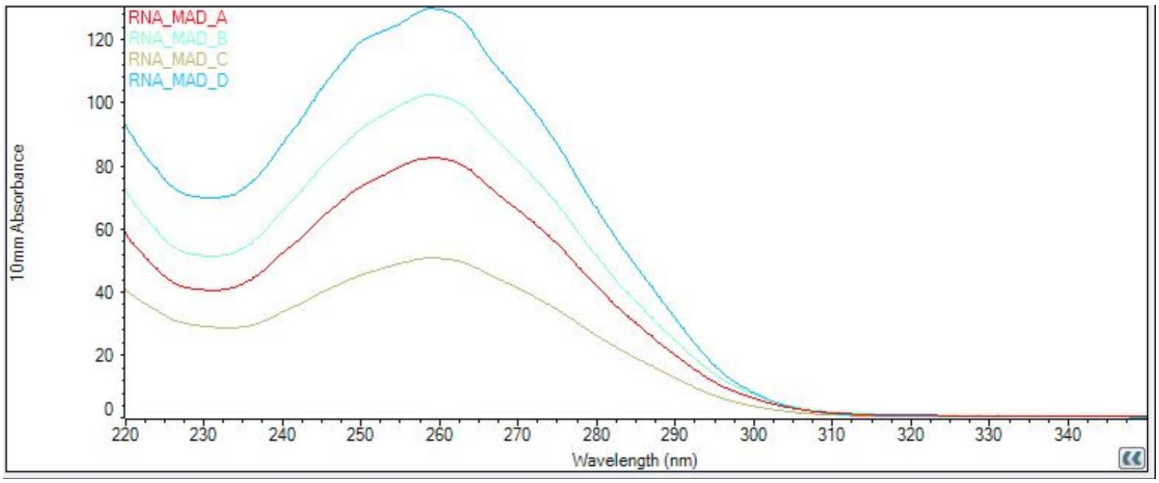

Figure C.1. Nanodrop spectrophotometry graph displaying the spectrum from 220-340 nm at 10 mm absorbance

APPENDIX D: MASS SPECTROMETRY SPECTRA

Atrazine was synthesized via organic synthetic methods, with the presence of similar compounds. Compounds synthesized with the target molecule being atrazine were characterized using mass spectrometry (MS). Three compounds were determined to be present and were matched to corresponding spectra from the MS library. Experimental spectra and library spectra are reported for peak one (Figure D.1), peak two (Figure D.2), and peak three (Figure D.3.) below.

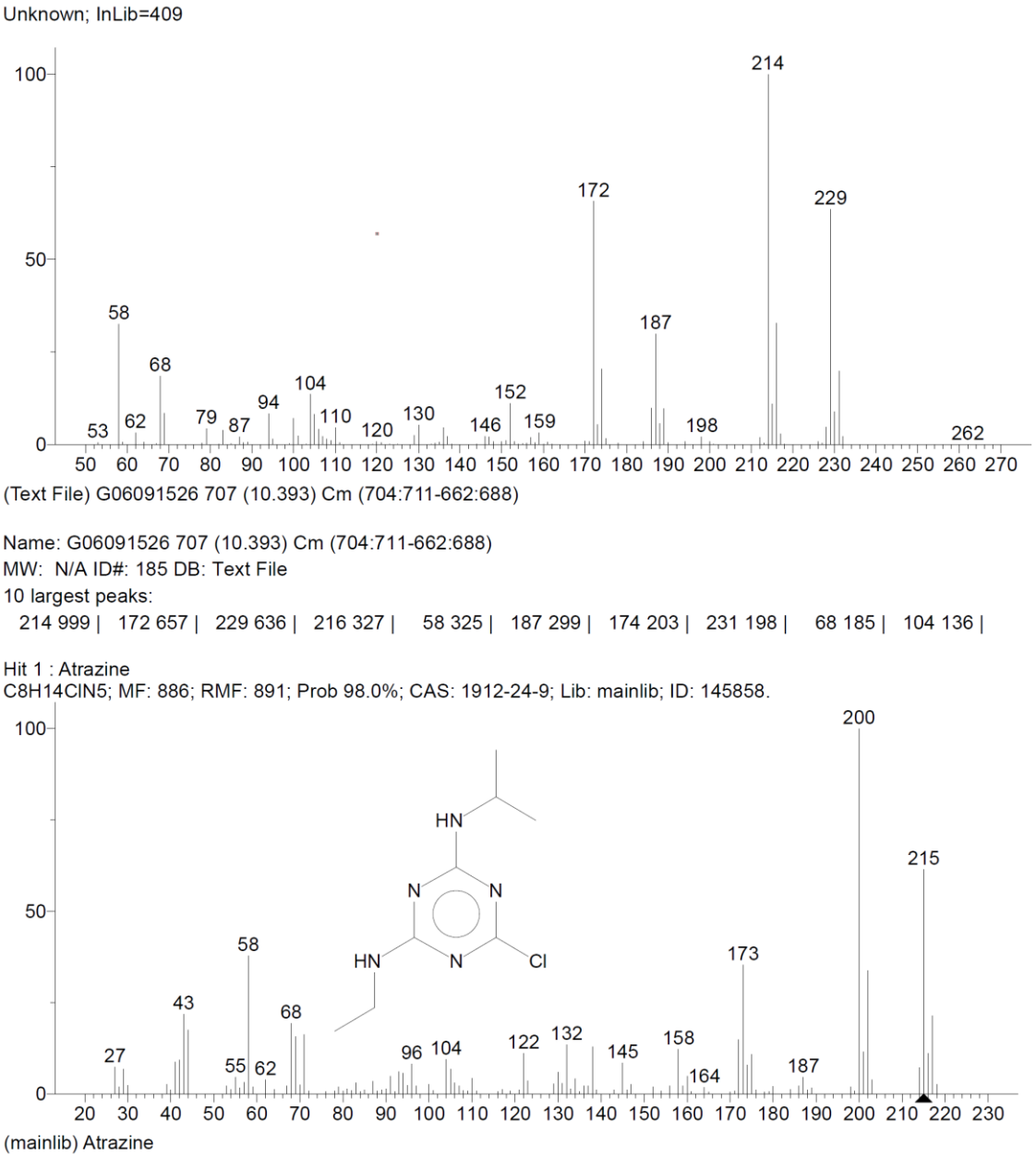

Figure D.1. The first peak reported from MS: atrazine. The experimental mass spectrum (top) along with the mass spectrum of the library hit for atrazine (bottom) is displayed.

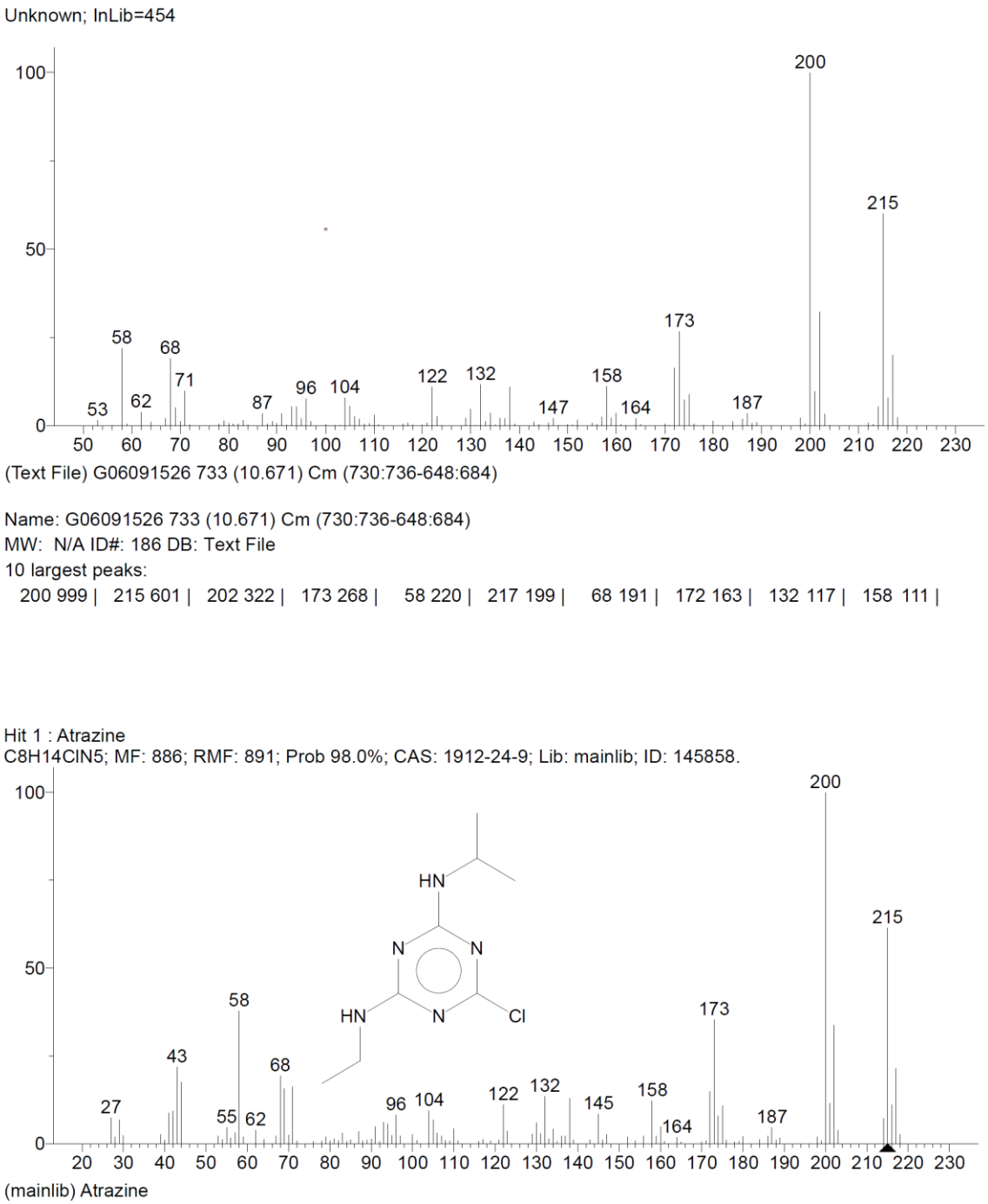

Figure D.2. The second peak reported from MS: atrazine. The experimental mass spectrum (top) along with the mass spectrum of the library hit for atrazine (bottom) is displayed.

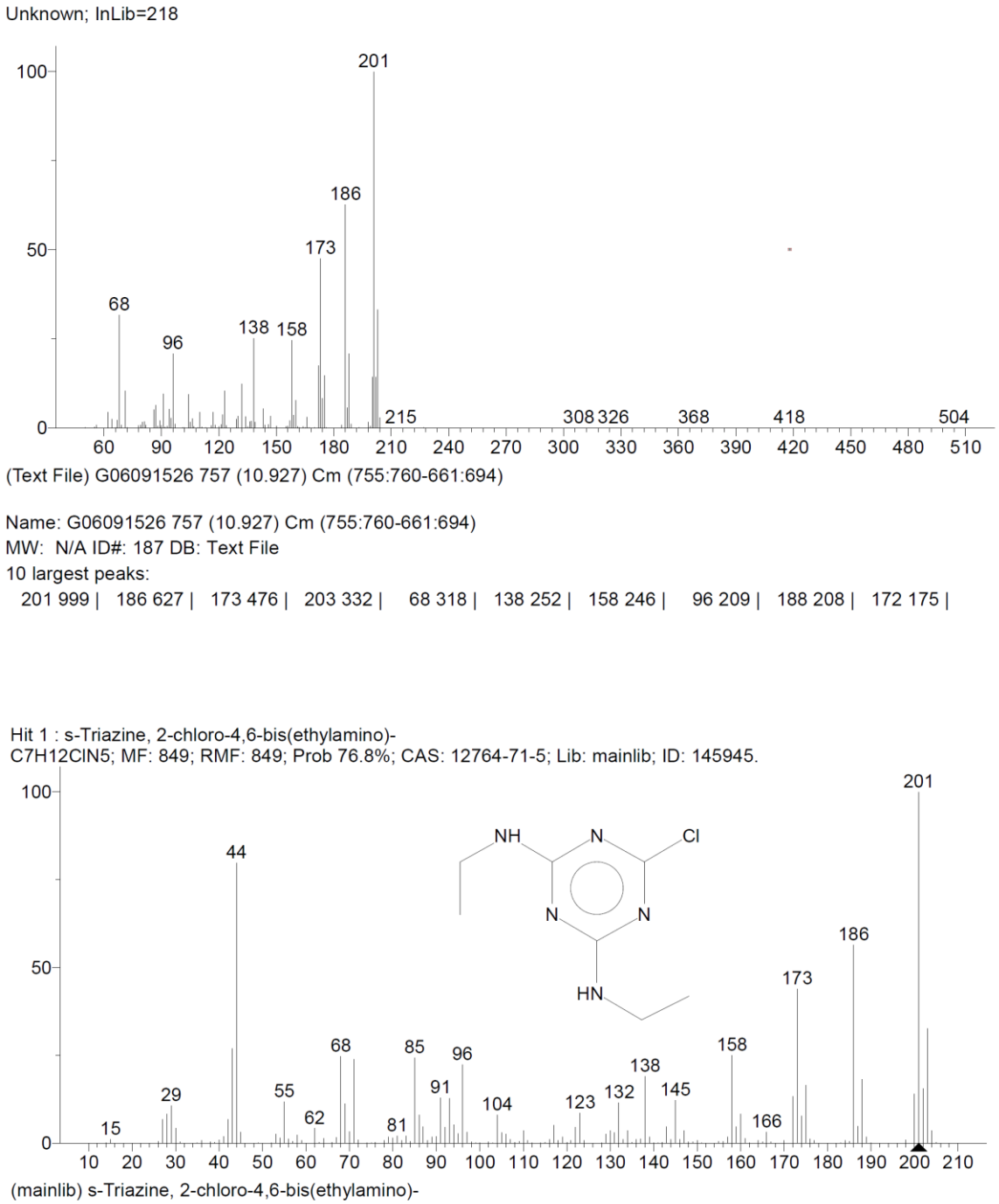

Figure D.3. The second peak reported from MS: atrazine. The experimental mass spectrum (top) along with the mass spectrum of the library hit for s-Triazine, 2-chloro-4,6-bis(ethylamino)- (bottom) is displayed.

APPENDIX E: FLUORESCENT LECTIN BINDING ANALYSIS

Fiji® aided in evaluating the mean intensity values for each constructed biofilm image from CLSM. Values from each biofilm sample image, along with each trial of collecting biofilm images with CLSM for the same sample were collected. The mean intensity was recorded for DAPI (blue), the counterstain for nucleic acid, and rhodamine (red), the primary stain for each lectin. The ratio of the mean intensities for each of these values represents the mean intensity ratio (MIR). The purpose of using the mean intensity for each lectin over the intensity of the counterstain serves to normalize the values to compare them across samples, and across different growth media used for biofilms. The standard deviation for each mean intensity value is reported below, along with the red to blue ratio, which is the ratio of the rhodamine fluorescence intensity to DAPI fluorescence intensity (MIR).

Table E.1. Sample calculations of Mean Intensity Ratio (MIR) for fluorescent lectin binding analysis (FLBA) of Concanavalin A (ConA). S designates sample, and T in table above designates trial. LB is the medium used for this set of samples.

Sample	Mean Intensity	Standard Deviation	Red to Blue Ratio
S1T1			
Red	5.979	7.728	1.387239
Blue	4.31	11.555	
S1T2			
Red	4.135	3.605	*19.32243*
Blue	0.214	0.785	
S1T3			
Red	4.514	5.462	2.2936992
Blue	1.968	4.903	
S2T1			
Red	1.76	2.041	1.4390842
Blue	1.223	1.851	
S3T1			
Red	2.7	2.656	2.525725
Blue	1.069	1.39	
S4T1			
Red	3.986	2.369	1.7240484
Blue	2.312	0.938	
		MIR	1.873959
Positive for Mannose (+)			

APPENDIX F: NOMENCLATURE TABLE

Abbreviation	Description
^{1}H-NMR	Proton Nuclear Magnetic Resonance
A_{225}	Absorbance at 225 nm
AF448	Alexa Fluor 488 Dye
ATZ	Atrazine
cDNA	Complementary Deoxyribose Nucleic Acid
CFU	Colony Forming Units
CLSM	Confocal Laser Scanning Microscopy
ConA	Concanavalin A
C_t	Threshold Number
CYA	Cyanuric Acid
DAPI	4',6-Diamidino-2-Phentylindole
DBA	Dolichos Biflorus Agglutinin
DEPC	Diethyl Pyrocarbonate
DFR	Drip Flow Reactor
DNA	Deoxyribose Nucleic Acid
DNase	Deoxyribonuclease
DOE	Design-of-Experiments
DSMZ	Medium Based on Deutsche Sammlung
EDC	Endocrine Disruptor Compound
ELISA	Enzyme Linked Immunosorbent Assay
EM	Electron Microscopy
EPA	Environmental Protection Agency
EPS	Extracellular Polymeric Substances
EUB338	Eubacterial Probe
FISH	Fluorescent In Situ Hybridization
FLBA	Fluorescent Lectin Binding Analysis
GAM42a	Gamma Proteobacterial Probe
GAPDH	Glyceraldehyde 3-Phosphate Dehydrogenase
GC	Gas Chromatography
GFP	Green Fluorescent Protein
HPLC	High Performance Liquid Chromatography
IMARIS	Bitplane Core Product
ISRT	In Situ Reverse Transcription
LB	Lysogeny Broth Growth Medium
MCL	Maximum Contaminant Level
MIC	Minimum Inhibitory Concentration
MIP	Maximum Intensity Projection
MIR	Mean Intensity Ratio
mRNA	Messenger Ribonucleic Acid
MS	Mass Spectroscopy
NGS	Next Generation Sequencing
NMR	Nuclear Magnetic Resonance
NRT	No Reverse Transcriptase Control

Abbreviation	Description
NTC	No Template Control
OD_{600}	Optical Density at 600 nm
P.ADP	*Pseudomonas* sp. strain ADP
pADP-1	Plasmid containing atrazine-degrading genes
PBS	Phosphate-Buffered Saline
PNA	Peanut Agglutinin
PPB	Parts Per Billion
PPM	Parts Per Million
EU	European Union
RCA	Ricin Communis Agglutinin
RFP	Red Fluorescent Protein
RIN	RNA Integrity Number
RNA	Ribonucleic Acid
RNase	Ribonuclease
RNA-Seq	Ribonucleic Acid Sequencing
ROS	Radical Oxygen Species
RSM	Response Surface Methodology
RT	Reverse Transcription
RT-qPCR	Reverse Transcription – Real Time Polymerase Chain Reaction
SBA	Soybean Agglutinin
SEM	Scanning Electron Microscopy
SNR	Signal-to-Noise Ratio
T_d	Doubling Time
TOF-MS-EI	Time-of-Flight Mass Spectrometry Electron Ionization
TY	Tryptone Yeast Growth Medium
UEA	Ulex Europeanus Agglutinin
UV-Vis	UV-Visible Spectrophotometry
UV-Vis	UV-Visible Spectrophotometry
WGA	Wheat Germ Agglutinin
$\Delta\Delta C_t$	Analysis for Fold-Change
μ	Specific Growth Rate

REFERENCES

1. Mandelbaum, R. T., Allan, D. l. & Wackett, L. P. Isolation and Characterization of a Pseudomonas sp . That Mineralizes the s -Triazine Herbicide Atrazine. *Appl. Environ. Microbiol.* **61,** 1451–1457 (1995).
2. Martinez, B., Tomkins, J., Wackett, L. P., Sadowsky, M. J. & Wing, R. O. D. Complete Nucleotide Sequence and Organization of the Atrazine Catabolic Plasmid pADP-1 from Pseudomonas sp . Complete Nucleotide Sequence and Organization of the Atrazine Catabolic Plasmid pADP-1 from Pseudomonas sp . Strain ADP. *J. …* **183,** 5684–5697 (2001).
3. Devers, M., Soulas, G. & Martin-Laurent, F. Real-time reverse transcription PCR analysis of expression of atrazine catabolism genes in two bacterial strains isolated from soil. *J. Microbiol. Methods* **56,** 3–15 (2004).
4. Kostakioti, M., Hadjifrangiskou, M. & Hultgren, S. J. Bacterial biofilms: development, dispersal, and therapeutic strategies in the dawn of the postantibiotic era. *Cold Spring Harb. Perspect. Med.* **3,** 1–23 (2013).
5. Thesis-Victoria Henry.
6. Mary Kensa, V. Bioremediation - An overview. *J. Ind. Pollut. Control* **27,** 161–168 (2011).
7. Flemming, H.-C. *et al.* Biofilms: an emergent form of bacterial life. *Nat. Rev. Microbiol.* **14,** 563–575 (2016).
8. Edwards, S. J. & Kjellerup, B. V. Applications of biofilms in bioremediation and biotransformation of persistent organic pollutants, pharmaceuticals/personal care products, and heavy metals. *Appl. Microbiol. Biotechnol.* **97,** 9909–9921 (2013).
9. Henry, V. A., Jessop, J. L. P. & Peeples, T. L. Differentiating Pseudomonas sp. strain ADP cells in suspensions and biofilms using Raman spectroscopy and scanning electron microscopy. *Anal. Bioanal. Chem.* **409,** 1441–1449 (2017).
10. Biglione, N., Rodgers, V. G. J. & Peeples, T. L. Determining design and scale-up parameters for degradation of atrazine with suspended Pseudomonas sp. ADP in aqueous bioreactors. *Biotechnol. Prog.* **24,** 588–592 (2008).
11. Carvalho, F. P. Agriculture, pesticides, food security and food safety. *Environ. Sci. Policy* **9,** 685–692 (2006).
12. Fernandez-Cornejo, J. & Vialou, A. Pesticide Use in U. S. Agriculture: 21 Selected Crops, 1960-2008. *USDA Econ. Inf. Bull.* 80 (2014). doi:10.2139/ssrn.2502986
13. Donley, N. EPA Finds Atrazine Likely Harming Most Species of Plants, Animals in U.S. *Center for Biological Diversity* 1–2 (2016). Available at: https://www.biologicaldiversity.org/news/press_releases/2016/atrazine-05-03-2016.html. (Accessed: 26th January 2018)
14. Mudhoo, A. & Garg, V. K. Sorption, Transport and Transformation of Atrazine in Soils, Minerals and Composts: A Review. *Pedosphere* **21,** 11–25 (2011).
15. Database, P. C. Atrazine Compound Summary for CID 2256. *National Center for Biotechnology Information* 1 (2018). Available at: https://pubchem.ncbi.nlm.nih.gov/compound/atrazine#section=Top. (Accessed: 26th January 2018)

16. Colborn, T., Vom Saal, F. S. & Soto, A. M. Developmental effects of endocrine-disrupting chemicals in wildlife and humans. *Environ. Health Perspect.* **101,** 378–384 (1993).
17. Rusiecki, J. A. *et al.* Cancer incidence among pesticide applicators exposed to Atrazine in the agricultural health study. *J. Natl. Cancer Inst.* **96,** 1375–1382 (2004).
18. Simpkins, J. W. *et al.* Atrazine and breast cancer: A framework assessment of the toxicological and epidemiological evidence. *Toxicol. Sci.* **123,** 441–459 (2011).
19. Cooper, R. L., Stoker, T. E., Tyrey, L., Goldman, J. M. & McElroy, W. K. Atrazine disrupts the hypothalamic control of pituitary-ovarian function. *Toxicol. Sci.* **53,** 297–307 (2000).
20. Hayes, T. B. *et al.* Hermaphroditic, demasculinized frogs after exposure to the herbicide atrazine at low ecologically relevant doses. *Proc. Natl. Acad. Sci.* **99,** 5476–5480 (2002).
21. Prasad, T. A. V., Srinivas, T., Janardan Reddy, S. & Reddy, D. C. Atrazine toxicity on transport properties of hemocyanin in the crab Oziotelphusa senex senex. *Ecotoxicology and Environmental Safety* **30,** 124–126 (1995).
22. Ramel, F. *et al.* Genome-wide interacting effects of sucrose and herbicide-mediated stress in Arabidopsis thaliana: Novel insights into atrazine toxicity and sucrose-induced tolerance. *BMC Genomics* **8,** 1–20 (2007).
23. Hayes, T. *et al.* Atrazine-induced hermaphroditism at 0.1 ppb in American leopard frogs (Rana pipiens): Laboratory and field evidence. *Environ. Health Perspect.* **111,** 568–575 (2003).
24. Sass, J. B. & Colangelo, A. European Union bans atrazine, while the United States negotiates continued use. *Int. J. Occup. Environ. Health* **12,** 260–267 (2006).
25. EPA Drinking Water Regulations for Atrazine. *US Environmental Protection Agency* 1 (2015). Available at: https://safewater.zendesk.com/hc/en-us/articles/212077787-4-What-are-EPA-s-drinking-water-regulations-for-atrazine-. (Accessed: 26th January 2018)
26. Wu, M., Quirindongo, M., Sass, J. & Wetzler, A. Still Poisoning the Well. *Nat. Resour. Def. Counc.* 1–32 (2010).
27. Fan, X. & Song, F. Bioremediation of atrazine: recent advances and promises. *J. Soil Sediments* **14,** 1727–1737 (2014).
28. Head, I. M. Bioremediation: Towards a credible technology. *Microbiology* **144,** 599–608 (1998).
29. Tyagi, M., da Fonseca, M. M. R. & de Carvalho, C. C. C. R. Bioaugmentation and biostimulation strategies to improve the effectiveness of bioremediation processes. *Biodegradation* **22,** 231–241 (2011).
30. Fava, F., Di Gioia, D. & Marchetti, L. Cyclodextrin effects on the ex-situ bioremediation of a chronically polychlorobiphenyl-contaminated soil. *Biotechnol. Bioeng.* **58,** 345–355 (1998).
31. Tongarun, R., Luepromchai, E. & Vangnai, A. S. Natural attenuation, biostimulation, and bioaugmentation in 4-chloroaniline-contaminated soil. *Curr. Microbiol.* **56,** 182–188 (2008).

32. Wackett, L., Sadowsky, M., Martinez, B. & Shapir, N. Biodegradation of atrazine and related s-triazine compounds: From enzymes to field studies. *Appl. Microbiol. Biotechnol.* **58,** 39–45 (2002).
33. Struthers, J. K., Jayachandran, K. & Moorman, T. B. Biodegradation of atrazine by Agrobacterium radiobacter J14a and use of this strain in bioremediation of contaminated soil. *Appl. Environ. Microbiol.* **64,** 3368–3375 (1998).
34. Behki, R., Topp, E., Dick, W. & Germon, P. Metabolism of the herbicide atrazine by rhodococcus strains. *Appl. Environ. Microbiol.* **59,** 1955–1959 (1993).
35. Mandelbaum, R., Allan, D. L. & Wackett, L. P. Isolation and characterization of a Pseudomonas sp. that mineralizes the *s*-triazine herbicide atrazine. *Appl. Environ. Microbiol.* **61,** 1451–1457 (1995).
36. García-González, V., Govantes, F., Shaw, L. J., Burns, R. G. & Santero, E. Nitrogen Control of Atrazine Utilization in Pseudomonas sp. Strain ADP. *Appl. Environ. Microbiol.* **69,** 6987–6993 (2003).
37. Seffernick, J. L., Johnson, G., Sadowsky, M. J. & Wackett, L. P. Substrate specificity of atrazine chlorohydrolase and atrazine-catabolizing bacteria. *Appl. Environ. Microbiol.* **66,** 4247–4252 (2000).
38. Adp, S., Souza, M. L. De, Wackett, L. P. & Michael, J. The atzABC Genes Encoding Atrazine Catabolism Are Located on a Self-Transmissible Plasmid in Pseudomonas The atzABC Genes Encoding Atrazine Catabolism Are Located on a Self-Transmissible Plasmid in Pseudomonas sp . Strain ADP †. **64,** 2323–2326 (1998).
39. Boundy-mills, K. L., Souza, M. L. D. E. & Mandelbaum, Raphi T, Wackett, L P, S. M. J. The atzB gene of Pseudomonas sp . strain ADP encodes the second enzyme of a novel atrazine degradation pathway . The atzB Gene of Pseudomonas sp . Strain ADP Encodes the Second Enzyme of a Novel Atrazine Degradation Pathway. *Appl. Environental Microbiol.* **63,** 916–923 (1997).
40. Sadowsky, M. J., Tong, Z., De Souza, M. & Wackett, L. P. AtzC is a new member of the amidohydrolase protein superfamily and is homologous to other atrazine-metabolizing enzymes. *J. Bacteriol.* **180,** 152–158 (1998).
41. Govantes, F. *et al.* Regulation of the atrazine-degradative genes in Pseudomonas sp. strain ADP. *FEMS Microbiol. Lett.* **310,** 1–8 (2010).
42. Platero, A. I., García-jaramillo, M., Santero, E. & Govantes, F. Transcriptional Organization and Regulatory Elements of a Pseudomonas sp . Strain ADP Operon Encoding a LysR-Type Regulator and a Putative Solute Transport System. **194,** 6560–6573 (2012).
43. García-gonzález, V., Govantes, F., Porrúa, O. & Santero, E. Regulation of the Pseudomonas sp . Strain ADP Cyanuric Acid Degradation Operon Regulation of the Pseudomonas sp . Strain ADP Cyanuric Acid Degradation Operon. **187,** 155–167 (2005).
44. Cheng, G., Shapir, N., Sadowsky, M. J. & Wackett, L. P. Allophanate hydrolase, not urease, functions in bacterial cyanuric acid metabolism. *Appl. Environ. Microbiol.* **71,** 4437–4445 (2005).
45. Donlan, R. M. Biofilms: Microbial life on surfaces. *Emerg. Infect. Dis.* **8,** 881–890 (2002).
46. Davey, M. E. & O'toole, G. A. Microbial Biofilms: from Ecology to Molecular Genetics. *Microbiol. Mol. Biol. Rev.* **64,** 847–867 (2000).

47. Van Houdt, R. & Michiels, C. W. Biofilm formation and the food industry, a focus on the bacterial outer surface. *J. Appl. Microbiol.* **109,** 1117–1131 (2010).
48. J., K.-J. Cheng, Gill G. Greesy, Timothy I. Ladd, J. Curtis Nickel, Mrinal Dasgupta, T. J. M. NATIJRE AND DISEASE. *Ann. Rev. Microbiol.* **41,** 435–464 (1987).
49. Davies, D. G. *et al.* The Involvement of Cell-to-Cell Signals in the Development of a Bacterial Biofilm The Involvement of Cell-to-Cell Signals in the Development of a Bacterial Biofilm. **295,** 295–299 (2011).
50. Singh, R., Paul, D. & Jain, R. K. Biofilms: implications in bioremediation. *Trends Microbiol.* **14,** 389–397 (2006).
51. Lear, G. Biofilms in Bioremediation Edited by.
52. De Souza, M. L., Wackett, L. P., Boundy-Mills, K. L., Mandelbaum, R. T. & Sadowsky, M. J. Cloning, characterization, and expression of a gene region from Pseudomonas sp. strain ADP involved in the dechlorination of atrazine. *Appl. Environ. Microbiol.* **61,** 3373–3378 (1995).
53. Solomon, R. D. J., Kumar, A. & Satheeja Santhi, V. Atrazine biodegradation efficiency, metabolite detection, and trzD gene expression by enrichment bacterial cultures from agricultural soil. *J. Zhejiang Univ. Sci. B* **14,** 1162–72 (2013).
54. Livak, K. J. & Schmittgen, T. D. Analysis of relative gene expression data using real-time quantitative PCR and the 2-ΔΔCT method. *Methods* **25,** 402–408 (2001).
55. Platero, A. I., Santero, E. & Govantes, F. Genetic evidence of a high-affinity cyanuric acid transport system in Pseudomonas sp. ADP. *FEMS Microbiol. Lett.* **352,** 150–156 (2014).
56. He, X. & Ahn, J. Differential gene expression in planktonic and biofilm cells of multiple antibiotic-resistant Salmonella Typhimurium and Staphylococcus aureus. *FEMS Microbiol. Lett.* **325,** 180–188 (2011).
57. Hugouvieux-Cotte-Pattat, N., Kohler, T., Rekik, M. & Harayama, S. Growth-phase-dependent expression of the Pseudomonas putida TOL plasmid pWW0 catabolic genes. *J. Bacteriol.* **172,** 6651–6660 (1990).
58. Croucher, N. J. & Thomson, N. R. Studying bacterial transcriptomes using RNA-seq. *Curr. Opin. Microbiol.* **13,** 619–624 (2010).
59. Chen, F. In situ reverse transcription , an approach to characterize genetic diversity and activities of In Situ Reverse Transcription , an Approach To Characterize Genetic Diversity and Activities of Prokaryotes. **63,** 4907–4913 (1997).
60. Ligasová, A. & Koberna, K. In situ reverse transcription: the magic of strength and anonymity. *Nucleic Acids Res.* **38,** e167 (2010).
61. Tawakoli, P. N., Neu, T. R., Busck, M. M., Kuhlicke, U. & Schramm, A. Visualizing the dental biofilm matrix by means of fluorescence lectin-binding analysis. *J. Oral Microbiol.* **0,** (2017).
62. Rolfe, M. D. *et al.* Lag phase is a distinct growth phase that prepares bacteria for exponential growth and involves transient metal accumulation. *J. Bacteriol.* **194,** 686–701 (2012).

63. Neumann, G. *et al.* Simultaneous Degradation of Atrazine and Phenol by Pseudomonas sp. Strain ADP: Effects of Toxicity and Adaptation. *Appl. Environ. Microbiol.* **70,** 1907–1912 (2004).
64. Matlock, B. Assessment of Nucleic Acid Purity. *Tech. Note 52646* 3 (2012). doi:10.7860/JCDR/2015/11821.5896
65. Labchip, E., Data, T. R. N. A., Ladder, R. N. A., The, R. & Rna, T. FAQ for Agilent 2100 Bioanalyzer Service.
66. Chen, S. *et al.* Synthesis of C-13-labeled atrazine. *J. Label. Compd. Radiopharm.* **56,** 305–306 (2013).
67. Heffernan, B., Murphy, C. D. & Casey, E. Comparison of planktonic and biofilm cultures of Pseudomonas fluorescens dsm 8341 cells grown on Fluoroacetate. *Appl. Environ. Microbiol.* **75,** 2899–2907 (2009).
68. Whiteley, M., Bangera, M. G. & Bumgarner, R. E. Gene expression in Pseudomonas aeruginosa bio ® lms. **413,** 860–864 (2001).
69. Schembri, M. A., Kjaergaard, K. & Klemm, P. Global gene expression in Escherichia coli biofilms. *Mol. Microbiol.* **48,** 253–267 (2003).
70. Nielsen, S., Meyer, R. & Nørskov-Lauritsen, N. Differences in Gene Expression Profiles between Early and Late Isolates in Monospecies Achromobacter Biofilm. *Pathogens* **6,** 20 (2017).
71. Madsen, J. S., Burmølle, M., Hansen, L. H. & Sørensen, S. J. The interconnection between biofilm formation and horizontal gene transfer. *FEMS Immunol. Med. Microbiol.* **65,** 183–195 (2012).
72. Giaouris, E. *et al.* Intra- and inter-species interactions within biofilms of important foodborne bacterial pathogens. *Front. Microbiol.* **6,** 1–26 (2015).
73. Mohan, S. V. *et al.* Anaerobic treatment of complex chemical wastewater in a sequencing batch biofilm reactor: Process optimization and evaluation of factor interactions using the taguchi dynamic DOE methodology. *Biotechnol. Bioeng.* **90,** 732–745 (2005).
74. Hoellein, T. J., Tank, J. L., Kelly, J. J. & Rosi-Marshall, E. J. Seasonal variation in nutrient limitation of microbial biofilms colonizing organic and inorganic substrata in streams. *Hydrobiologia* **649,** 331–345 (2010).
75. Biosystems, A. Guide to performing relative quantitation of gene expression using real-time quantitative PCR. *Guid. to Perform. Relat. Quant. Gene Expr. Using Real-Time Quant. PCR* 1–61 (2004). doi:10.1007/978-3-642-31107-9
76. Siddique, T., Okeke, B. C., Arshad, M. & Frankenberger, W. T. Temperature and pH effects on biodegradation of hexachlorocyclohexane isomers in water and a soil slurry. *J. Agric. Food Chem.* **50,** 5070–5076 (2002).
77. Lim, B. R., Huang, X., Hu, H. Y., Goto, N. & Fujie, K. Effects of temperature on biodegradation characteristics of organic pollutants and microbial community in a solid phase aerobic bioreactor treating high strength organic wastewater. *Water Sci. Technol.* **43,** 131–137 (2001).
78. Lew, D. Atrazine Degradation by Pseudomonas sp. ADP is nitrogen regulated. *Environmental Microbiology* 1 (2017). Available at: https://www.drdarrinlew.us/environmental-microbiology/atrazine-degradation-by-pseudomonas-sp-adp-is-nitrogen-regulated.html. (Accessed: 27th February 2018)

79. Govantes, F., Porru, O. & Santero, E. Regulation of the Pseudomonas sp . Strain ADP Cyanuric Acid Degradation Operon. **187,** 155–167 (2005).
80. Platero, A. I., Santero, E. & Govantes, F. Genetic evidence of a high-affinity cyanuric acid transport system in Pseudomonas sp. ADP. **352,** 150–156 (2018).
81. Govantes, F., Porrúa, O., García-González, V. & Santero, E. Atrazine biodegradation in the lab and in the field: Enzymatic activities and gene regulation. *Microb. Biotechnol.* **2,** 178–185 (2009).
82. García-González, V. *et al.* Distinct roles for NtrC and GlnK in nitrogen regulation of the Pseudomonas sp. strain ADP cyanuric acid utilization operon. *FEMS Microbiol. Lett.* **300,** 222–229 (2009).
83. Harrison, J. J. *et al.* The use of microscopy and three-dimensional visualization to evaluate the structure of microbial biofilms cultivated in the Calgary biofilm device. *Biol. Proced. Online* **8,** 194–213 (2006).
84. De Carvalho, C. C. C. R. & Da Fonseca, M. M. R. Assessment of three-dimensional biofilm structure using an optical microscope. *Biotechniques* **42,** 616–620 (2007).
85. Hannig, C., Follo, M., Hellwig, E. & Al-Ahmad, A. Visualization of adherent micro-organisms using different techniques. *J. Med. Microbiol.* **59,** 1–7 (2010).
86. Asahi, Y. *et al.* Simple observation of Streptococcus mutans biofilm by scanning electron microscopy using ionic liquids. *AMB Express* **5,** 0–8 (2015).
87. Baum, M. M. *et al.* Characterization of structures in biofilms formed by a Pseudomonas fluorescens isolated from soil. *BMC Microbiol.* **9,** 1–13 (2009).
88. Gjermansen, M., Nilsson, M., Yang, L. & Tolker-Nielsen, T. Characterization of starvation-induced dispersion in Pseudomonas putida biofilms: Genetic elements and molecular mechanisms. *Mol. Microbiol.* **75,** 815–826 (2010).
89. Wolfahrt, S., Kleine, B. & Rossmanith, W. G. Detection of gonadotrophin releasing hormone and its receptor mRNA in human placental trophoblasts using in-situ reverse transcription-polymerase chain reaction. *Mol. Hum. Reprod.* **4,** 999–1006 (1998).
90. Yang, Y. & Zeyer, J. Specific Detection of Dehalococcoides Species by Fluorescence In Situ Hybridization with 16S rRNA-Targeted Oligonucleotide Probes Specific Detection of Dehalococcoides Species by Fluorescence In Situ Hybridization with 16S rRNA-Targeted Oligonucleotide Pr. *Society* **69,** 2879–2883 (2003).
91. Rhee, S. *et al.* Detection of Genes Involved in Biodegradation and Biotransformation in Microbial Communities by Using 50-Mer Oligonucleotide Microarrays Detection of Genes Involved in Biodegradation and Biotransformation in Microbial Communities by Using 50-Mer Oligonucl. *Appl. Environ. Microbiol.* **70,** 4303–4317 (2004).
92. Mesarch, M. B., Nakatsu, C. H. & Nies, L. Development of Catechol Monitoring Bioremediation by Competitive Quantitative PCR Development of Catechol 2 , 3-Dioxygenase-Specific Primers for Monitoring Bioremediation by Competitive Quantitative PCR. *Appl. Environ. Microbiol.* **66,** 678–683 (2000).
93. Zippel, B. & Neu, T. R. Characterization of glycoconjugates of extracellular polymeric substances in tufa-associated biofilms by using fluorescence lectin-binding analysis. *Appl. Environ. Microbiol.* **77,** 505–516 (2011).

94. Neu, T. R., Swerhone, G. D. W. & Lawrence, J. R. Assessment of lectin- binding analysis for in situ detection of glycoconjugates in biofilm systems. *Microbiology* **147,** 299–313 (2001).
95. Trizol_RNeasy hybrid. 8–9
96. Harbor, cold S. Paraformaldehyde in PBS Recipe. *Cold Spring Harbor Laboratory Press* 1 (2018). Available at: http://cshprotocols.cshlp.org/content/2006/1/pdb.rec9959.full?text_only=true. (Accessed: 5th March 2018)
97. Sinigalliano, C. D., Kuhn, D. N., Jones, R. D. & Guerrero, M. A. In situ reverse transcription to detect the cbbL gene and visualize RuBisCo in chemoautotrophic nitrifying bacteria. *Lett. Appl. Microbiol.* **32,** 388–393 (2001).
98. Moltz, A. G. & Martin, S. E. Formation of biofilms by Listeria monocytogenes under various growth conditions. *J. Food Prot.* **68,** 92–97 (2005).
99. Tristan, C., Shahani, N., Sedlak, T. W. & Sawa, A. The diverse functions of GAPDH : Views from different subcellular compartments. *Cell. Signal.* **23,** 317–323 (2011).
100. Article, O. β -Actin and GAPDH housekeeping gene expression in asthmatic airways is variable and not suitable for normalising mRNA levels. 765–770 (2002).
101. Chevalier, J., Yi, J., Michel, O. & Tang, X. Biotin and Digoxigenin as Labels for Light and Electron Microscopy in Situ Hybridization Probes : Where Do We Stand ? **45,** 481–491 (1997).
102. Picchi, S., Cristina, T. & Castellane, L. Monosaccharides Composition of Biofilm Produced by Xylella Fastidiosa Wild Type and Rpf Mutants. (2014).
103. Koo, H., Xiao, J., Klein, M. I. & Jeon, J. G. Exopolysaccharides Produced by Streptococcus mutans Glucosyltransferases Modulate the Establishment of Microcolonies within Multispecies Biofilms □. **192,** 3024–3032 (2010).
104. Kreft, J. & Wimpenny, J. W. T. EFFECT OF EPS ON BIOFILM STRUCTURE AND FUNCTION AS REVEALED BY AN INDIVIDUAL-BASED MODEL OF BIOFILM GROWTH.
105. Wimpenny, J., Manz, W. & Szewzyk, U. Heterogeneity in bio ¢ lms. **24,** 661–671 (2000).
106. Xu, K. D., Stewart, P. S., Xia, F. & Huang, C. Spatial Physiological Heterogeneity in Pseudomonas aeruginosa Biofilm Is Determined by Oxygen Availability. **64,** 4035–4039 (1998).
107. Chai, Y., Beauregard, P. B., Vlamakis, H., Losick, R. & Kolter, R. Galactose Metabolism Plays a Crucial Role in Biofilm Formation by Bacillus subtilis. **3,** 1–11 (2012).
108. Zippel, B. & Neu, T. R. Characterization of Glycoconjugates of Extracellular Polymeric Substances in Tufa-Associated Biofilms by Using Fluorescence Lectin-Binding Analysis □ †. **77,** 505–516 (2011).
109. Bejarano, E. M. & Schneider, P. Use of Fluorescent Lectin Probes for Analysis of Footprints from Pseudomonas aeruginosa MDC on Hydrophilic and Hydrophobic Glass Substrata. **70,** 4356–4362 (2004).
110. Kanissery, R. G. & Sims, G. K. Biostimulation for the Enhanced Degradation of Herbicides in Soil. *Appl. Environ. Soil Sci.* **2011,** 1–10 (2011).

111. Newcombe, D. A. & Crowley, D. E. Bioremediation of atrazine-contaminated soil by repeated applications of atrazine-degrading bacteria. *Appl. Microbiol. Biotechnol.* **51,** 877–882 (1999).
112. Biglione, N. K. Fundamental Kinetic Parameters of Suspended and Biofilm. (2007).
113. Debasmita, N. & Rajasimman, M. Optimization and kinetics studies on biodegradation of atrazine using mixed microorganisms. *Alexandria Eng. J.* **52,** 499–505 (2013).
114. Verhagen, P., de Gelder, L., Hoefman, S., de Vos, P. & Boon, N. Planktonic versus biofilm catabolic communities: Importance of the biofilm for species selection and pesticide degradation. *Appl. Environ. Microbiol.* **77,** 4728–4735 (2011).
115. Chen, J. L., Au, K. C., Wong, Y. S. & Tam, N. F. Y. Using orthogonal design to determine optimal conditions for biodegradation of phenanthrene in mangrove sediment slurry. *J. Hazard. Mater.* **176,** 666–671 (2010).
116. Yuan, S. Y., Wei, S. H. & Chang, B. V. Biodegradation of polycyclic aromatic hydrocarbons by a mixed culture. *Chemosphere* **41,** 1463–1468 (2000).
117. Strong, L. C., Rosendahl, C., Johnson, G., Sadowsky, M. J. & Wackett, L. P. Arthrobacter aurescens TC1 Metabolizes Diverse s -Triazine Ring Compounds Arthrobacter aurescens TC1 Metabolizes Diverse s -Triazine Ring Compounds. *Appl. Environ. Microbiol.* **68,** 5973–5980 (2002).
118. Lutosławski, K., Cibis, E. & Krzywonos, M. The effect of temperature on the efficiency of aerobic biodegradation of sugar beet distillery stillage: Removal of pollution load and biogens. *Brazilian J. Chem. Eng.* **34,** 985–996 (2017).
119. Spear, R. N., Li, S., Nordheimb, E. V & Andrewsa, J. H. ofMicrobiological Methods Quantitative imaging and statistical analysis of fluorescence in situ hybridization (FISH) of Aureobasidium pullulans. **35,** (1999).
120. Gunst, R. F. Response Surface Methodology: Process and Product Optimization Using Designed Experiments. *Technometrics* **38,** 284–286 (1996).
121. Churchill, G. A. Fundamentals of experimental design for cdna microarrays. *Nat. Genet.* **32,** 490–495 (2002).
122. VanGuilder, H. D., Vrana, K. E. & Freeman, W. M. Twenty-five years of quantitative PCR for gene expression analysis. *Biotechniques* **44,** 619–626 (2008).
123. Marguerat, S. & Bähler, J. RNA-seq: From technology to biology. *Cell. Mol. Life Sci.* **67,** 569–579 (2010).
124. Ozsolak, F. & Milos, P. M. NIH Public Access. *Nat. Rev. Genet.* **12,** 87–98 (2011).
125. Costa, V., Angelini, C., De Feis, I. & Ciccodicola, A. Uncovering the complexity of transcriptomes with RNA-Seq. *J. Biomed. Biotechnol.* **2010,** (2010).
126. Grabherr, M. G. *et al.* Full-length transcriptome assembly from RNA-Seq data without a reference genome. *Nat. Biotechnol.* **29,** 644–652 (2011).
127. Li, B. & Dewey, C. N. RSEM: Accurate transcript quantification from RNA-Seq data with or without a reference genome. *BMC Bioinformatics* **12,** (2011).
128. Schulz, M. H., Zerbino, D. R., Vingron, M. & Birney, E. Oases: Robust de novo RNA-seq assembly across the dynamic range of expression levels. *Bioinformatics* **28,** 1086–1092 (2012).

129. Haas, B. J. *et al.* De novo transcript sequence reconstruction from RNA-seq using the Trinity platform for reference generation and analysis. *Nat. Protoc.* **8,** 1494–1512 (2013).
130. Rumbo-Feal, S. *et al.* Whole Transcriptome Analysis of Acinetobacter baumannii Assessed by RNA-Sequencing Reveals Different mRNA Expression Profiles in Biofilm Compared to Planktonic Cells. *PLoS One* **8,** 1–19 (2013).
131. Qin, N. *et al.* RNA-Seq-based transcriptome analysis of methicillin-resistant staphylococcus aureus biofilm inhibition by ursolic acid and resveratrol. *Sci. Rep.* **4,** 1–9 (2014).
132. Dötsch, A. *et al.* The pseudomonas aeruginosa transcriptome in planktonic cultures and static biofilms using rna sequencing. *PLoS One* **7,** (2012).
133. Atagana, H. I., Haynes, R. J. & Wallis, F. M. Optimization of soil physical and chemical conditions for the bioremediation of creosote-contaminated soil. *Biodegradation* **14,** 297–307 (2003).
134. Rigas, F. *et al.* Biodegradation of lindane by Pleurotus ostreatus via central composite design. *Environ. Int.* **31,** 191–196 (2005).
135. Chang, B. ., Shiung, L. . & Yuan, S. . Anaerobic biodegradation of polycyclic aromatic hydrocarbon in soil. *Chemosphere* **48,** 717–724 (2002).
136. Zahed, M. A., Aziz, H. A., Isa, M. H., Mohajeri, L. & Mohajeri, S. Optimal conditions for bioremediation of oily seawater. *Bioresour. Technol.* **101,** 9455–9460 (2010).
137. Park, C. *et al.* Optimization for biodegradation of 2,4,6-trinitrotoluene (TNT) by Pseudomonas putida. *J. Biosci. Bioeng.* **95,** 567–571 (2003).
138. J.M., L. Biodegradation of a polymeric dye in a packed-bed bioreactor by immobilized Phanerochaete chrysosporium. *Water Res.* **36,** 1896 (2002).